Quaternary structures of the cyanide dihydratases of *Bacillus pumilus* C1 and *Pseudomonas stutzeri* AK61

by

Mark Nicholas Berman

Department of Molecular and Cell Biology
and Electron Microscope Unit,
Faculty of Science
University of Cape Town

A thesis submitted in fulfillment of the requirements
for the degree of Master of Science

Cape Town
May 2003

PREFACE

The experimental work presented in this thesis was carried out in the Department of Molecular and Cell Biology and in the Electron Microscope Unit at the University of Cape Town under the supervision of Prof Trevor Sewell and Dr Paul Meyers.

I hereby declare that this thesis is original and has not been submitted in any form to any other institution. Where use is made of work of others due acknowledgement is made of this.

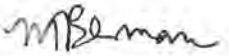

Mark Berman
May 2003

ACKNOWLEDGEMENTS

I am deeply grateful to my supervisors Trevor Sewell and Paul Meyers, for their outstanding support and friendship, their wealth of knowledge and for providing me with a fascinating research project.

Many thanks also to Mohamed Jaffer for sharing his expertise with me and for many patient hours spent helping me find my way around the microscopes. Thanks to Brendon Price and my father Peter Berman for valuable conversations and insightful advice. I am very grateful to Dennis Burford who out of kindness produced the wonderful programme MODEL VIEWER on which the models could be easily visualised. Thanks to William Williams, for developing the films, Anke Fiedler for doing the mass spectrometry and Ed Rybicki for the use of his fraction collector.

I would like to thank Laura Bremme for sacrificing many sun-filled days to be with me while I was writing this thesis. I wish to thank her and my parents for all their love and support.

Finally, I gratefully acknowledge the National Research Foundation for providing me with a subsistence grant in order to carry out this research.

Table of contents

Abstract

Nitrilases catalyse the conversion of a nitrile to its corresponding acid and ammonia by the addition of two water molecules. Cyanide dihydratases, a subgroup of nitrilases, specifically hydrolyse cyanide to formic acid and ammonia. Nitrilases are found in a diverse collection of organisms that includes plants, bacteria and fungi. They form one branch of a superfamily of structurally related enzymes that are believed to have in common a unique cys-glu-lys catalytic triad. Many nitrilases exist as a large molecular weight oligomers of more than 300kDa. In the current study the structures of two cyanide dihydratases, from *Pseudomonas stutzeri* AK61 and *Bacillus pumilus* C1, have been solved at a resolution of 2.9nm and 3.2nm respectively by single particle reconstruction from electron micrographs of enzyme particles stained in uranyl acetate. Each enzyme consists of a spiral structure of well-defined length. It is proposed that this arrangement of subunits occurs in many other nitrilases and that a number of unexplained observations in the literature can be reconciled by this model.

Chapter 1. Introduction

1.1 Cyanide dihydratase

Cyanide dihydratases are bacterial enzymes that catalyse the double hydrolysis of cyanide to formic acid and ammonia. These enzymes fit naturally into a larger class of enzymes, the nitrilases, which catalyse the double hydrolysis of larger nitriles. Nitrilases can be used in many synthetic processes to produce commodity chemicals and pharmaceuticals (Kobayashi *et al.*, 1994). Successful adaptation of nitrilases for use in industry will require a fundamental understanding of their enzymology and structure.

1.2 The nitrilase superfamily

The nitrilase superfamily encompasses a wide variety of proteins that are homologous to nitrilases. These proteins have been divided into thirteen distinct branches by Pace and Brenner (Pace and Brenner, 2001; Brenner, 2002) on the basis of amino acid sequence homology. Every sequence contains cysteine, glutamic acid and lysine residues at three conserved positions. Surrounding these residues are signature sequences which differ between branches and are conserved within each branch. The branches are labelled according to known and inferred function as follows:

1. Nitrilase
2. Aliphatic amidase
3. Amino-terminal amidase
4. Biotinidase
5. β-Ureidopropionase
6. Carbamylase
7. Prokaryotic NAD synthetase
8. Eukaryotic NAD synthetase
9. Apolipoprotein *N*-acyltransferase
10. Nit and NitFhit (substrate unknown)
11. *N*-carbamyl putrescine amidohydrolase

Abbreviations

BSA	bovine serum albumin
CFE	cell free extract
CHCA	α-cyano-4-hydroxycinnamic acid
DE sample	anion exchange sample
DE52	diethylaminoethyl cellulose
EDTA	ethylenediamine tetra-acetic acid
GF sample	gel filtration sample
IPTG	isopropyl-β-D-thiogalactopyranoside
LB	Luria broth
MALDI-TOF	Matrix-assisted laser desorption/ionisation-time of flight
MES	2-(*N*-Morpholino)ethanesulfonic acid
OD	optical density
PAGE	Polyacrylamide gel electrophoresis
PMSF	phenylmethylsulfonyl fluoride
SDS	sodium dodecyl sulphate
TEA	triethylamine
TRIS	Tris(hydroxymethyl)aminomethane
UV	Ultraviolet

12. NB12

13. NB13

The proteins in branches 12 and 13 have unknown functions. The nitrilase branch has been further subdivided into auxin-producing nitrilase, aliphatic nitrilase and β-cyano-L-alanine hydratase/nitrilase, while branch 4 has been subdivided into biotinidase and pantetheinase. Enzymes of all of the characterised branches perform nitrilase or amidase reactions, with the exception of branch 9 enzymes which catalyse a carbon-nitrogen condensation reaction.

1.3 The nitrilase branch

Nitrilases are defined by their ability to catalyse the conversion of a nitrile to its corresponding acid and ammonia. There is an alternative pathway, in which two successive hydration reactions are performed by a nitrile hydratase and an amidase, as depicted in Figure 1.1. Nitrile hydratases are metalloenzymes that are structurally distinct from nitrilases (Banerjee *et al.*, 2002). The plant AtNIT1 nitrilase homologue is exceptional in that it possesses both nitrilase and nitrile hydratase activities (Osswald *et al.*, 2002). The fungal cyanide hydratases are homologous to nitrilases even though they convert cyanide to formamide with the addition of a single water molecule.

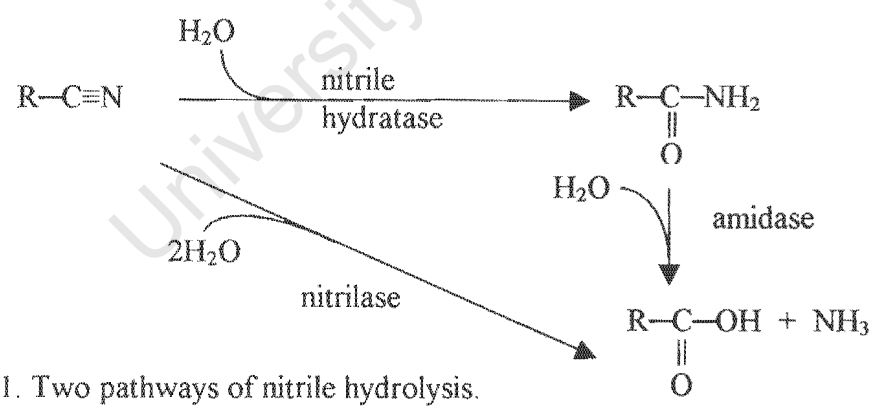

Figure 1.1. Two pathways of nitrile hydrolysis.

1.4 Biological roles of nitrilases

Nitrilases were first isolated from barley by Thimann and Mahadevan in 1964. The enzyme was shown to convert indole-3-acetonitrile (IAN) to indole-3-acetic acid (IAA), an important plant growth hormone. At least two metabolic pathways for IAA synthesis

in *Arabidopsis thaliana* have been identified (Bartling *et al.*, 1994), each of which involves the action of a nitrilase to convert IAN to IAA in the final step. Of the four nitrilase homologues in *A. thaliana* (NIT1-4), NIT4 is distinguished from the others by its inability to cleave IAN and its specificity for β-cyano-L-alanine, an intermediate in the detoxicification of cyanide during ethylene biosynthesis (Piotrowski *et al.*, 2001).

In fungi such as *Fusarium solani*, *Fusarium lateritium* and *Gloeocercospora sorghi* (Barclay *et al.*, 1998; Cluness *et al.*, 1993; Fry and Munch, 1975) cyanide hydratase enzymes are strongly induced in the presence of cyanide. These fungi are pathogens of cyanogenic plants. Disruption of the gene encoding the *G. sorghi* cyanide hydratase causes sensitivity of the organism to cyanide but also shows that pathogenicity of the fungus does not depend on a functional enzyme (Wang *et al.*, 1999).

A role for cyanide dihydratase in bacteria has not been found. Cells of *Bacillus pumilus* C1 were not able to utilise cyanide as a sole source of nitrogen (Meyers *et al.*, 1991). Expression of cyanide dihydratase in *Bacillus pumilus* C1 and *Pseudomonas stutzeri* AK61 is cyanide-independent (Meyers *et al.*, 1991; Watanabe *et al.*, 1998a), while in *Alcaligenes xylosoxidans* subsp. *denitrificans* strain DF3 it is induced by cyanide (Invorsen *et al.*, 1991). Cells of the latter organism are tolerant to cyanide at concentrations of up to 0.5 M. While expression of cyanide dihydratase in *B. pumilus* C1 is independent of cyanide, it is dependent on the presence of manganese ions.

In bacteria nitrilases may serve to utilise exogenous nitriles as a source of nitrogen. Supportive evidence is provided by the nitrilase of *Pseudomonas fluorescens* DSM 7155. The expression of this nitrilase was induced in cells grown in media containing phenylacetonitrile, but not when both phenylacetonitrile and ammonia were present (Layh *et al.*, 1998). The authors explained this as N-catabolite repression. This suggests that the *in vivo* role of this nitrilase may be to use arylacetonitriles as a source of nitrogen for growth. Induction by nitriles is common in other bacteria that possess nitrilases. For instance, the nitrilases of *Rhodococcus rhodochrous* K22, *Alcaligenes faecalis* JM3 and *Rhodococcus* ATCC 39484 were all expressed when these organisms were grown in the

presence of isovaleronitrile (Kobayashi *et al.*, 1990a; Nagasawa *et al.*, 1990; Stevenson *et al.*, 1992). Exceptions include the nitrilases of *Klebsiella ozaenae* and *Acinetobacter* sp. AK 226, which were both found to be constitutively expressed (Stalker and McBride, 1987; Yamamoto and Komatsu, 1991). The aromatic nitrilase of *Rhodococcus rhodochrous* NCIMB 11216 was shown to differentially express two different nitrilases depending on whether benzonitrile or propionitrile was used as the inducer (Hoyle *et al.*, 1998). The two enzymes had similar substrate specificities for the compounds tested. By contrast, the single aromatic nitrilase of *Fusarium oxysporum* F. sp. *melonis* was shown to be induced by a wide variety of aromatic and aliphatic nitriles (Goldlust and Bohak, 1989).

1.5 Substrate specificity

Nitrilases can be split into classes according to their substrate specificities, as aromatic, aliphatic, arylaceto- and bromoxynil-specific nitrilases, cyanide dihydratases and cyanide hydratases, as indicated in Table 1.2. The relative rates of hydrolysis (based on V_{max}) for prototype substrates as well as special substrates are shown for each enzyme in Table 1.3.

The first class contains nitrilases that act on aromatic and heterocyclic nitriles. These enzymes act on a broad range of aromatic substrates and most of them are inactive on aliphatic nitriles such as acrylonitrile. However, unsaturated aliphatic dinitriles are good substrates for the nitrilase of *Rhodococcus rhodochrous* 11216 (Hoyle *et al.*, 1998), while the *Bacillus pallidus* Dac521 nitrilase is active on 4-chlorobutyronitrile and other aliphatic nitriles (Almatawah *et al.*, 1999). The aromatic nitrilase of *Rhodococcus rhodochrous* J1 is inactive on aliphatic nitriles such as acrylonitrile (Kobayashi *et al.*, 1989). Under conditions leading to oligomerisation of the enzyme, activity on aliphatic nitriles is acquired (Nagasawa *et al.*, 2000), as discussed below. Nitrilases of *Rhodococcus rhodochrous* 11216, *Alcaligenes faecalis* JM3 and *Rhodococcus* ATCC 39484 act readily on fluoro-, chloro-, bromo-, methyl- and hydroxyl- substituted benzonitriles when the substitution is in the para- or meta- position, but are vitually inactive when the substitution is in the ortho- position (Harper, 1977a; Kobayashi *et al.*, 1989; Stevenson *et al.*, 1992). This is observed also in the fungal aromatic nitrilases of

Fusarium solani and *Fusarium oxysporum* F. sp. *melonis* (Harper, 1977b; Goldlust and Bohak, 1989). The nitrilases of *Bacillus pallidus* Dac521 and *Rhodococcus rhodochrous* NCIMB 11215 are able to cleave ortho-substituted benzonitrile, but only if the substitutient is a small atom such as fluorine (Harper, 1985; Almatawah *et al.*, 1999).

The second class of nitrilases contains enzymes that act primarily on aliphatic nitriles. These enzymes are less active on aromatic than aliphatic nitriles. In particular the nitrilase of *Comamonas testosteroni* sp. has a 25-fold higher activity on adiponitrile than on benzonitrile (Lévy-Schil *et al.*, 1995), while the AtNIT1 nitrilase of *Arabidopsis thaliana* has a 270-fold higher activity on 3-phenylpropionitrile than on benzonitrile (Osswald *et al.*, 2002).

Certain nitrilases specifically cleave arylacetonitriles. These enzymes are inactive on benzonitrile, and so differ from typical aromatic nitrilases. The arylacetonitrilase of *Pseudomonas fluorescens* DSM 7155 does not act on aliphatic nitriles (Layh *et al.*, 1998) while that of *Alcaligenes faecalis* JM3 is weakly active on acrylonitrile (Nagasawa *et al.*, 1990).

Cyanide dihydratases comprise a fourth class. The enzyme of *Alcaligenes xylosoxidans* subsp. *denitrificans* strain DF3 has been tested on a number of aromatic and aliphatic nitriles, and is specific for cyanide (Invorsen *et al.*, 1991). The cyanide dihydratase of *Bacillus pumilus* C1 is inactive on acetonitrile (Meyers *et al.*, 1993a).

The nitrilase of *Klebsiella ozaenae* differs from all other known nitrilases in that it is highly specific for bromoxynil (3,5-dibromohydroxybenzonitrile) (Stalker *et al.*, 1988a). The enzyme is inactive on benzonitrile.

The fungal cyanide hydratases specifically convert cyanide to formamide. However, in a recent study (Nolan *et al.*, 2003) it was shown that the cyanide hydratase of *Fusarium lateritium* is weakly active on benzonitrile and acrylonitrile.

A general feature of nitrilases is that they do not act on amides, and do not produce amides as by-products of their reactions with nitriles. Exceptions include the nitrilases of *Rhodococcus* ATCC 39484, *Fusarium oxysporum* F. sp. *melonis*, *Pseudomonas fluorescens* DSM 7155, the AtNIT1 nitrilase of *Arabidopsis thaliana* and the fungal cyanide hydratases. The AtNIT1 nitrilase was shown to convert crotononitrile to the corresponding acid, with 5% formation of amide, whereas the acid and amide products of its action on 3-nitroacrylonitrile were formed in the reverse ratio (Osswald *et al.*, 2002). The *Rhodococcus* ATCC 39484 enzyme formed 2% amide as a by-product in its reaction with phenylacetonitrile but not with other substrates (Stevenson *et al.*, 1992). On the other hand the *Fusarium oxysporum* F. sp. *melonis* nitrilase formed 4-6% amide as a by-product in its reaction with each of benzonitrile, propionitrile and acrylonitrile (Goldlust and Bohak, 1989).

The nitrilase of *Rhodococcus rhodochrous* J1 has extremely weak but detectable amidase activity. This enzyme has K_m values of 2.1 and 2.9mM for benzonitrile and benzamide respectively, but cleaves benzamide less efficiently by six orders of magnitude (Kobayashi *et al.*, 1998).

1.6 Catalysis

Crystal structures of two nitrilase homologues have been determined. These are the *Caenorhabditis elegans* NitFhit protein (Pace *et al.*, 2000) (a fusion of Nit - a nitrilase homologue, and Fhit - a centrally important tumor suppressor protein) and the *Agrobacterium N*-Carbamoyl-D-Amino Acid Amidohydrolase (DCase, also known as D-NCAase) (Nakai *et al.*, 2000; Chen *et* al., 2003; Wang *et al.*, 2001). These proteins belong respectively to Branch 10 and Branch 6 of the nitrilase superfamily. Both of these structures revealed a cys-glu-lys triad of closely positioned residues that were postulated to form the catalytic site (Nakai *et al.*, 2000; Pace *et* al., 2000; Wang *et al.*, 2001; Chen *et* al., 2003 with reviews in Pace and Brenner, 2001; Brenner, 2002). This catalytic triad is unique to members of the nitrilase superfamily, the closest similar active site being cys-asp-lys found in *N*-carbamoylsarcosine amidohydrolase (Romão *et al.*, 1992).

Table 1.2. Activities and sizes of nitrilases.

Description	Organism	Typical substrate(s) (Specific activity in $\mu mol.min^{-1}.mg^{-1}$)	amino acids	Subunit mw (SDS PAGE / sequence data)		Complex mw	Subunits	Reference
Aromatic nitrilase	*Arthrobacter* sp. strain J1	benzonitrile (1.31)	—	30kDa	—	30kDa	1	Bandyopadathy *et al.*, 1986
	Bacillus pallidus Dac521	benzonitrile (1.06) 4-cyanopyridine (2.46)	—	41kDa	—	600kDa	14	Almatawah *et al.*, 1999
	(fungal) *Fusarium solani*	benzonitrile (1.66)	—	76kDa	—	620kDa	8	Harper, 1977b
	(fungal) *Fusarium oxysporum* F. sp. *melonis.*	benzonitrile (143)	—	37kDa	—	550kDa	14	Goldlust and Bohak, 1989
	Rhodococcus rhodochrous sp. NCIMB 11215	benzonitrile (1.74), p-hydroxybenzonitrile (0.395)	—	46 kDa	—	560kDa	12	Harper, 1985
	Rhodococcus rhodochrous sp. NCIMB 11216	benzonitrile (15.7)	—	(45kDa, 45.8kDa)	—	44.5kDa, 560kDa	1, 12	Harper, 1977a; Hoyle *et al*,. 1998
	Rhodococcus rhodochrous J1	benzonitrile (15.9)	366	41.5kDa	40.2 kDa	78kDa, 410kDa	2, 10	Kobayashi *et al.*, 1989, 1992a; Nagasawa *et al.*, 2000
	Rhodococcus ATCC 39484	benzonitrile (84)	—	40.3kDa (mass spec.)	—	46kDa, 100kDa, 225kDa, 560kDa	1, 2, 6, 14	Stevenson *et al.*, 1992
	Rhodococcus rhodochrous PA-34	benzonitrile (24.5), α-aminoisocapronitrile	—	45kDa	—	45kDa	1	Bhalla *et al.*, 1992
Aliphatic nitrilase	*Rhodococcus rhodochrous* K22	acrylonitrile (2.56), crotonitrile (0.737)	383	41kDa	42.3kDa	(604kDa,650kDa)	15 or 16	Kobayashi *et al.*, 1990a, 1992b
	Comamonas testosteroni sp.	adiponitrile (68), cyanovaleric acid (15)	354	38kDa	38.7kDa	oligomeric, no estimate	—	Lévy-Schil *et al.*, 1995
	Acinetobacter sp. AK226	acrylonitrile (22.5)	—	41,43kDa	—	580 kDa	13 or 14	Yamamoto & Komatsu, 1991
	Arabidopsis thaliana (AtNIT1)	3-phenylpropionitrile (34.1)	346	38kDa	38kDa	450kDa	11-13	Osswald *et al.*, 2002
Arylaceto-nitrilase	*Alcaligenes faecalis* JM3	2-thiopheneacetonitrile (144)	356	44kDa	38.9kDa	(260kDa, 275kDa)	6	Nagasawa 1990; Kobayashi *et al.*, 1993
	Pseudomonas fluorescens DSM 7155	phenylacetonitrile (90)	—	38,40kDa	—	130kDa	2 or 3	Layh *et al.*, 1998
Bromoxynil-specific nitrilase	*Klebsiella ozaenae*	Bromoxynil (15)	349	37kDa	38.1kDa	72kDa	2	Stalker *et al.*, 1988
Cyanide dihydratase	*Alcaligenes xylosoxidans* subsp. *denitrificans* strain DF3	HCN (81)	—	39,40kDa	—	>300kDa	—	Ingvorsen *et al.*, 1991
	Bacillus pumilus C1	HCN (88)	—	(41.2, 44.6, 45.6 kDa)	—	417kDa	11	Meyers *et al.*, 1993b
	Pseudomonas stutzeri AK61	HCN (54.6)	334	38kDa	37.4kDa	>100kDa	—	Watanabe *et al.*, 1998a, 1998b
Cyanide hydratase	(fungal) *Fusarium lateritium*	HCN (1109)	355	43kDa	39.9kDa	>300kDa, 272-1217kDa	—	Cluness *et al.*, 1993
	(fungal) *Fusarium solani*	KCN (1.7), $K_2Ni(CN)_4$,$K_4Fe(CN)_6$	—	45kDa	—	>300kDa	—	Barclay *et al.*, 1998
	(fungal) *Gloeocercospora sorghi*	HCN (555)	369	45kDa	40.9kDa	>300 kDa, 2000-10 000 kDa	—	Fry and Munch, 1975; Wang and vanEtten, 1992b

Table 1.3. Substrate specificities of nitrilases.

Organism	Relative activities on different substrates (nt=not tested) Values are independently normalised for each enzyme						Amide by-product	Activity on amide	Reference
	Benzo-nitrile	4-Cyano-pyridine	Acrylonitrile	2-Thiophene-acetonitrile	cyanide	other			
Arthrobacter sp. strain J1	100	44	nt	nt	nt	—	–	–	Bandyopadathy *et al.*, 1986
Bacillus pallidus Dac521	43	100	4	nt	nt	0.3 (Phenylacetonitrile) 110 (4-Chlorobutyronitrile)	–	–	Almatawah *et al.*, 1999
(fungal) *Fusarium solani*	80	100	nt	nt	nt	0 (Acetonitrile)	–	–	Harper, 1977b
(fungal) *Fusarium oxysporum* F. sp. *melonis.*	100	25	35	nt	nt	25 (3-Cyanopyridine)	+ (4-6% for benzonitrile)	nt	Goldlust and Bohak, 1989
Rhodococcus rhodochrous sp. NCIMB 11215	37	100	nt	nt	nt	—	–	–	Harper, 1985
Rhodococcus rhodochrous sp. NCIMB 11216	100	26	nt	nt	nt	0 (Acetonitrile) 183 (Fumaronitrile)	–	–	Harper, 1977a
Rhodococcus rhodochrous J1	100	26	0 (dimeric) 59 (decameric)	11	nt	139 (2-Furonitrile)	–	+ (weak)	Kobayashi *et al.*, 1989; Nagasawa *et al.*, 2000
Rhodococcus ATCC 39484	100	nt	0	nt	nt	28 (3-Cyanopyridine)	+ (2% for phenyl-acetonitrile)	–	Stevenson *et al.*, 1992
Rhodococcus rhodochrous PA-34	100	nt	22	nt	nt	0.8 (Phenylacetonitrile) 14 (a-Aminoisocapronitrile)	–	–	Bhalla *et al.*, 1992
Rhodococcus rhodochrous K22	8	3	100	21	nt	—	–	–	Kobayashi *et al*,1990a,1992b
Comamonas testosteroni sp.	17	nt	100	nt	nt	435 (Adiponitrile)	–	–	Lévy-Schil *et al.*, 1995
Acinetobacter sp. AK226	65	36	100	32	0.06	—	–	nt	Yamamoto & Komatsu, 1991
Arabidopsis thaliana (AtNIT1)	0.4	nt	nt	nt	nt	100 (3-Phenylpropionitrile) 14 (Butyronitrile)	+ (95% for 3-nitroacrylonitrile)	–	Osswald *et al.*, 2002
Alcaligenes faecalis JM3	0	0	8	100	nt	—	–	–	Nagasawa 1990
Pseudomonas fluorescens DSM 7155	0	nt	nt	nt	nt	100 (Phenylacetonitrile) 0 (3-Cyanopyridine) 0 (Propionitrile)	+ (5% for 2-(methoxy)-mandelonitrile)	–	Layh *et al.*, 1998
Klebsiella ozaenae	0	nt	nt	nt	nt	100 (Bromoxynil)	–	–	Stalker *et al.*, 1988
Alcaligenes xylosoxidans subsp. *denitrificans* strain DF3	0	nt	0	nt	100	—	–	–	Ingvorsen *et al.*, 1991
Bacillus pumilus C1	nt	nt	nt	nt	100	0 (Acetonitrile)	–	–	Meyers *et al.*, 1993b
Pseudomonas stutzeri AK61	nt	nt	nt	nt	100	—	nt	nt	Watanabe *et al.*, 1998a
(fungal) *Fusarium lateritium*	0.033	nt	nt	nt	100	0.013 (acetonitrile) 0.009 (propionitrile)	+ (100%)	–	Cluness *et al.*, 1993
(fungal) *Fusarium solani*	nt	nt	nt	nt	100	—	+ (100%)	–	Barclay *et al.*, 1998
(fungal) *Gloeocercospora sorghi*	nt	nt	nt	nt	100	—	+ (100%)	–	Fry and Munch, 1975; Wang and vanEtten, 1992b

The cysteine residue of the presumptive catalytic triad was shown by site-directed mutagenesis to be absolutely required for activity in *Rhodococcus rhodochrous* J1 (Kobayashi *et al.*, 1992a), *Alcaligenes faecalis* JM3 (Kobayashi *et al.*, 1993) and *Pseudomonas stutzeri* AK61 (Watanabe *et al.*, 1998c). In all three cases, the mutant enzymes with cysteine substituted by alanine or serine were found to have molecular masses and far-UV circular dichroism spectra indistinguishable from that of wild type enzymes, which was taken to indicate that no significant conformational change had occurred. The involvement of cysteine was also supported by studies on a number of nitrilases in which thiol-reducing reagents were shown to enhance activity (Kobayashi *et al.*, 1989; Layh *et al.*, 1998) whereas thiol-complexing reagents were inhibitory (Brown *et al.*, 1995; Harper, 1977a; Harper, 1977b; Harper, 1985; Goldlust and Bohak, 1989; Kobayashi *et al.*, 1989; Layh *et al.*, 1998; Meyers *et al.*, 1993a; Stalker *et al.*, 1988a; Stevenson *et al.*, 1992; Wang *et al.*, 1992a; Watanabe *et al.*, 1998a; Yamamoto and Komatsu, 1991).

The aliphatic amidase of *Pseudomonas aeruginosa* is a member of Branch 2 of the nitrilase superfamily. Mutations at each of the catalytic triad residues, Cys166Ser, Glu59Gln and Lys134Asn caused inactivation; nevertheless the protein remained stable (Farnaud *et* al., 1999; Novo *et al.*, 2002). The D-NCAase of *Agrobacterium radiobacter*, belonging to Branch 6 of the nitrilase superfamily, was mutated to replace the putative active site cysteine with serine (Chen *et al.*, 2003). This C172S mutant was crystallised bound with *N*-carbamoyl-D-*p*-hydroxyphenylglycine (HPG) substrate and the structure was solved at 2.2Å resolution by molecular replacement. The hydroxyl group of S172 was seen to point directly towards the carbon of the carbamoyl moiety, with an O-C interatomic distance of 2.9Å. Side chains of the other presumptive catalytic residues, E47 and K127, were observed to form a cluster with S172 and both faced the carbamoyl group.

The optimal pH for activity of nitrilases is typically in the region of 7.5-8.5. The pH maximum for some enzymes is sharp, as with *Klebsiella ozaenae* nitrilase, *Acinetobacter* sp. AK226 nitrilase and *Bacillus pumilus* C1 cyanide dihydratase (Stalker *et al.*, 1988a;

Yamamoto and Komatsu, 1991; Meyers *et al.*, 1993a). Other nitrilases exhibit activity over a broad range of pH. These include the nitrilases of *Bacillus pallidus* Dac521 (pH 6-9), *Fusarium oxysporum* f. sp. *melonis* (pH 6-11), *Rhodococcus rhodochrous* NCIMB 11215 (pH 7-10), *Rhodococcus rhodochrous* K22 (pH 5-9), *Pseudomonas fluorescens* DSM 7155 (pH 6-10), and *Comamonas* sp. (pH 4-7) (Almatawah *et* al., 1999; Goldlust and Bohak, 1989; Harper, 1985; Kobayashi *et* al., 1990a; Layh *et al.*, 1998; Lévy-Schil *et al.*, 1995). This is consistent with the involvement of a deprotonated Glu and protonated Lys in the reaction, but would depend also on the stabilising effect on these residues by neighbouring residues at the extreme pH values of 4 and 11 (which are close to the respective pKa values of the sidechains of free glu and lys). The cyanide dihydratase of *Bacillus pumilus* C1 was inactive above pH 8.4. However, its activity at this pH could be restored by the addition of chromium or terbium ions to 200μM (Meyers *et al.*, 1993a).

A reaction mechanism for nitrilase was proposed as early as 1964 by Hook and Robinson for a Pseudomonad ricinine nitrilase. This has been refined by Nakai *et al.* and Pace *et al.* along with their independent discoveries of the cys-glu-lys catalytic triad. In this mechanism, the carboxyl group of glu acts as a general base, activating cys for nucleophilic attack on the nitrile carbon, as indicated in Figure 1.4. Lys (or glu) may then activate a water molecule for further attack on the carbon, leading to a tetrahedral intermediate. The positively charged lys may also stabilise the oxyanion of the tetrahedral intermediate. The fate of this intermediate is determined by the relative strength of the C-S and C-N bonds (indicated in red as A and B), (Hook and Robinson, 1964; Osswald *et al.*, 2002) which in turn will be determined by the geometry and chemistry of both the active site and the substrate. In most nitrilases C-N cleavage is favoured, followed by the release of ammonia. A notable exception is the nitrilase of *Arabidopsis thaliana*, which can cleave the C-S bond (to release an amide) or the C-N bond, depending on the substrate (Osswald *et al.*, 2002). Following C-N cleavage, a second water molecule is activated by glu to attack the thioester, resulting in a second tetrahedral intermediate, formation of a carboxylic acid and its release from the enzyme. An interesting observation made by Pace and Brenner is that the presence of a bulky aromatic sidechain

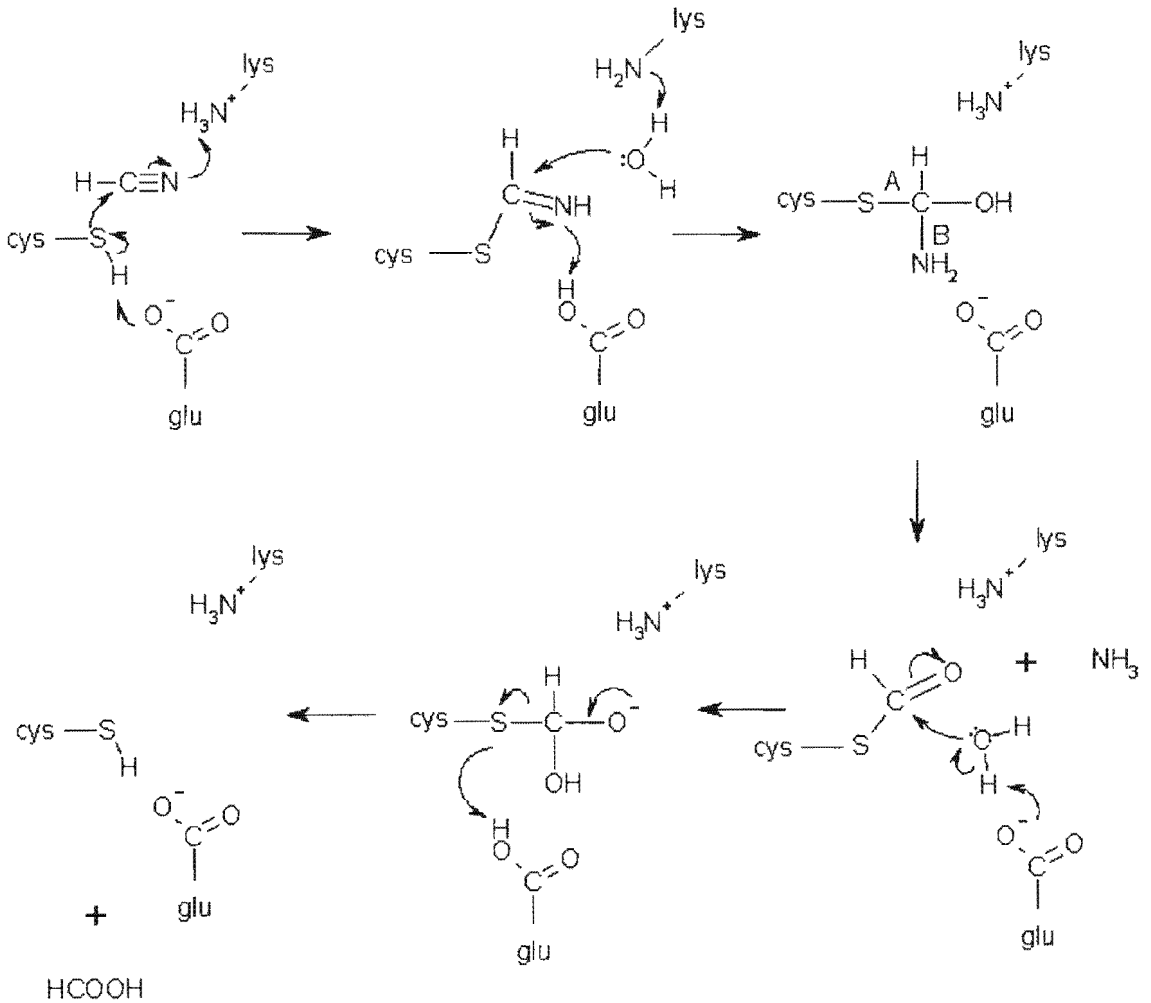

Figure 1.4. Proposed reaction mechanism for nitrilase, with cyanide shown as prototype substrate. Nucleophilic attack by the sulfhydryl moeity is activated by glu, which acts as a general base. This leads to the formation of the first covalent intermediate. The first hydrolysis is catalysed by lys acting as a general base, increasing the nucleophilicity of the lone pair of the water. Spontaneous breakdown of the tetrahedral intermediate can proceed in two ways, depending on the relative strengths of the C-S and C-N bonds (indicated in red as A and B). In the nitrilase reaction the C-N is cleaved and ammonia is released. Activation of a second water molecule by glu leads to the second hydrolysis and release of the substrate.

in the substrate may help to distort the bond angles in the nitrile closer to the 120° angles at the nitrile carbon required for the first planar intermediate, thus favouring the reaction. This may help to explain the fact that many nitrilases act most readily on bulky substrates.

The nitrilase of *Rhodococcus* ATCC 39484 was analysed by mass spectrometry in the presence of benzonitrile (Stevenson *et al.*, 1990; Stevenson *et al.*, 1992). An adduct was detected having a mass consistent with the masses expected for either of the two planar enzyme-substrate intermediates (the second and fourth intermediates in Figure 1.4), which differ by only one Dalton.

1.7 Oligomerisation

Many nitrilases exist as a homo-oligomers of molecular weight greater than 300kDa and subunit molecular weight in the range 37-45kDa, as shown in Table 1.2. Exceptions include the 76 kDa subunits of *Fusarium solani* (Harper, 1977b) and the 30kDa subunit of *Arthrobacter* (Bandyopadathy *et al.*, 1986). The fungal cyanide hydratases of *Fusarium lateritium* and *Gloeocercospora sorghi* exist as large aggregates in excess of 1000 kDa (Cluness *et al.*, 1993; Fry and Munch, 1975). The purified cyanide dihydratase of *Bacillus pumilus* C1 was examined by negative stain electron microscopy (Meyers *et al.*, 1993a). Particles heterogeneous in size were observed of diameter 9nm and length up to 50nm. A spiral quaternary structure was postulated for this enzyme.

The cyanide dihydratases of *Alcaligenes xylosoxidans* subsp. *denitrificans* strain DF3 and of *Bacillus pumilus* C1 migrate as multiple bands on SDS PAGE gel electrophoresis (Invorsen *et al.*, 1991; Meyers *et al.*, 1993a), and this is observed also in the purified nitrilases of *Acinetobacter* sp. AK226, *Bacillus pallidus* strain Dac521 and *Pseudomonas fluorescens* DSM 7155 (Yamamoto and Komatsu, 1991; Almatawah *et al.*, 1999; Layh *et al.*, 1998). Partial N-terminal sequences were determined for each band of the latter three preparations (Yamamoto and Komatsu, 1991; Almatawah *et al.*, 1999; Layh *et al.*, 1998). This revealed copurification of chaperonin-related polypeptides with the *Bacillus pallidus* and *Pseudomonas fluorescens* enzymes. The partial sequences also showed that

Pseudomonas fluorescens nitrilase is a heterodimer or heterotrimer and indicated that *Acinetobacter* nitrilase is a homo-oligomer.

The aromatic nitrilases of *Rhodococcus rhodochrous* NCIMB 11216, *Rhodococcus* ATCC 39484 and *Rhodococcus rhodochrous* J1 are interesting in that their subunits associate in the presence of benzonitrile, which is a substrate for all of them (Harper, 1977a; Nagasawa *et al.*, 2000; Stevenson *et al.*, 1992).

Specifically, the nitrilase of *Rhodococcus* ATCC 39484 was shown to partially assemble in the presence of various substrate analogues (Stevenson *et al.*, 1992). Benzyl alcohol - a weak inhibitor of the enzyme, induced assembly into a hexamer. Benzoic acid, the reaction product, induced dimerisation. Benzaldehyde, a strong inhibitor of the enzyme, induced full assembly into a 14-mer, as did the substrate benzonitrile.

The nitrilase of *Rhodococcus rhodochrous* J1, normally found as dimers, was induced to form decamers at higher concentrations of enzymes, elevated temperatures, dehydrating conditions (such as the addition of organic solvents or ammonium sulfate) and in the presence of benzonitrile (Nagasawa *et al.*, 2000). Concommitant with assembly, the enzyme acquired an ability to hydrolyse acrylonitrile and other aliphatic nitriles. In the dimeric state the enzyme was virtually inactive on acrylonitrile, and acrylonitrile could not induce assembly. The rate of acrylonitrile hydrolysis by the decameric enzyme was 59% of the rate of benzonitrile hydrolysis. Interestingly, assembly was not induced by benzonitrile in the presence of $HgCl_2$; neither was the enzyme active under these conditions. However, at elevated enzyme concentrations in the absence of benzonitrile, $HgCl_2$ did not inhibit assembly.

The monomeric nitrilase of *Rhodococcus rhodochrous* NCIMB 11216 was induced to form a dodecamer by benzonitrile and this process was favoured at pH 7.3 and at temperatures higher than 20°C (Harper, 1977a). Association was initially detected by gel filtration and subsequently by measuring activation times for benzonitrile degradation.

The nitrilases of *Rhodococcus rhodochrous* NCIMB 11216 and *Rhodococcus* ATCC 39484 are inactive on aliphatic nitriles (Harper, 1977a; Stevenson *et al.*, 1992). The activity of the assembled enzymes on aliphatic nitriles has not been investigated, and would be interesting to test in view of the behaviour of the *Rhodococcus rhodochrous* J1 nitrilase.

The nitrilase of *Fusarium oxysporum* f. sp. *melonis* (Goldlust and Bohak, 1989) was reported to consist of partially assembled oligomers under certain conditions. Active complexes corresponding to hexamers, decamers and 14-mers were detected by native polyacrylamide gel electrophoresis, despite the presence of a single active gel filtration peak corresponding to the 14-mer.

Exceptions to the general pattern of oligomerisation are the nitrilases of *Arthrobacter* sp. strain J1 and *Rhodococcus rhodochrous* PA-34, which exist as monomers, and the nitrilases of *Pseudomonas fluorescens* DSM 7155 and *Klebsiella ozaenae*, which exist as dimers or trimers. The sizes of these enzymes have not been determined in the presence of substrate.

The crystal structures of both NitFhit and DCase reveal a homotetramer with 222 symmetry and two types of interacting surfaces. The dimer interface designated as east-west is formed by the symmetry-related mating of two pairs of alpha helices and anti-parallel β-interaction (Pace *et al.*, 2000). Some of the salt bridges stabilising the north-south dimer interface are absent in the sequences of other Branch 10 Nit proteins. These structures will be useful in the future to model subunit interactions in nitrilases.

1.8 Industrial applications

While chemical methods exist for the production of carboxylic acids from nitriles, the reactions require extreme conditions and result in the damage to catalysts, undesirable polymerisation of the products and the build-up of by-products such as salts or cyanide (Banerjee *et al.*, 2002; Nagasawa and Yamada, 1995). Nitrilases offer an attractive alternative as they operate efficiently under mild conditions. Moreover the diversity of

substrate specificities occurring amongst nitrilases allows flexibility in the choice of biocatalyst. The nitrilase of *Rhodococcus rhodochrous* J1 was shown to act on acrylonitrile (Nagasawa *et al.*, 2000), a compound used in the manufacture acrylic fibres, whilst the nitrilase of *Comomonas testosteroni* sp. converts the dinitrile adiponitrile into cyanovaleric acid and adipic acid, which are used in the production of nylon (Lévy-Schil *et al.*, 1995).

The nitrilase of *Acinetobacter* sp. AK 226 converts 2-(4'-isobutylphenyl)propionitrile (Ibu-CN) to S-(+)-ibuprofen, a non-steroidal anti-inflammatory drug. This enzyme is highly selective for the S-(-)-Ibu-CN enantiomer, producing 94% S-(+)-Ibuprofen at 50% yield. Other enantioselective nitrilases include the propionitrile-induced nitrilase of *R. rhodochrous* NCIMB 11216 (Gradley and Knowles, 1994) and the phenylacetonitrile-induced arylacetonitrilase of *Pseudomonas fluorescens* DSM 7155 (Layh *et al.*, 1998). These enzymes may be useful in the pharmaceutical industry for producing optically pure compounds.

The *Rhodococcus rhodochrous* K22 nitrilase was shown to specifically cleave one of the two nitrile groups in glutaronitrile (Kobayashi *et al.*, 1990b). Regiospecificity has also been reported in the nitrilases of *Rhodococcus rhodochrous* J1, *Rhodococcus rhodochrous* NCIMB 11216, *Rhodococcus rhodochrous* LL100-21 and *Arabidopsis thaliana* (Kobayashi *et al.*, 1988; Bengis-Garber and Gutman, 1989; Dadd *et al.*, 2001; Effenberger and Osswald, 2001). This type of selectivity is virtually impossible to achieve chemically.

Cyanide dihydratases and cyanide hydratases are potentially useful as biological agents in the remediation of toxic cyanide waste, which is produced in large amounts by the gold mining industry. *Pseudomonas paucimobilis* was used as a biocatalyst in the wastewater of Homestake Mine, in South Dakota, and led to a removal of 98% of weak-acid-dissociable cyanide (Dubey and Holmes, 1995). The cyanide hydratase activity of *Fusarium solani* was shown to convert $K_2Ni(CN)_4$ and $K_4Fe(CN)_6$ to ammonia under neutral and acidic conditions (Barclay *et al.*, 1998), and may be a useful alternative in the

remediation of wastewaters containing metal-cyanide complexes, which are often resistant to attack by cyanide degrading organisms.

The nitrilase of *Klebsiella ozaenae*, which specifically cleaves the herbicide bromoxynil (Stalker *et al.*, 1988a), has been successfully transfected into tobacco plants to confer bromoxynil-resistance in these plants (Stalker *et al.*, 1988b).

1.9 Motivation

Nitrilases are interesting because they are able to cleave a wide variety of nitrile substrates using a glu-lys-cys catalytic triad (unique to the nitrilase superfamily) and their biological roles are largely unknown. In addition, these enzymes exhibit stereo- and regio-specificities that make them attractive as biocatalysts.

In spite of their sequence similarity the nitrilases are reported to form oligomers of widely differing sizes. An important step on the way to understanding the structure-function relationships of these enzymes is to determine the principle that leads to this diversity.

In this work the cyanide dihydratases of *Bacillus pumilus* C1 and *Pseudomonas stutzeri* AK61 were expressed and purified. Electron micrographs of negatively stained single particles were used to generate models of the enzymes at a resolution of 2.9 nm - 3.4 nm by three dimensional reconstruction. The structures of these enzymes provide insight into what may be a general pattern of assembly in nitrilases that is compatible with the range of sizes reported in the literature.

Chapter 2. Materials and Methods

A Purification of cyanide dihydratase from *B. pumilus* C1 and from recombinant clones MB2784 and MB2890

In this section purification protocols for the cyanide dihydratases are given. These are based on the method described in Meyers *et al.*, 1993a. The enzyme of *B. pumilus* C1 was purified both from the native organism and from an overexpressing clone, which is designated *E. coli* MB2890. The *P. stutzeri* AK61 enzyme was purified from an overexpressing clone, designated *E. coli* MB2784.

2.1 Origin and nature of the clones

Both the recombinant clones MB2890 and MB2784 were generous gifts from Dr Michael J. Benedik, Department of Biology and Biochemistry, University of Houston, Texas. The host for both of these is *E. coli* strain BL21(DE3)pLysS, which is chloramphenicol resistant, and the expression vector is pET26b, which confers kanamycin resistance. The inserted sequence in MB2890 is the coding region of the cyanide dihydratase gene of *B. pumilus* C1, while that in MB2784 is the coding region of the cyanide dihydratase gene of *P. stutzeri* AK61. The stop codon of the original genes prevents expression of the plasmid-encoded hexahistidine tag.

2.2 Growth conditions

B. pumilus

- Liquid medium was Luria Broth (1% tryptone (Biolab), 0.5% Yeast Extract (Biolab), 0.5% NaCl in Milli-RO water), with the addition of $MnSO_4$, usually to 25μM. Manganese was filter sterilised as a 5mM stock in Millipore water (autoclaving the solution caused precipitation).
- Solid medium was as for liquid medium, with the addition of Agar (Biolab) to 1.5% and the omission of $MnSO_4$.

Cells were maintained on LB agar plates in the absence of any antibiotic selection.

In each purification, freshly plated colonies were used to inoculate an initial culture of 100ml LB containing 25μM $MnSO_4$. This was grown for 8-12 hours. 1ml of this culture was then added to each of six 2-litre flasks each containing 250ml LB, 25μM $MnSO_4$ and grown for 12 hours. All liquid cultures were grown at 30°C with shaking. Stationary phase cells were imaged on a Nikon Diaphot phase contrast microscope fitted with a Zeiss Axiocam camera and Axiovision 2.05 software.

MB2890 and MB2784

- Liquid medium was Luria broth (prepared as above), containing 30μg/ml kanamycin sulphate for antibiotic selection.
- Solid medium was as for liquid medium, with the addition of Agar (Biolab) to 1.5%.

In each enzyme purification, freshly plated colonies were used to inoculate an initial culture of 5ml Luria broth containing kanamycin. This was grown overnight. This culture was then used to inoculate each of eight flasks each containing 100ml LB with kanamycin, in such a way as to bring the final OD_{600} to 0.015. The liquid culture occupied one tenth of the flask capacity. All liquid cultures were grown at 37°C.

2.3 Induction

Initial induction experiment

For the recombinant clones, separate batches of cells were grown either to OD_{600}=0.1 or OD_{600}=0.5. IPTG was then added to a final concentration of 1mM. Cells were incubated at 37°C with shaking and harvested at various time points. Samples of 2ml were spun down, washed twice in 10mM Tris, 50mM NaCl pH 8, resuspended in 300μl of the same buffer, and sonicated for 45 seconds in the absence of protease inhibitors. Five microlitres of the cell free extracts were then electrophoresed on an SDS PAGE gel.

General induction method

Cells were grown to OD_{600} = 0.9 at 37°C, induced by the addition of IPTG to 1mM, and harvested after 6.5 hours (MB2890) or 9.75 hours (MB2784) further incubation at 37°C.

2.4 Harvesting and lysis

Cells were washed twice in 10mM Tris, 50mM NaCl pH 8 and harvested by centrifugation for 10 minutes at 8000 rpm in a Beckman J2-21M/E centrifuge using JA 14 and JA 20 rotors. They were resuspended in the same buffer containing 1mM EDTA, 0.5μg/ml Leupeptin and 2μg/ml Aprotinin. The resuspension volume was 1/40th that of the growth medium. The suspension was placed in a universal bottle and sonicated with a 0.5 inch titanium disrupter for 2 to 3 minutes on level 7 of a Virsonic Digital 475 Ultrasonicator (Virtis, USA), with ON times of 5 seconds alternating with OFF times of 15 seconds. An ethanol/ice slurry was used as a bath to cool the sample. The lysate was then centrifuged in a JA 20 rotor at 15000 rpm for 30 minutes. The supernatant was passed through a 0.45μm Millipore filter and loaded onto the DE52 anion exchange column. All cells (MB2784, M2890, *B. pumilus*) were lysed in this manner.

2.5 Amicon ultrafiltration

Samples were concentrated in either a 50ml or 250ml Amicon cell (Amicon Corporation, Lexington, Mass.) and PM10 membrane (this has a molecular weight cut-off of approximately 10kDa). N_2 gas was used to pressurise the cell, and the solution was stirred continuously. Where appropriate the buffer was replaced by another buffer by concentrating the sample and re-diluting in the desired buffer, and repeating this procedure several times.

2.6 Dialysis

Samples were dialysed against the appropriate buffers at 4°C, in a micro-dialysis device. Spectrum® Spectra/Por® dialysis tubing was used. This has a nominal molecular weight cut-off of 12-14kDa. The tubing was not specially pre-treated.

2.7 Anion exchange chromatography

All steps from here onward were performed at 4°C. Pre-swollen Whatman® diethylaminoethyl cellulose (DE52) microgranular anion exchanger was prepared according to the manufacturer's instructions, and packed onto a 55×1.6cm column.

The column was equilibrated with 10mM Tris, 50mM NaCl pH 8. Cell-free extract was loaded using a peristaltic pump, after which the column was flushed with at least one column volume of equilibration buffer.

Elution of B. pumilus *and MB2890 enzymes*

The column was further flushed with 10mM Tris, 250mM NaCl pH 8 until the OD_{280} had decreased to less than 0.1. A linear salt gradient from 250 to 360mM NaCl in 10mM Tris pH 8 was then applied over 1.8 column volumes. Fractions were collected with an Isco Foxy® Jr. fraction collector at 3 minute intervals at a flow rate of 2 ml/min (*B. pumilus*), or at 4 minute intervals at a flow rate of 1.2 ml/min (MB2890). The active fractions were pooled and concentrated to 1ml (*B. pumilus*) or 1.2 ml (MB2890) by ultrafiltration. The used DE52 matrix was washed with 10mM Tris, 1M NaCl, 0.1% sodium azide pH 8 and stored at 4°C.

Pilot experiment to determine the elution point of MB2784 enzyme

In order to determine the appropriate salt gradient for elution of MB2784 enzyme, 1ml of freshly prepared cell free extract was adsorbed for 30 minutes onto a miniature DE52 column packed in a syringe barrel and stoppered with glass wool, with a bed volume of 1.5ml. This was exhaustively flushed with 10mM Tris, 50mM NaCl pH 8, after which a 10mM Tris pH 8 step gradient was applied with successive sodium chloride concentrations of 50mM, 150mM, 250mM, 360mM, and 450mM. At each salt concentration, three successive fractions (of volumes 2, 4 and 6ml, respectively) were collected. These fractions were assayed for activity.

Elution of MB2784 enzyme

The column was flushed with 10mM Tris, 50mM NaCl pH 8 until the OD_{280} had decreased to less than 0.1. A linear salt gradient from 50 to 250mM NaCl in 10mM Tris pH 8 was then applied over a total of 3.6 column volumes. An initial flow rate of 0.57 ml/min was used. This was increased to 0.95 ml/min at elution volume of 364ml (=3.3 column volumes). The active fractions were pooled and concentrated to 0.8ml by ultrafiltration.

2.8 Gel filtration chromatography

A pre-packed, 60×1.6cm Sephacryl 300 HR column was obtained from AP Biotech. This matrix had a nominal molecular-weight cut-off of 1.5 MDa. The column was partially flushed with water, and then equilibrated with 120 ml of 10mM Tris, 360mM NaCl pH 8. All solutions used for this column were filtered and degassed. The concentrated, partially purified enzyme was applied to the column. Elution was by gravity flow, at a rate of 90µl/min. *B. pumilus* fractions were collected at 6 minute intervals. Fractions of MB2784 and MB2890 were collected at 24 minute intervals. Active fractions were pooled and Amicon concentrated to 200µl. After purification of *B. pumilus* enzyme, the buffer containing the concentrated enzyme was exchanged, by repeated ultrafiltration, into 10mM triethanolamine (TEA), 50mM NaCl pH 8. The procedure adopted was different for the *P. stutzeri* enzyme. After gel filtration chromatography, the active fractions were concentrated to 0.5ml by ultrafiltration, and then diluted to 12ml in 10mM citrate, 360mM NaCl pH 5.4. This was concentrated by ultrafiltration to 1ml and centrifuged at 4°C for one hour. The supernatant was loaded onto the gel filtration column that had been pre-equilibrated with 10mM citrate, 360mM NaCl pH 5.4. Active fractions were pooled and concentrated without buffer exchange. The column was partially flushed with water, and then fully flushed with 20% absolute ethanol after use.

2.9 Continuous absorbance monitoring

The protein concentration of column eluates was continuously monitored by digitally coupling a Philips PU 8620 UV/VIS/NIR Spectrophotometer (with a flow-through cell) to a portable PC1600 microcomputer, on which data points were continuously plotted and could later be downloaded onto a conventional PC. This system was devised and implemented by James Duncan, Electron Microscope Unit, University of Cape Town.

2.10 Measurement of activity

Cyanide degradation was assayed according to the method of Fisher and Brown, 1952. Twenty microlitres of the test sample was added to 20µl of 25mM KCN, 125mM Tris pH 8 in an eppendorf tube and incubated at 37°C for 30 minutes. To this, 80µl of picric acid mix was added (this consisted of freshly mixed, equal volumes of

1% picric acid and 0.5M Na_2CO_3). The tube was clipped shut and boiled for 5 minutes. Once cooled, the sample was brought to 1ml with deionised water and its absorbance measured at 520nm. Measurements in each assay were normalised with respect to a sample prepared in duplicate with cyanide but no enzyme. The cyanide stock of 100mM KCN in 500mM Tris pH 8 was kept in a tightly sealed container at 4°C. Tips and eppendorfs were decontaminated in 3.5 % sodium hypochlorite. Liquid picric acid/cyanide complex waste was treated as cyanide waste and disposed of accordingly by Waste-Tech.

One unit was defined to be the amount of enzyme that degrades 1µmole of cyanide in one minute under the conditions described above. Activity is quoted in these units in Table 3.5. Elsewhere the activity is expressed in arbitrary units.

2.11 Protein Assay

Protein concentrations of the cell-free extract, the anion exchange concentrate, and the gel filtration concentrate were measured using the Bradford assay with bovine serum albumin as a standard (Bradford, 1976).

2.12 SDS PAGE

For SDS polyacrylamide gel electrophoresis a Bio-Rad Protean II xi 20cm cell was used. Sample application buffer was stored at 4°C as a five-times stock, consisting of 60mM Tris-HCl pH 6.8, 25% glycerol, 2% SDS, 14.4 mM 2-mercaptoethanol and 0.1% bromophenol blue. Gels and buffers were prepared according to the method developed by Laemmli, 1970 and described in Bollag and Edelstein, 1991, except that the mass:mass ratio of acrylamide to bisacrylamide was 200:1. Purification gels contained an acrylamide concentration of 15%, gels used to analyse the induction experiment contained 12% acrylamide and gels in the crosslinking experiments contained 10% acrylamide. Samples were boiled for 2 minutes at 95°C prior to loading on the gel.

A constant current of 16mA per gel was used while the samples migrated through the stacking gel. Thereafter, a constant voltage of 180V was applied.

B Trypsin digest and mass spectrometry of native cyanide dihydratase from *B. pumilus*

2.13 Trypsin digestion

Cyanide dihydratase was purified from *Bacillus pumilus* C1 and run on SDS PAGE, comprising 12% acrylamide, 0.06% bisacrylamide, together with molecular weight markers that included carbonic anhydrase. The reagents used for the staining and destaining solutions were of analytical grade, to avoid unwanted reactions with the proteins. Bands were excised from the gel as slices of approximately $15mm^3$ in volume and prepared for trypsin digestion. These included the single band of carbonic anhydrase and each of the three bands of cyanide dihydratase. A blank piece of gel was excised as a control. In order to remove the stain several washing steps were carried out. Following a protocol obtained from the website http://info.med.yale.edu/wmkeck/geldig3.htm, each gel piece was successively washed in 50% acetonitrile (5 minutes), 50% acetonitrile, 50mM NH_4HCO_3 (30 minutes) and 50% acetonitrile, 10mM NH_4HCO_3 (30 minutes). The sample was vacuum spun to complete dryness to remove the acetonitrile, then incubated in 15µl of 6.6µg/ml trypsin in 10mM NH_4HCO_3 (10 minutes), mixed with 20µl of 10mM NH_4HCO_3 and incubated at 37°C (several hours or overnight).

2.14 MALDI-TOF spectrometry

One microlitre of the in-gel trypsin digest was extracted by centrifuging the gel slice in an eppendorf tube. It was mixed with an equal volume of a standard solution of the matrix α-cyano-4-hydroxycinnamic acid (CHCA, MW 189.17)) or sinapinic acid (MW 224.21), and placed on a sample grid to dry. This was then placed in a calibrated Perseptive Biosystems DE-PRO MALDI-TOF spectrometer for mass measurements.

2.15 Analysis of spectra

Trypsin fragment sizes were predicted from known sequences. The programme GPMAW, Version 4.1, was used to perform virtual trypsin/chymotrypsin digests of the sequences of interest.

C Crosslinking of *B. pumilus* cyanide dihydratase

2.16 Initial crosslinking with formaldehyde and glutaraldehyde

Cyanide dihydratase was purified from *B. pumilus* C1. In the first experiment, freshly prepared formaldehyde and EM grade glutaraldehyde were diluted as appropriate in 10mM triethanolamine, 50mM NaCl pH 8. A volume of 0.5µl of diluted formaldehyde or glutaraldehyde was added to 2µl of purified enzyme to give a final protein concentration of 4.8mg/ml. After a 15 hour incubation at room temperature, the reaction was stopped by the addition of 5.5µl of 0.5 M glycine. The sample was added to 2µl of sample application buffer, boiled for 2 minutes and loaded onto a 10% SDS PAGE gel.

2.17 Further crosslinking with glutaraldehyde

In the second experiment, 1µl of purified enzyme was added to 30µl of glutaradehyde at concentrations ranging from 0 to 0.2% in 10mM TEA, 50mM NaCl pH 8, to give a final protein concentration of 0.2mg/ml. Samples were incubated at room temperature for 75 minutes, and the reaction was stopped by the addition of 6µl of 0.5M glycine. After the addition of 9µl of sample application buffer, the samples were boiled for 2 minutes and loaded onto a 10% SDS PAGE gel.

D Negative staining, electron microscopy and three-dimensional reconstruction of the enzymes

2.18 Preparation of carbon-coated copper grids

To prepare carbon-coated copper grids, carbon was deposited on the surface of a freshly cleaved piece of mica using an electron beam evaporator (Balzers Union). The carbon was floated onto the surface of distilled water and then transferred onto the grids. The carbon-coated grids were dried under a tungsten lamp.

2.19 Preparation of negatively stained enzyme particles

The purified enzyme preparation was diluted in a specific buffer. The following table summarises the buffers used, the dilution factors and the final protein concentrations.

Source of enzyme	Original buffer	Diluting buffer	Dilution factor	Final protein concentration
Native *B.pumilus*	10mM TEA, 50mM NaCl, pH 8	10mM TEA, 50mM NaCl, pH 8	1:40	0.15 mg/ml
MB2890	10mM TEA 50mM NaCl, pH 8	10mM MES, 50mM NaCl, pH 6	1:40	0.14 mg/ml
MB2784	10mM citrate, 360mM NaCl, pH 5.4	10mM TEA, 50mM NaCl, pH 8	1:40	0.32 mg/ml

One drop of the diluted enzyme was placed on Parafilm and a carbon-coated grid was floated on the drop for 10 minutes. The grid was blotted, and placed onto a drop of 2% uranyl acetate (unbuffered) for 3 minutes. The grid was then blotted and air-dried.

2.20 Electron microscopy

The Jeol 1200CX microscope was aligned according to standard practice, and the grid placed in the eucentric position (this was confirmed by tilting the specimen holder). The microscope was stigmated at high magnification (150 000 times). Micrographs were taken at 50 000 times magnification, with spot size 4, using minimum dose technique to minimise exposure of molecules to the electron beam. The level of underfocus was 0-224nm throughout, and was consistent for each set of micrographs, with the exception of MB2890 where some were at an underfocus of 224nm and others at 112nm.

2.21 Scanning and reconstruction

The micrographs were developed and then scanned on an Ilford Leafscan^{TM} 45. The resolution of the scans was 2540dpi which corresponds to 2Å on the actual specimen.

Image processing was performed on a UP2000 computer which had two 667MHz Alpha Processors (Alpha Processor Inc.) and 512MB of RAM. The programme SPIDER (Frank *et* al., 1996a) was used for calculations and to generate processed images and models. (Details on SPIDER can be found at http://www.wadsworth.org/spider_doc/spider/docs/spider.html). The programme WEB was used to view the images and two-dimensional projections of the models (Frank *et* al., 1996a). MODEL VIEWER (written by Dennis Burford, Department of Computer Science, University of Cape Town) was used to interactively view the models.

The raw files were converted to *mrc* format. Adjacent pixels were averaged using the programme *label*, to reduce the resolution by a factor of two in both dimensions. Thus 1 pixel corresponds to 4Å. Each micrograph was viewed in the programme Ximdisp (Crowther *et* al., 1996) and individual particles were selected. The coordinates of these particles were written to a separate file on which basis a 64×64 pixel box was excised around each coordinate to generate an image file. This was later increased to 80×80 pixels.

Each image was filtered by performing a fourier transform (FT), followed by high- and low-pass fourier filters (FF) to partially exclude noise as well as low frequency variation within the image. The Gaussian used for the high frequency threshold was set so as to attenuate the signal by 50% at a spatial frequency corresponding to 15Å in real-space.

The images were classified into 84 classes using the method of Penczek et al., 1996. Membership of these classes was refined by several cycles of multireference alignment (Joyeux and Penczek, 2002) and the exclusion of poorly matching images. The angular relationship of the most populous classes was determined by a common-lines based method (Penczek et al., 1996). A starting model was created by the iterative 3-D reconstruction method of Penczek et al., 1992 according to these angular relationships. Projections of the starting model were then made using a set of 84 quasi-equivalently spaced projection directions, spanning an entire hemisphere with a step size of 15° to produce a set of reference images. Multiple cycles of refinement

were performed, comprising: 1. multireference alignment, 2. averaging the sets of image classes thus determined to match each projection, 3. iterative 3-D reconstruction (Penczek et al., 1992) of the class averages to create a model and 4. re-projecting this model to create the next generation of reference images. In the 3D-reconstruction, a radius of 26 pixels was used for back-projecting in early refinements of the model. This was later increased to 38 pixels.

After many cycles it became apparent by visual inspection that the structure had a global two-fold axis. The orientation of the two-fold axis was determined and the model was relocated in the box so that the two-fold axis was located along the x-axis. In subsequent cycles of refinement two-fold averaging was performed. The procedure was terminated when no further changes in the map were visible.

The resolution was determined by dividing the images into two equally populated sets, reconstructing separately and determining the Differential Phase Residual and Fourier shell correlation (Harauz and van Heel, 1986) in shells of one pixel thickness.

In the final structure, it was necessary to determine the appropriate threshold density with which to contour the surface of the model. The number of subunits was counted by increasing the contour level until the subunits could be unambiguously identified. The theoretical volume of the protein was estimated by multiplying the number of subunits by the molecular weight of each subunit. A value of 0.73 daltons/$(Å)^3$ was used as average protein density (Richards, 1974). The volume was converted into voxels by dividing by the volume of a voxel, which is 4^3=64. The programme MODEL VIEWER allowed direct calculation of the volume, in voxels, for any contour level and so the desired contour could be readily found.

E Structural transition in *B. pumilus* cyanide dihydratase

2.22 Removal of salt and buffer

Purified samples of recombinant and native *B. pumilus* enzymes at concentrations of 13mg/ml and 6mg/ml respectively were dialysed against a 10 000-fold excess of distilled water overnight at 4°C, diluted in distilled water or 10mM citrate, 50mM NaCl pH 5.4 and examined by negative stain electron microscopy as described above. Concentrations of enzyme used for negative staining were 150µg/ml (native enzyme in water), 650 µg/ml (recombinant enzyme in water) and 20 µg/ml (recombinant enzyme in citrate pH 5.4).

2.23 Effects of NaCl concentration and pH

The *B. pumilus* native enzyme, prepared in 10mM TEA, 50mM NaCl, pH 8, was diluted either 20- or 40-fold in each of the following buffers: (a) 20mM glycine, 25mM NaCl pH 2 (b) 20mM glycine, 25mM NaCl pH 3 (c) 20mM sodium acetate 25mM NaCl pH 4.6 (d) 20mM sodium acetate, 25mM NaCl pH 5.0 (e) 20mM sodium citrate, 25mM NaCl pH 5.4 (f) 10mM sodium citrate, 500mM NaCl pH 5.4 (g) 20mM MES, 25mM NaCl pH 6.0 (h) 10mM TEA, 25mM NaCl pH 8. The specimen was then prepared for electron microscopy as described above.

For molecular size estimation, purified, frozen and re-thawed recombinant *B. pumilus* enzyme in 10mM TEA, 50mM NaCl pH 8, was diluted 25-fold in 10mM citrate, 360mM NaCl pH 5.4 and reconcentrated by ultrafiltration to 0.9ml. This was then run on the Sephacryl 300HR gel filtration column in 10mM citrate, 360mM NaCl pH 5.4. Fractions were collected and assayed, and active fractions were pooled and concentrated. In a separate experiment, the purified recombinant enzyme of *P. stutzeri* was diluted in elution buffer (10mM citrate, 50mM NaCl pH 5.4), negatively stained and examined by electron microscopy.

Chapter 3. Purification of *B. pumilus* and *P. stutzeri* cyanide dihydratases

In this chapter purifications of the cyanide dihydratases of *P. stutzeri* AK61 and *B. pumilus* C1 are described.

Recall from Chapter 2 that MB2890 is an *E. coli* clone bearing an expression vector for cyanide dihydratase of *B. pumilus*, while MB2784 bears an expression vector for cyanide dihydratase of *P. stutzeri*. Cyanide dihydratase purified directly from *Bacillus pumilus* C1 will be referred to as the native *B. pumilus* enzyme (as a matter of convenience). This convention will also be used in later chapters.

A Optimising the purification procedures

3.1 Optimising growth and inducing conditions for recombinant strains MB2890 and MB2784

In working with *E. coli* strain BL21(DE3)pLysS, it was found that chloramphenicol at the recommended concentration of 30μg/ml reduced the cell density by approximately 40% at stationary phase (results not shown). Therefore kanamycin was used as the sole antibiotic for all work with this strain.

The respective cyanide dihydratase-expressing cells were induced with 1mM IPTG either at $OD_{600} \approx 0.1$, or $OD_{600} = 0.5$. The progression of induction was assessed by harvesting cells at various time points and analysing cell free extracts by SDS PAGE. Figure 3.1(a) shows that MB2784 cells produced an inducible band at 37.6 kDa and a subsidiary band at 36.3 kDa. Similarly, MB2890 cells produced a predominant, inducible band at 41.4 kDa, and subsidiary bands at 39.8 and 38.6 kDa (Figure 3.1(b)). These compare (and contrast) with the theoretical sizes of 37.383 kDa and 37.329 kDa for the *P. stutzeri* and *B. pumilus* enzymes, respectively. Note that the pattern of induced bands in MB2890 closely resembles the pattern of bands in the

purified, native enzyme (Fig 3.1(b), lane 1). Induction of the enzyme in MB2784 was strongest from 6.6 hours onwards, with addition of IPTG at OD_{600} = 0.49. Induction of the enzyme in MB2890 was strongest from 5.9 hours onwards, with addition of IPTG at OD_{600} = 0.51. From these data a reasonable choice of inducing conditions was made for later use.

3.2 Optimising growth and lysis conditions for native *B. pumilus* C1

Gram-stained *B. pumilus* C1 cells are shown in Figure 3.2(c). Initial purifications yielded insufficient quantities of enzyme to be detected by the picric acid assay. The production and detection of enzyme was improved in two ways.

Manganese ions are essential for the induction of cyanide dihydratase activity in *B. pumilus* C1 cells, and also affect growth of the cells. Therefore, the optimal concentration of manganese was investigated. Cells were grown in Luria broth with exogenous manganese ranging from 0.25 to 25μM in concentration. Cells grown at 0.25μM were 2- to 3- fold less dense than cells grown at higher concentrations of manganese (results not shown). Figure 3.2(a) shows that the enzyme production (per volume of growth medium) increased substantially with increasing manganese concentration up to $[Mn^{2+}]$=25μM. Activity per dry cell weight was not determined.

In early experiments various protease inhibitors were used to protect against degradation of the enzyme. An experiment was carried out to test the effects of these protease inhibitors on enzyme activity. PMSF, EDTA and aprotinin were added individually or in combination to cell-free extracts of *B. pumilus* which were assayed for activity. As shown in Figure 3.2(b), EDTA and aprotinin have no effect, whereas PMSF strongly inhibits the enzyme. Leupeptin was not tested but in later purification experiments it did not appear to adversely affect yields.

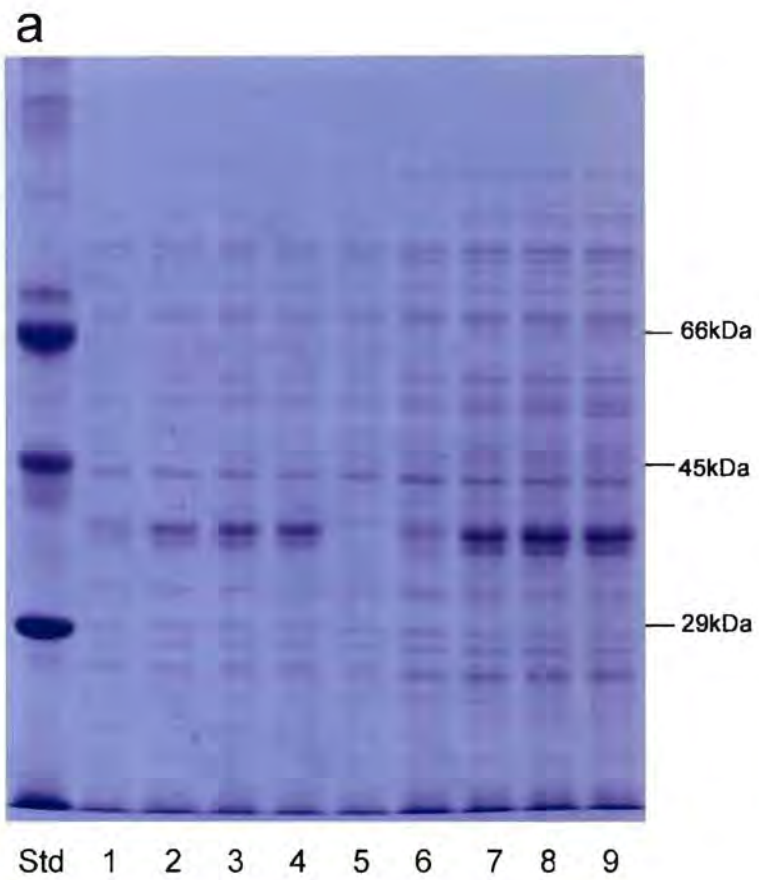

Fig 3.1. 12% SDS PAGE of recombinant cyanide dihydratase induced in MB2784 and MB2890 (bearing the *P. stutzeri* and *B. pumilus* clones, respectively).
Each sample was derived from an equal volume of cell culture. Molecular weight markers: Carbonic anhydrase, Ovalbumin, Bovine serum albumin

(a) Samples of MB2784 cells taken at various times after induction with IPTG. Lanes 1-4, cells treated at OD(600) = 0.08; lanes 5-9, cells treated at OD(600) = 0.49. Time after induction (hours):

lane	time	lane	time
1	1.5	5	0
2	3.3	6	1.5
3	6.7	7	4.4
4	8.9	8	6.6
		9	8.4

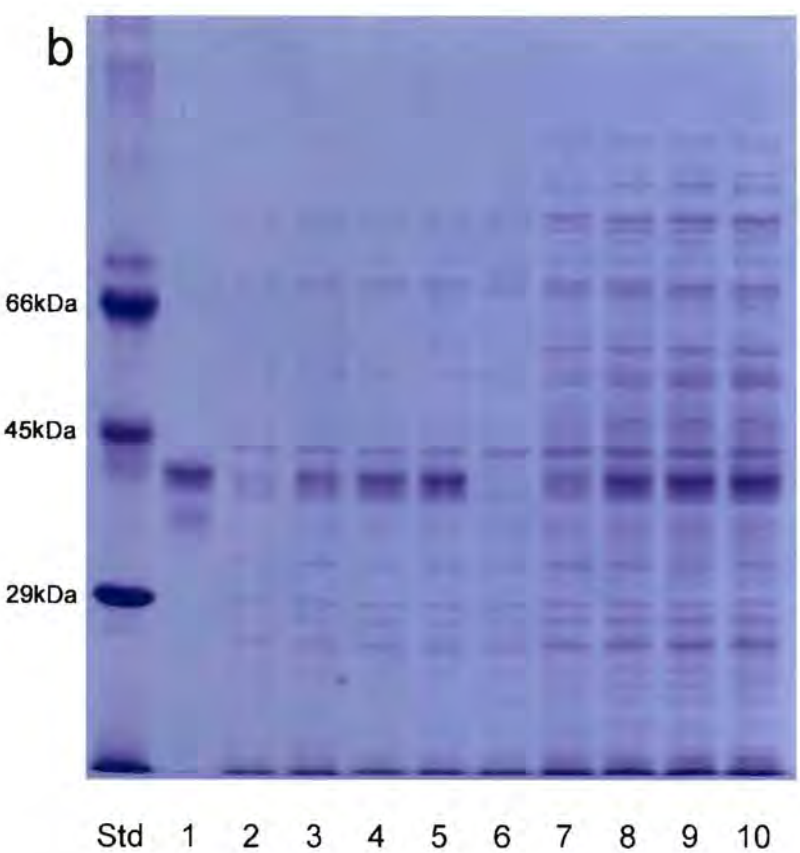

(b) Samples of MB2890 cells taken at various times after induction with IPTG. Lane 1, enzyme purified from native *B. pumilus* C1; lanes 2-5, MB2890 cells treated at OD(600) = 0.16; lanes 6-10, cells treated at OD(600) = 0.51. Time after induction (hours):

lane	time	lane	time
2	1.8	6	0
3	4.1	7	1.9
4	6.3	8	4.1
5	8.1	9	5.9
		10	8.0

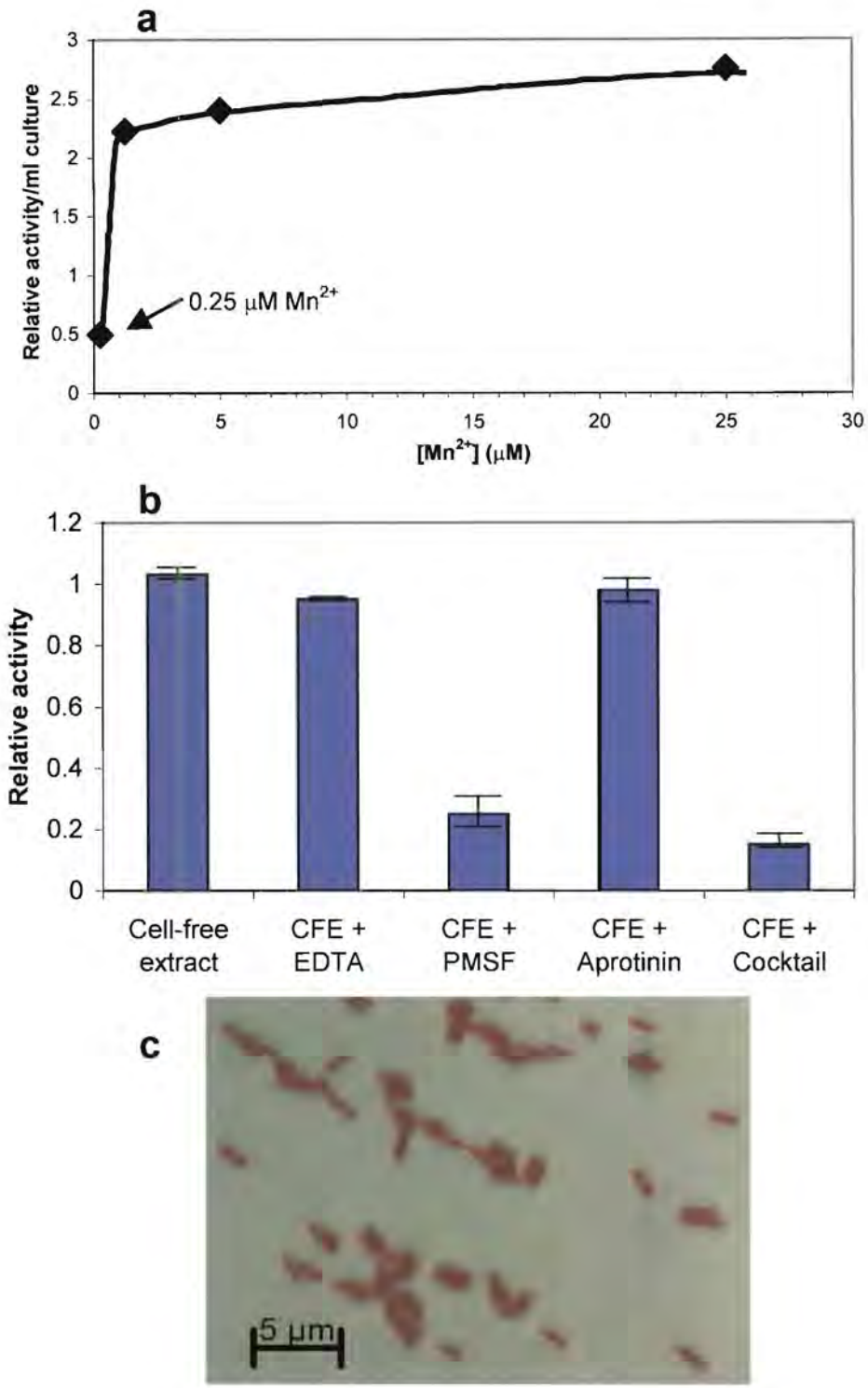

Figure 3.2. (a) Cyanide degrading activities of cell-extracts of cultures of *B. pumilus* C1 grown to stationary phase in various concentrations of manganese. **(b)** Activities of cell-free extract incubated with 1mM EDTA, 1mM PMSF, 2mg/ml Aprotinin or all of these (cocktail). **(c)** Gram-stained *B. pumilus* C1 cells grown to stationary phase. Relative activity in (a) and (b) represents arbitrarily normalised activity. Data points are in duplicate.

3.3 Linearity of the protein and cyanide assays

Cyanide assay

A standard curve was determined for cyanide, as shown in Figure 3.3(a). This was used to determine amounts of cyanide degraded by the enzyme from the change in absorbance at 520nm.

Protein assay

A standard curve was generated for the Bradford assay, for each experiment. Shown in Figure 3.3(b) is the curve used to determine protein concentrations of partially purified cyanide dihydratase.

Linearity of activity assay

An experiment was carried out to determine the relationship between the amount of purified enzyme (as determined by the Bradford assay) and the amount of cyanide degraded under the standard assay conditions. Figure 3.3(c) and (d) show that this relationship was approximately linear in the case of *P. stutzeri*, whereas in the case of *B. pumilus* a strong deviation (towards lower activity) occurred with small amounts of enzyme. One possible explanation for the latter is that the enzyme may be inhibited at the high concentration (12.5mM) of cyanide used. In this case the catalytic rate would increase over the course of the incubation. Further experiments would be necessary to test this.

3.4 Optimising salt gradient chromatography of the *P. stutzeri* enzyme

The binding of cyanide dihydratase of MB2784 to the DE52 anion exchange matrix was tested. MB2784 cells were induced, harvested, lysed and adsorbed onto a miniature column of bed volume 1.5ml. A series of step gradients were applied, ranging from 50mM to 450mM NaCl. The enzyme eluted completely in the range 50-250mM NaCl (Figure 3.4).

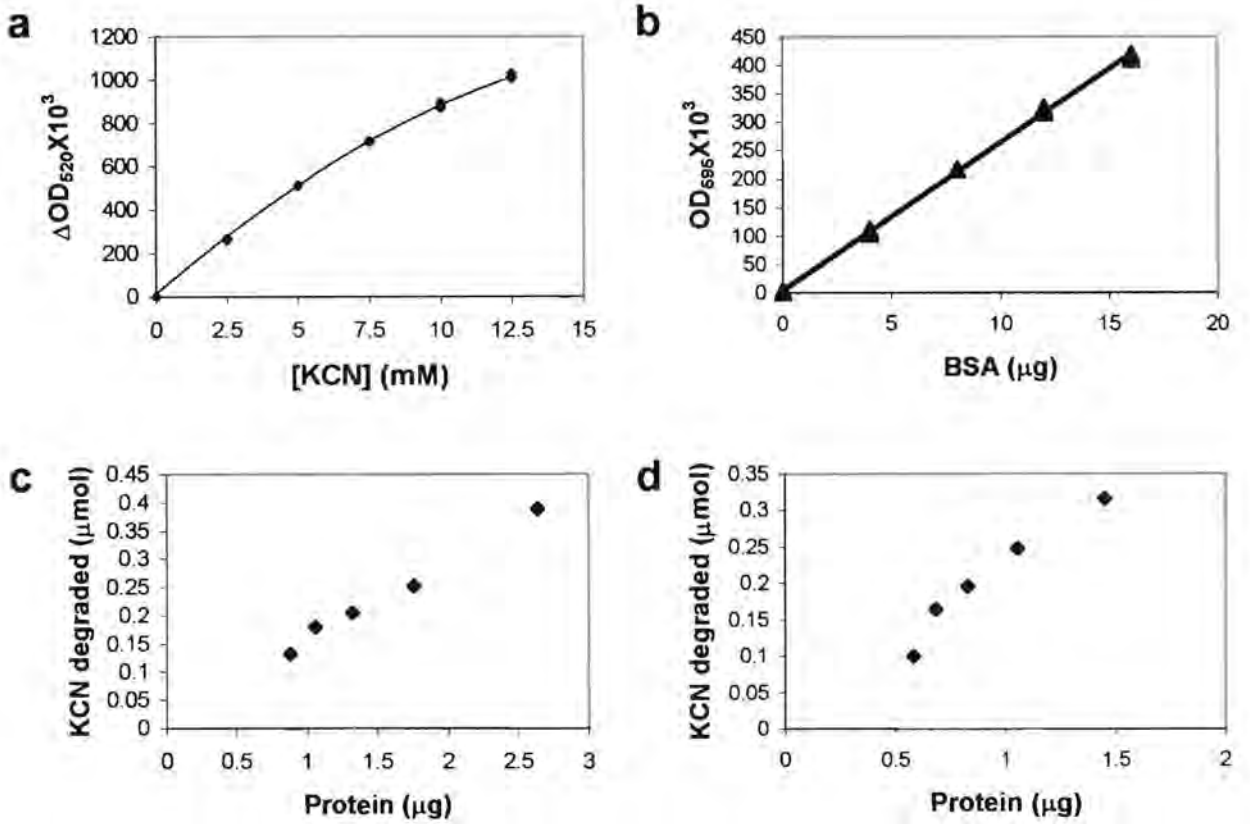

Figure 3.3. Standard curves for **(a)** the cyanide assay and **(b)** the Bradford assay. Correlation between protein concentration and KCN degraded in 30 minutes for purified **(c)** *P. stutzeri* and **(d)** **(d)** *B. pumilus* cyanide dihydratase. Assays in (b) were performed in duplicate; all other measurements were in triplicate.

B Purification of the enzymes

3.5 Purity

Purification parameters for recombinant *P. stutzeri* and *B. pumilus* enzymes and native *B. pumilus* enzyme are presented in Table 3.5. The yield of each purified recombinant enzyme was 10- to 15- fold greater than that of the native enzyme. The specific activities of the purified enzymes are lower than the values reported in the literature, which are 88 units/mg for the *B. pumilus* enzyme (Meyers, 1993a) and 54.6 units/mg for the *P. stutzeri* enzyme (Watanabe *et al.*, 1998a). This may have to do with substrate inhibition at the high concentration of 12.5mM cyanide used in the current study. Elution profiles of chromatographic steps in the purification of each of the three enzymes are shown in Figures 3.6, 3.7 and 3.8. In the final gel filtration run of each enzyme, the activity peak coincides with a protein peak, both of which are symmetrical (the exception being deviation from symmetry on the trailing edge of the native enzyme profile). These data suggested that the enzyme preparations were homogeneous.

SDS PAGE gel electrophoresis (Figures 3.9 (a) and 3.10(e)), revealed characteristic dominant bands. The pattern of bands of the *B. pumilus* enzyme consists of two sets of doublets. The dominant upper pair is well-resolved in Figure 3.9 (a) lane 12, and the lower pair in Figure 3.10 (c). This banding pattern was also observed by Meyers (1993a). In *P. stutzeri*, three bands are observed - a dominant lower doublet and single band above this (Figure 3.9 (a) lane 5). These bands may belong to the enzyme or they may be copurified, unrelated polypeptides. Evidence will be presented in Chapters 4 and 5 showing that these bands are part of the enzyme (at least) for the *B. pumilus* cyanide dihydratase.

3.6 Native and recombinant *B. pumilus* enzymes

The purified native and recombinant proteins give the same banding pattern on SDS PAGE (Figure 3.9 (a) lanes 11 and 12). However, on gel filtration the native enzyme elutes at a volume of 46.5ml and the recombinant enzyme at a volume of 48ml. The significance of these observations is discussed below.

3.7 Tracking a contaminant of the native *B. pumilus* enzyme

A contaminating protein of subunit molecular weight 66 kDa was observed during the purification of the cyanide dihydratase from *B. pumilus*. To investigate whether this protein simply co-eluted with the enzyme or was bound to it, successive fractions from each of the chromatographic steps were collected and analysed by SDS PAGE. The intensity of the contaminating band reached its maximum at a slightly lesser elution volume than that of the cyanide dihydratase, both with the ion exchange and gel filtration runs (Figure 3.10 (a), (b), (c) and (d)). This indicates that the contaminating protein does not bind the cyanide dihydratase. It is possible that this protein is a homologue of the chaperonin GroEL, as molecules resembling GroEL were regularly seen on micrographs of purified native *B. pumilus* cyanide dihydratase, and these were always observed to be spatially separated from the cyanide dihydratase molecules.

3.8 Sodium citrate precipitation

The first gel filtration profile of the *P. stutzeri* enzyme indicates a significant degree of impurity. This is confirmed by the SDS PAGE gel of fractions containing enzyme activity (Figure 3.9 (b)). Quite fortuitously, the buffer exchange from Tris pH 8 to sodium citrate pH 5.4 immediately following this purification step resulted in precipitation of a large amount of protein that did not include the cyanide dihydratase. As a result, the product of this step was seen by gel filtration to be extremely pure (Figure 3.6 (c)) and SDS PAGE (Figure 3.9 (a) lane 3).

3.9 Conclusions

Cyanide dihydratases of *P. stutzeri* AK61 and *B. pumilus* C1 were purified to a high degree of homogeneity. Induction of cyanide dihydratase activity in *B. pumilus* cells was found to be approximately 5-fold higher at 25μM Mn^{2+} than at the concentration of 0.25μM used by Meyers *et al.*, 1993a. The protease inhibitor PMSF was found to inhibit cyanide dihydratase activity in the cell free extract of induced *B. pumilus* cells. The purification of *P. stutzeri* cyanide dihydratase was improved by adding sodium citrate to selectively precipitate contaminants.

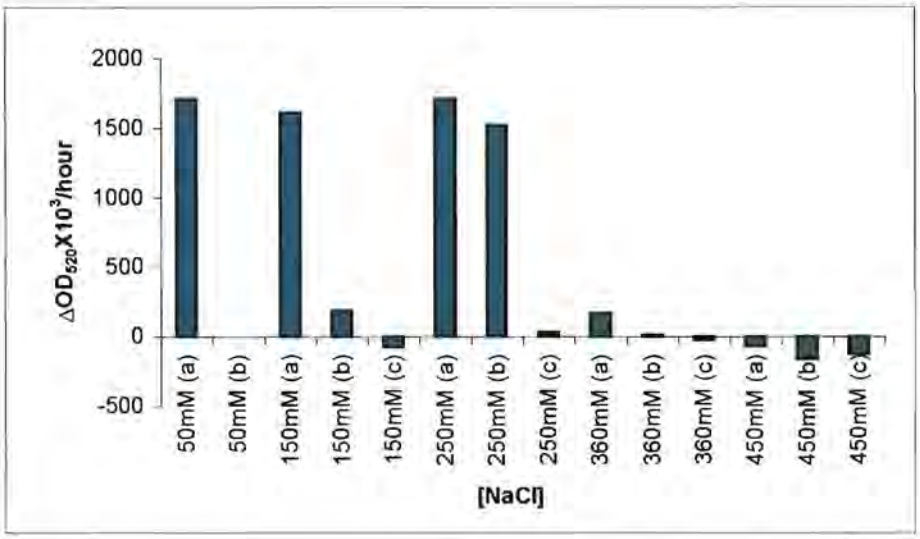

Figure 3.4. Activities of fractions from a miniature DE52 column loaded with cell-free extract of MB2784 cells. NaCl step gradients were applied at the concentrations indicated above. In each case (a), (b) and (c) are successive fractions.

Table 3.5 Purification tables for **(a)** recombinant *P. stutzeri*, **(b)** recombinant *B. pumilus* and **(c)** native *B. pumilus* cyanide dihydratase. Values in these tables are based on triplicate readings and were converted using standard curves.

a

P. stutzeri (rec.)	Volume (ml)	Concentration (mg/ml)	Total protein (mg)	Total activity (units)	Specific activity (units/mg)	Yield (%)	Purification Factor
Cell-free extract	24	19.5	468	1460	3.10	100	1.00
Anion exchange	0.79	106	84.0	445	5.30	30.5	1.70
Gel filtration 1[1]	1.0	24.4	24.4	210	8.70	14.4	2.76
Gel filtration 2	1.0	13.2	13.2	108	8.10	7.30	2.59

b

B. pumilus (rec.)	Volume (ml)	Concentration (mg/ml)	Total protein (mg)	Total activity (units)	Specific activity (units/mg)	Yield (%)	Purification Factor
Cell-free extract	14.5	29.4	427	790	1.85	100	1.00
Anion exchange	1.20	15.0	18.0	245	13.6	31.0	7.37
Gel filtration	1.47	7.30	10.7	160	15.0	13.1	8.15

c

B. pumilus (nat.)	Volume (ml)	Concentration (mg/ml)	Total protein (mg)	Total activity (units)	Specific activity (units/mg)	Yield (%)	Purification Factor
Cell-free extract	28.0	17.3	483	95.0	0.200	100	1.00
Anion exchange	0.55	not determined	not determined	36.0	not determined	38.0	not determined
Gel filtration	0.18	6.60	1.20	10.5	8.80	11.0	44.0

[1]This step includes buffer exchange.

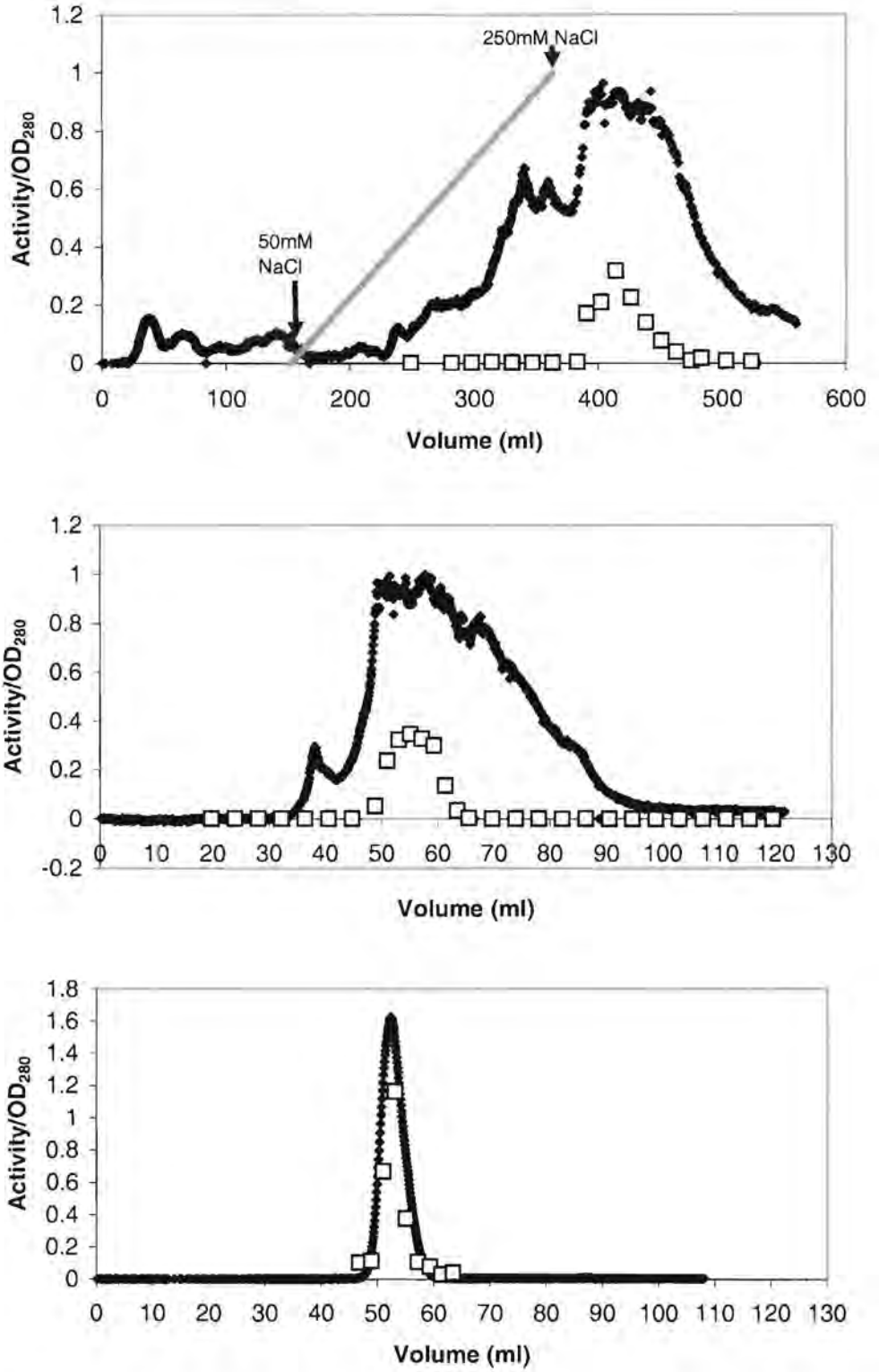

Figure 3.6. Elution profiles of recombinant *P.stutzeri* cyanide dihydratase. **(a)** DE52 anion exchange; **(b)** Gel filtration at pH 8; **(c)** Gel filtration at pH 5.4. OD_{280}, black diamonds; relative activity, open squares; salt gradient, grey line.

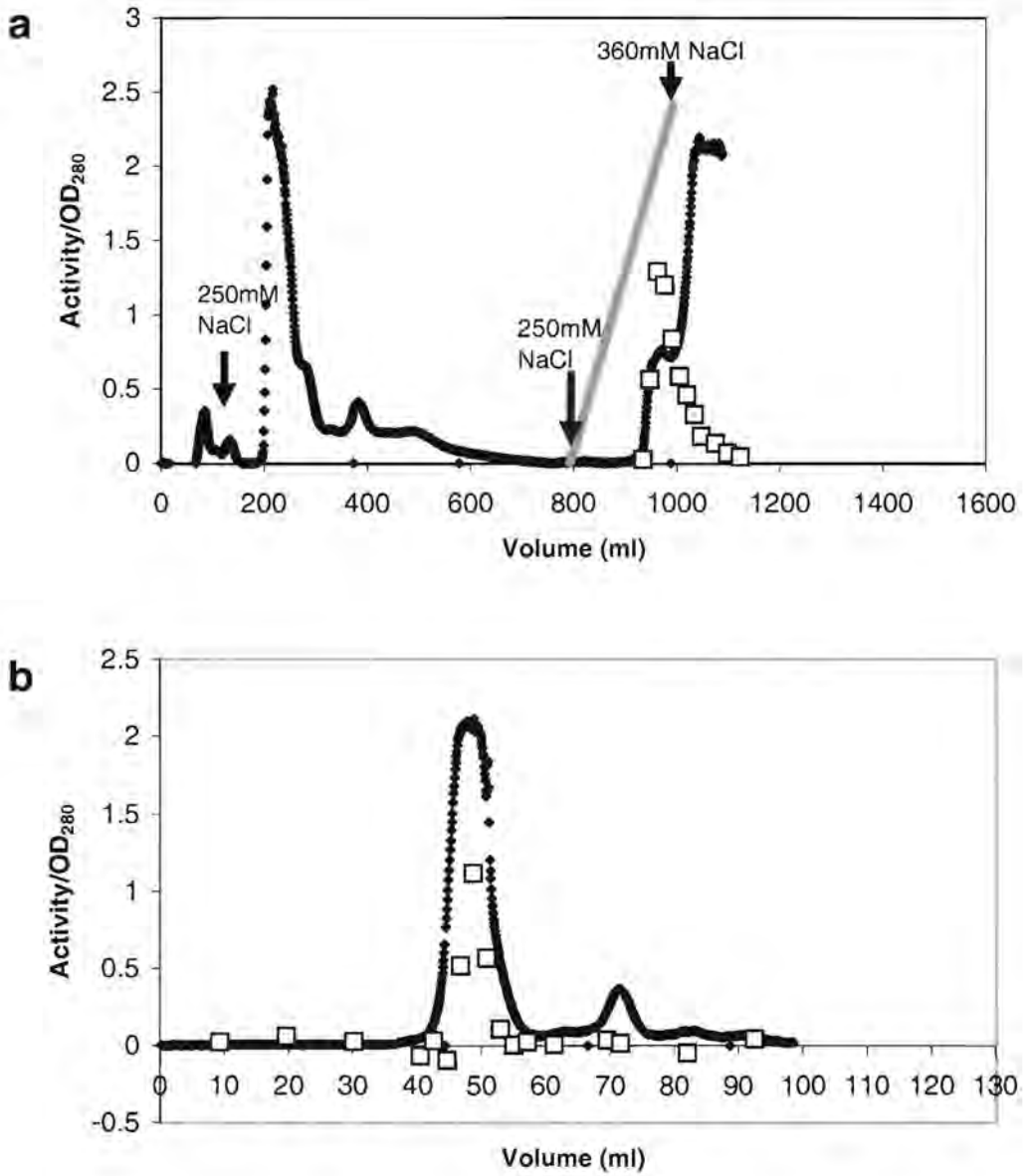

Figure 3.7. Elution profiles of recombinant *B.pumilus* cyanide dihydratase. **(a)** DE52 anion exchange; **(b)** Gel filtration, pH 8. OD_{280}, black diamonds; relative activity, open squares; salt gradient, grey line.

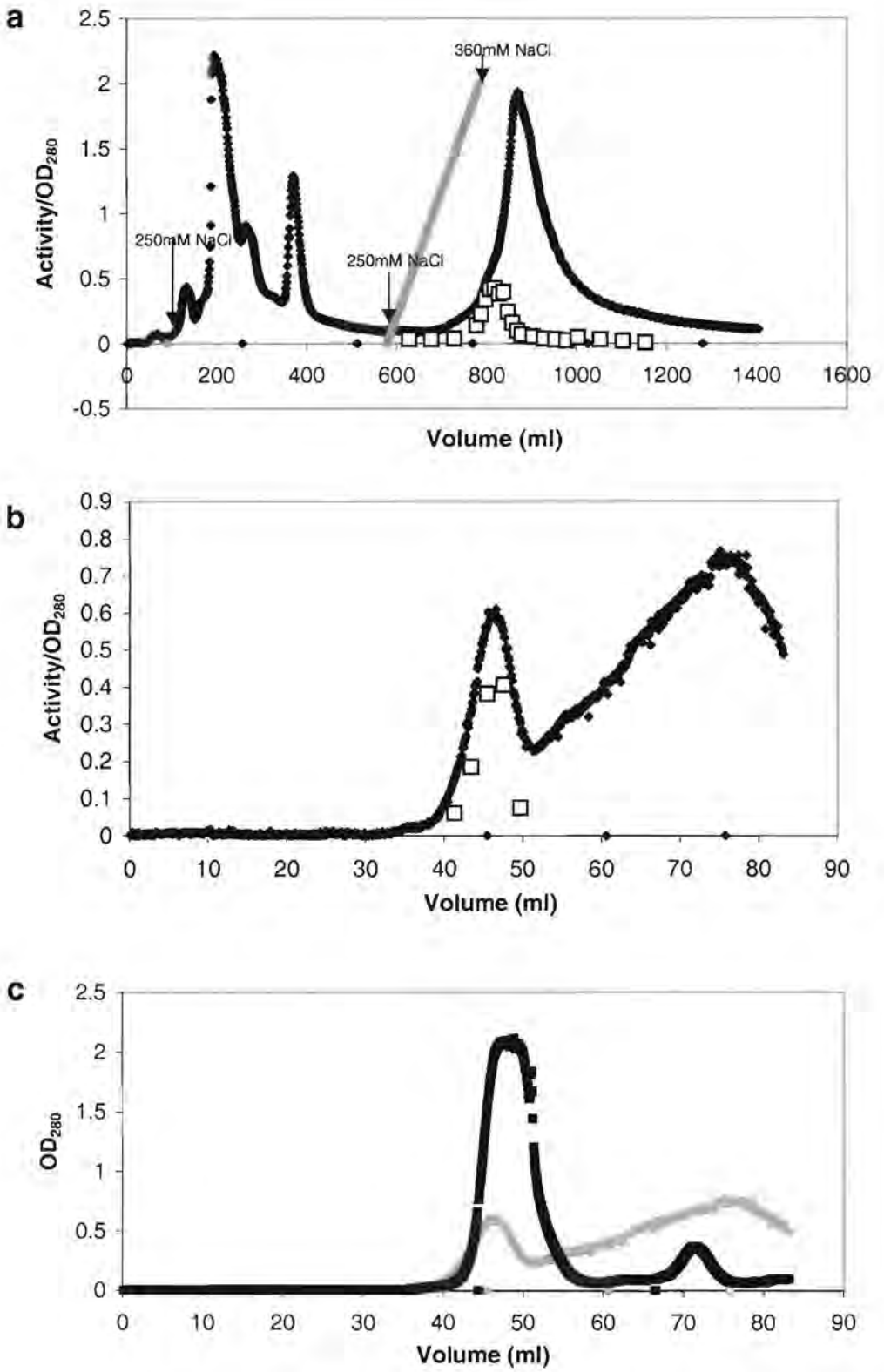

Figure 3.8. Column chromatography of native *B. pumilus* cyanide dihydratase. **(a)** DE52 anion exchange; **(b)** Gel filtration, pH 8; **(c)** Gel filtration profiles of native (grey) and recombinant (black) *B.pumilus* cyanide dihydratase, pH 8. $OD_{280,}$ black diamonds; relative activity, open squares.

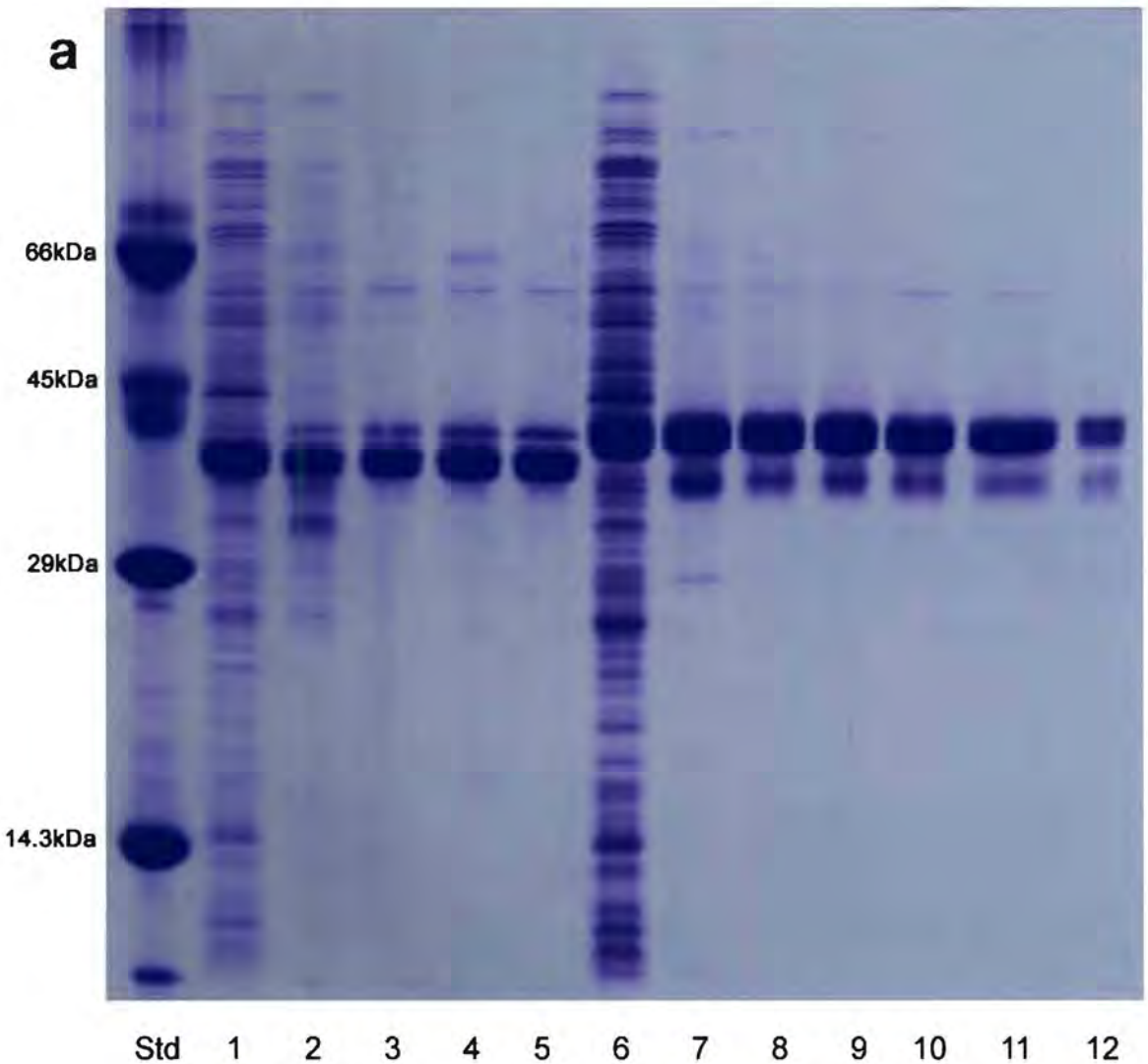

Fig 3.9 (a) 15% SDS PAGE of partially purified, recombinant cyanide dihydratase of *P. stutzeri* (lanes 1-5) and *B. pumilus* (lanes 6-11). Lane 1, CFE; lane 2, DE; lane 3, GF1 (pH 5.4); lane 4, GF2 (pH 5.4); lane 5, GF3 (pH 5.4); lane 6, CFE; lane 7, DE; lane 8, GF1a (pH 8); lane 9, GF1b; lane 10, GF1a transferred to citrate, pH 5.4; lane 11, GF2 (pH 5.4); lane 12, purified native *B.pumilus* C1 cyanide dihydratase. **(b)** 15% SDS PAGE of gel filtration fractions (GF1) of recombinant *P. stutzeri* cyanide dihydratase. Corresponding elution volumes are as follows. Lane 1, 45ml; lane 2, 49ml; lane 3, 53ml; lane 4, 57ml; lane 5, 61ml; lane 6, 65ml. Abbreviations: CFE, cell free extract; DE, pooled ion exchange active fractions; GFn, pooled gel filtration active fractions, nth pass through column; GF1a, pooled leading-edge active fractions; GF1b, pooled trailing-edge active fractions. Molecular weight standards: Lysozyme, Carbonic anhydrase, Ovalbumin, Bovine serum albumin.

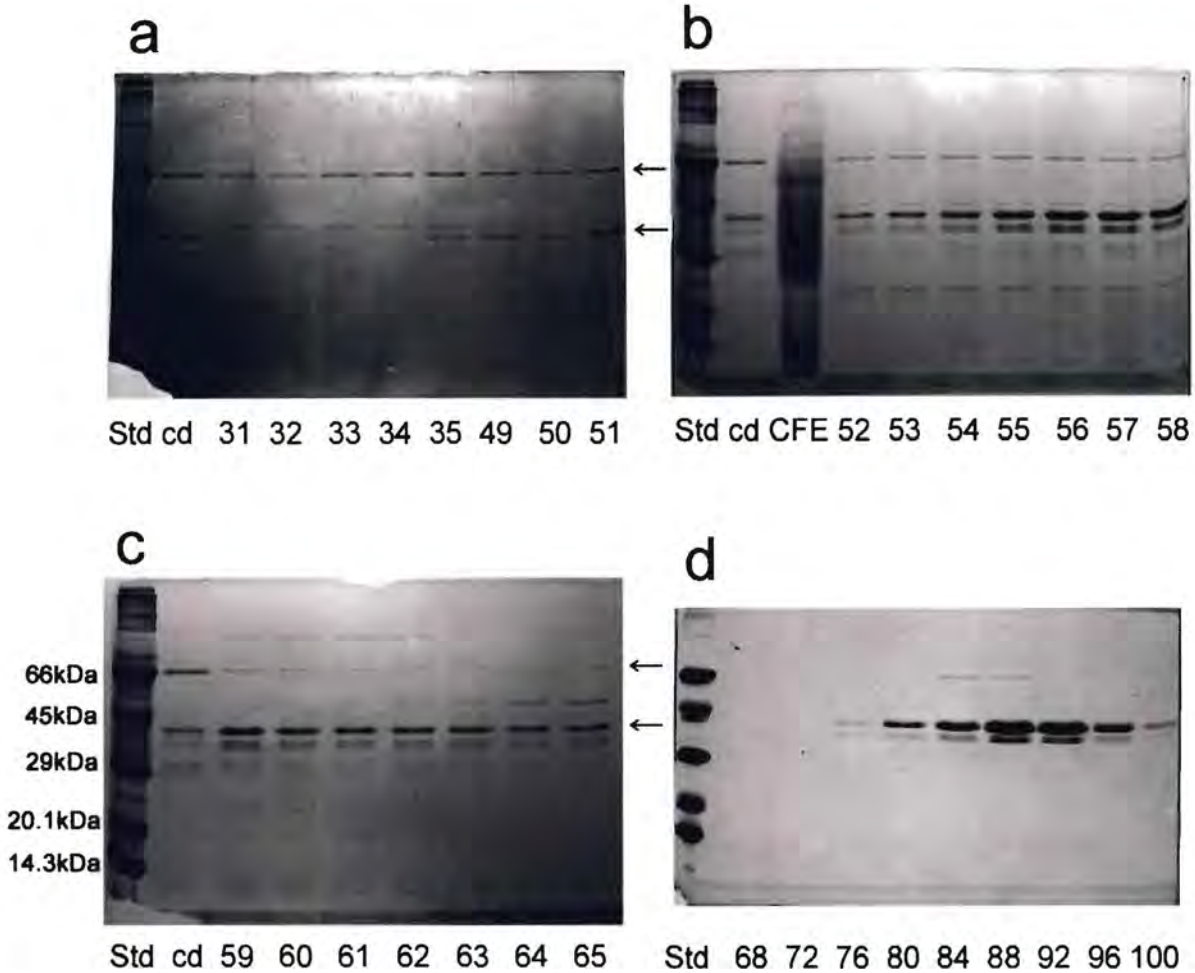

Fig 3.10. 15% SDS PAGE of partially purified native *B.pumilus* C1 cyanide dihydratase; and co-purification of an unknown protein of size 66kDa (indicated by arrows). **(a),(b),(c)** DE52 anion exchange fractions. **(d)** Gel filtration fractions. **(e)** Lane 1, Ovalbumin, lane 2, CFE; lane 3, DE; lane 4, GF. Molecular weight markers Lysozyme, Trypsin Inhibitor, Carbonic anhydrase, Ovalbumin, Bovine serum albumin. cd: partially purified cyanide dihydratase. Other abbreviations are as in Figure 3.9.

The native *B. pumilus* enzyme eluted slightly earlier than the recombinant form on gel filtration, indicating that the former complex may be slightly larger than the latter.

A contaminating protein, tentatively identified as a GroEL homogue, was copurified in the preparation of native *B. pumilus* enzyme, but apparently did not associate with the cyanide dihydratase. This is in contrast to the claims of Almatawah *et al.*, 1999 and Layh *et* al., 1998 that the nitrilases of *B. pallidus* Dac521 and *P. fluorescens* DSM7155 each form a complex with GroEL.

Complex patterns of bands on SDS PAGE were observed both in the case of *P. stutzeri* and *B. pumilus* purified cyanide dihydratase. The pattern in the native *B. pumilus* enzyme was indistinguishable from that of its recombinant form. Multiple bands have been seen previously in the purified cyanide dihydratase of *Alcaligenes xylosoxidans* subsp. *denitrificans* DF3 (Ingvorsen *et* al., 1991) and in the purified nitrilases of *Acinetobacter* sp. AK226 and *P. fluorescens* DSM 7155 (Yamamoto and Komatsu, 1991; Layh *et al.*, 1998). The interpretation of these bands in the *B. pumilus* cyanide dihydratase will be discussed further in Chapter 5.

Chapter 4. Mass spectrometry of trypsin digested *B. pumilus* cyanide dihydratase

At the outset of this project, the cyanide dihydratase gene of *Bacillus pumilus* C1 had not been cloned. The current chapter describes work that was done to assist Dakshina Jandhyala and Michael Benedik (Dept of Biology and Biochemistry, University of Houston) in their efforts to clone the gene (the work described in this chapter therefore pre-dates the work presented in Chapter 3).

Bacillus pumilus cyanide dihydratase was purified and analysed by MALDI-TOF spectrometry. Molecular weight determinations were compared with fragment sizes computed for the *P. stutzeri* cyanide dihydratase amino acid sequence. The hope was that any region of sequence identity between the two cyanide dihydratases would manifest as identical masses of trypsin fragments. These common stretches of sequences could be used to design degenerate oligonucleotide primers to amplify the *B. pumilus* gene.

4.1 Mass spectra

In this section the raw data is presented. Shown in Figure 4.1 (c) is the SDS PAGE gel from which bands were excised. The intense band at ~40kDa (which is in fact a poorly resolved doublet) will be referred to as the upper band, and the fainter, faster migrating doublet will be labelled (in order of increasing migration) lower band 1 and lower band 2.

The data collected from mass spectrometry of fragments were the result of five separate experiments. The first, third and fourth experiments involved overnight digestions, the second was for five days and the fifth was for several hours. In the fifth experiment purified enzyme was not extracted from a gel but instead digested directly with trypsin. The matrix used to ionise the peptide fragments was CHCA except in experiment 4, in which sinapinic acid was used.

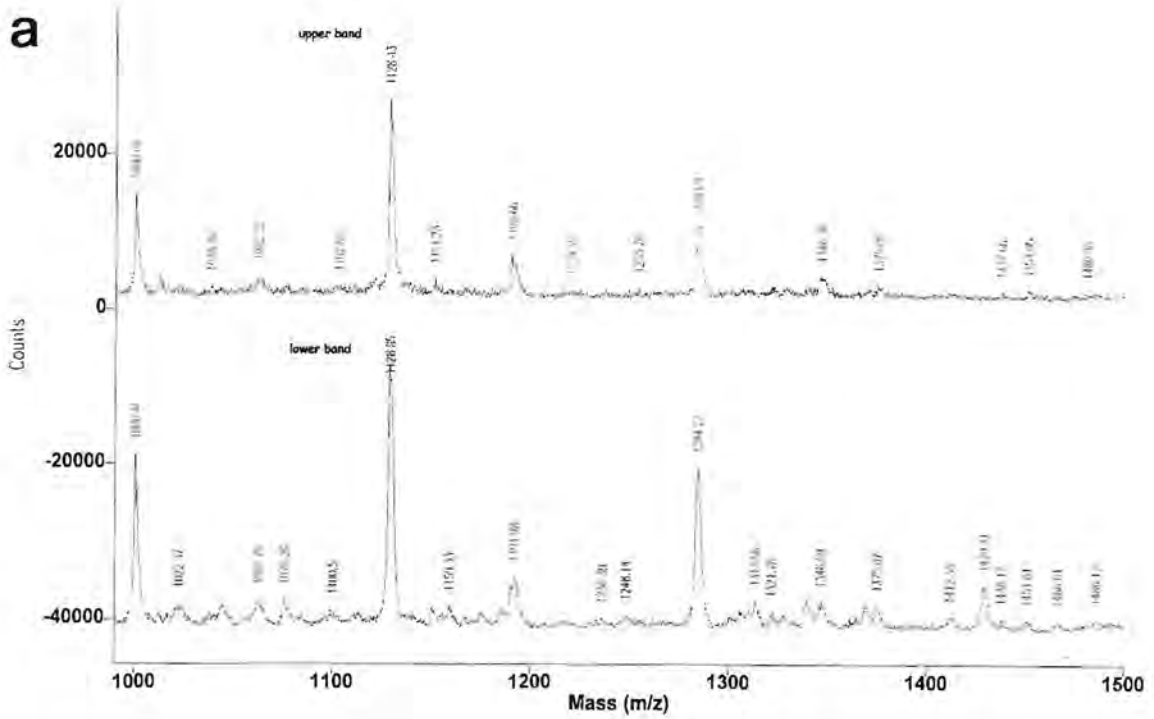

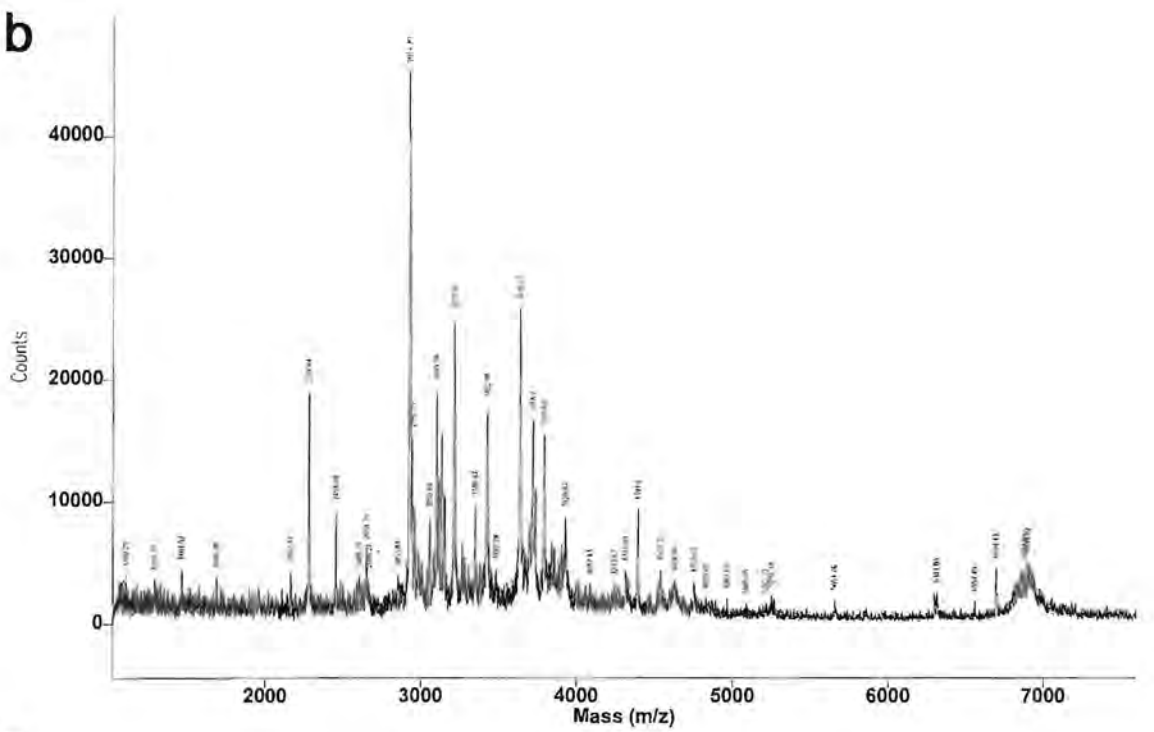

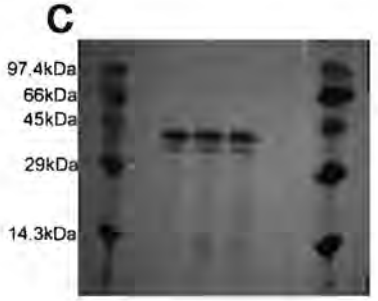

Figure 4.1(a) MALDI-TOF mass spectra of upper and lower bands of native *B. pumilus* cyanide dihydratase prepared in CHCA and **(b)** upper band prepared in sinapinic acid. **(c)** 15% SDS PAGE gel of purified *B. pumilus* cyanide dihydratase. Outer lanes: Phosphorylase b, bovine serum albumin, ovalbumin, carbonic anhydrase, lysozyme. Three central lanes: purified enzyme.

Many common fragment sizes were observed in the mass spectra of cyanide dihydratase upper and lower bands. A typical example is shown in Figure 4.1 (a). This suggests that the different bands are at least partially identical in amino acid sequence.

Tables 4.2 and 4.3 show mass measurements of trypsin-cleaved cyanide dihydratase and carbonic anhydrase, respectively. Mass measurements of samples derived from the same band are seen to differ by up to 0.15% between experiments.

Table 4.2. Masses of fragments of the *Bacillus pumilus* cyanide dihydratase bands after digestion with trypsin (all masses are in daltons). Averages were taken in such a way as to give each experiment equal weighting.

Upper band Expt 1	Lower bands Expt 1	Upper band Expt 2	Upper band Expt 3	Lower band 1 Expt 3	Lower band 2 Expt 3	Upper band Expt 4	Weighted average
	635.8						635.8
					684.3		684.3
	694.7						694.7
	709.0		708.6				708.8
	757.3		756.6				757.0
775	775.1	773.2	774.6	774.5	774.6		774.3
	830.8						830.8
	846.2						846.2
	871.7		870.4				871.1
	888.5		887.4				888.0
919.9	920.1	918.0	919.3	919.3	919.2		919.1
935.9	936.1		935.3	935.3	935.3		935.7
	941.6						941.6
949.9	950.3	947.9	949.2		949.2		949.1
	982.0						982.0
1000.0		997.9	999.2	999.2	999.2		999.0
			1015.2				1015.2
	1022.4			1019.6			1021.0
	1062.8						1062.8
	1076.3						1076.3
1128.4	1128.9	1125.8	1127.4	1127.4	1127.4		1127.3
			1149.9				1149.9
			1188.9				1188.9
	1192.0						1192.0
1283.9	1284.3	1280.8	1282.4	1282.6	1282.4		1282.5
			1304.0				1304.0
			1344.8				1344.8
			1372.8				1372.8
	1429.3						1429.3
1530.7	1531.0		1529.0	1529.1	1528.7		1529.9
		1556.9					1556.9

Table 4.2 (cont.)

Upper band Expt 1	Lower bands Expt 1	Upper band Expt 2	Upper band Expt 3	Lower band 1 Expt 3	Lower band 2 Expt 3	Upper band Expt 4	Weighted average
	1629.7				1627.4		1628.6
			1881.0				1881.0
				1950.9			1950.9
	1961.0	1956.3	1957.2				1958.2
				1975.1			1975.1
			2036.9				2036.9
			2127.8				2127.8
			2161.7	2162.0	2161.4		2161.7
			2261.1				2261.1
	2276.2					2278.8	2277.5
		2334.0					2334.0
			2390.7				2390.7
			2453.5			2454.7	2454.1
	2651.4	2647.0	2646.1				2648.2
		2849.2					2849.2
			2922.8			2926.3	2924.6
						3055.5	3055.5
3101.6		3096.9	3096.8			3099.4	3098.7
			3113.7				3113.7
3214.5		3209.9	3210.0			3213.0	3211.9
		3271.8					3271.8
			3345.2			3348.5	3346.9
		3421.0	3420.4			3423.0	3421.5
						3635.3	3635.3
			3714.9			3718.2	3716.6
			3731.5				3731.5
						3791.7	3791.7
						4391.6	4391.6

Table 4.3. Masses of fragments of bovine carbonic anhydrase after digestion with trypsin (all masses are in daltons).

Carbonic anhydrase Expt 1	Carbonic anhydrase Expt 2	Carbonic anhydrase Expt 3
2199.7	872.7	875.3
2355.7	979.3	980.3
2416.5	1002.3	1014.8
2836.7	1013.3	1020.3
2853.9	1018.2	1046.9
3131.4	1066.4	1159.9
3191.1	1158.4	1204.2
4120.9	1202.5	1392.2
4179.9	1222.4	1429.9
	1284.3	1583.8
	1391	1642.7

Table 4.3 (cont.)

Carbonic anhydrase Expt 1	Carbonic anhydrase Expt 2	Carbonic anhydrase Expt 3
	1425.5	1687.5
	1686.3	1711.7
	2125.3	1755.8
	2198.8	1840.2
	2260.7	1893
	2327	1969.9
	2355	2004.6
	2417.7	2083.4
	2585	2100.9
	2714.2	2126.1
	2853.4	2142.9
	2869.6	2200.3
	3124	2256.5
	3138.4	2328.3
	3155.2	2356.6
	3183.6	2418.3
	3201.7	2586.3
	3338	2714.3
	3472.1	2854.8
	4121.4	2871.2
	4183	3125.7
		3139.8
		3157.1
		3339.9
		3474.7
		3631.3
		3648.6
		4123.9

4.2 Carbonic anhydrase: a test case

The spectra obtained for bovine carbonic anhydrase were analysed to see whether this approach could be used to identify the fragments. Since the sequence of the polypeptide is known, it was possible to assign experimental peaks, using a tolerance of 0.1% for differences in molecular weight. Fragments in Table 4.3 arising from trypsin self-digestion were eliminated from the analysis.

Experimental and theoretical carbonic anhydrase masses are shown in Table 4.4. Since the supply of trypsin was not specially treated to inhibit traces of other enzymes, it may have possessed residual chymotrypsin activity. Also, trypsin may not have completely digested the polypeptide. Therefore, in the assignment of experimental masses, partial

digestion by trypsin and/or chymotrypsin was taken into account, including up to 7 uncleaved sites (trypsin or chymotrypsin) per fragment. Sodium and potassium adducts and chemical modifications were also considered. For instance, oxidation of tryptophan residues and deamination of peptides have been observed previously in trypsin- digested polypeptides (Wolf Brandt, personal communication).

Of these matches only 20 of the 47 masses could be simply explained in terms of the known sequence of this enzyme, and nine of the measurements did not appear to have a satisfactory explanation.

Table 4.4. Experimental masses of trypsin fragments of bovine carbonic anhydrase, and presumptive matching stretches of sequence. Shown in bold are the experimental peaks that represent an average of several closely matching values taken from different carbonic anhydrase spectra. In italics are masses that can be accounted for by chemical modification of an amino acid residue. In blue are peptides that would arise from chymotrypsin cleavage. Where both the parent peptide and its adduct are present, these are both indicated in red. Abbreviations: tryp. = oxidation of a tryptophan residue, deamin.= deamination of residue, Na add. = sodium adduct, K add = potassium adduct.

Measured mass	Theoreti-cal mass	Amino acid residues	No. of uncleaved trypsin sites	Measured mass	Theoreti-cal mass	Amino acid residues	No. of uncleaved trypsin sites
874.0	-------	-------	---	**2199.6**	2199.6	36-56	0
979.8	980.1	80-88	0	2256.5	2256.4	57-75	1
1002.3	1002.1	27-35	0	2260.7	-------	---	---
1014.1	1014.1	1-8	0	**2327.7**	2326.5	7-26	2
1066.4	-------	-------	---	**2355.8**	2355.7	36-57	1
1159.2	*1159.2 (Tryp)*	*9-17*	0	**2417.5**	*2416.8 (K add.)*	*230-250*	0
1203.3	1203.4	158-168	1	**2585.7**	2585.8	66-88	2
1222.4	*1222.4 (Deamin.)*	*113-122*	0	**2714.3**	2713.0	167-190	2
1284.3	1284.4	16-26	1	2836.7	-------	-------	---
1391.6	1391.6	76-88	1	**2853.9**	2854.3	226-250	0
1425.5	*1426.7 (K add.)*	*158-170*	2	**2870.4**	2870.4	88-111	2
1429.9	*1429.6 (K add.)*	*76-88*	1	**3124.8**	3124.6	226-252	1
1583.8	1582.8	113-125	0	3131.4	-------	-------	---
1642.7	-------	-------	---	**3139.1**	3138.4	1-26	2

Table 4.4 (cont.)

Measured mass	Theoretical mass	Amino acid residues	No. of uncleaved trypsin sites	Measured mass	Theoretical mass	Amino acid residues	No. of uncleaved trypsin sites
1686.9	*1685.8 (Na add.)*	*51-65*	2	**3156.2**	3157.7	224-250	1
1711.7	1711.0	112-125	0	3183.6	3182.6	27-56	1
1755.8	*1755.1 (Deamin.)*	*130-147*	0	3191.1	3191.6	148-177	4
1840.2	1839.2	111-125	2	3201.7	———	———	---
1893.0	1893.3	244-259	3	**3473.4**	3472.8	58-88	2
1969.9	1968.3	148-166	1	3631.3	3632.0	95-125	3
2004.6	———	———	---	3648.6	———	———	---
2083.4	*2083.2 (Deamin.)*	*58-75*	0	**4122.1**	4121.4	1-35	3
2125.7	2126.5	212-229	2	**4181.5**	4182.7	18-56	2
2142.9	2143.3	9-26	1				

The sequence of bovine carbonic anhydrase is given below. All parts of the sequence that were represented by experimental masses are underlined. The symbol b designates a sequence ambiguity between Asp and Asn, and z designates an ambiguity between Glu and Gln. In the calculating the theoretical sizes Asp and Glu were assumed for b and z respectively as these gave the best matches.

SHHWGYGK[9]HBGPZHWHKDFPIANGER[27]QSPVNIDT[36]KAVVQDPALKPLAL

VYGEATSR[57]R[58]MVN[61]NGHSF[66]NVEYDDSQDK[76]AVLKDGPLTGTYR[89]LVQF

HFHWGSSBBQGSEHTVDRK[112]KY[114]AAELHLV[121]HWNTK[126]YGDFGTAAQQ

PDGLAVVGVFLK[148]VGDANPALQK[158]VLDALDSIK[167]TKGKSTDFPNFDPG

[181]SLLPNVLDYW[191]TYPGSLTTPPLLESVTWIVLK[212]EPISVSSQQMLKFR[226]TL

NF[230]NAEGEPELLML[241]ANWRPAQPLK[251]NRQVRGFPK

4.3 Cyanide dihydratase fragments

Experimental peaks obtained from the spectra of *B. pumilus* cyanide dihydratase were compared with the theoretical fragment sizes computed for the cyanide dihydratase amino acid sequence of *P. stutzeri*. Of the 59 distinct experimental fragment sizes (Table 4.2), several were found to match a theoretical value to within 0.1% (Table 4.5). The theoretical fragment sizes were generated assuming digestion only by trypsin, and partial cleavage allowing up to 7 internal trypsin sites.

Table 4.5. Experimental masses of trypsin fragments of *B. pumilus* cyanide dihydratase, and presumptive matching stretches of sequence of *P. stutzeri* cyanide dihydratase. Averages of masses were taken so as to give equal weighting to each experiment.

Spectrum	Measured mass	Theoretical size of *P. stutzeri* fragment	Amino acid residues (in *P. stutzeri*)	No. of internal trypsin sites (*P. stutzeri*)
Lower band, expt 1	**635.8**	**635.8**	**271-275**	**0**
Lower band, expt 1	709.0			
Upper band, expt 3	708.6			
Weighted average of above	**708.8 ***	**not applicable**	**not applicable**	**not applicable**
Upper band, expt 1	935.9			
Lower band, expt 1	936.1			
Upper band, expt 3	935.3			
Lower band 1, expt 3	935.3			
Lower band 2, expt 3	935.3			
Weighted average of above	**935.7**	**935.0**	**230-236**	**0**
Upper band, expt 1	949.9			
Lower band, expt 1	950.3			
Upper band, expt 2	947.9			
Upper band, expt 3	949.2			
Lower band 2, expt 3	949.2			
Weighted average of above	**949.1**	**948.1**	**129-136**	**1**
Lower band, expt 1	**1076.3**	**1076.3**	**128-136**	**1**
Upper band, expt 2	2260.0			
Upper band, expt 3	2261.1			
Weighted average of above	**2260.6**	**2259.6**	**8-29**	**1**
Upper band, expt 3	**2922.8**	**2921.4**	**67-92**	**2**
Upper band, sinapinic acid, expt 4	2926.3	2927.38	41-65	0
Upper band, expt 3	3345.2			
Upper band, sinapinic acid, expt 4	3348.5			
Average of above	**3346.85**	**3343.8**	**8-40**	**2**
Upper band, sinapinic acid, expt 4	**3791.7**	**3789.37**	**92-125**	**2**

* The peak at 708.8 Da matches the size of the N-terminal trypsin fragment TSIYPK of the *Bacillus pumilus* C1 enzyme, which has molecular weight 708.83 Da (Meyers *et al.*, 1993a)

This assumption was made to reduce the chances of a random mismatch. Peaks known to arise from trypsin self-digestion were eliminated. These presumptive matches are indicated below in the full sequence of the *P. stutzeri* cyanide dihydratase.

AHYPKFK[8]AAAVQAAPVYLNLDATVEKSVK[30]LIEEAASNGAK[41]LVA

FPEAFIPGYPWFAFLGHPEYTR[66]R[67]FYHTLYLNAVEIPSEAVQKISAAAR[92]K[93]NKIYVCISC

SEKDGGSLYLAQLWFNPEGDLIGK[126]HR[128]K[129]MRVSVAER[137]LCWGDGNGSMMPVFETEIGN

LGGLMCWEHNVPLDIAAMNSQNEQVHVAAWPGFFDDETASSHYAICNQAFVLMTSSIYSEE

MK[220]DMLCETQEER[230]DYFNTFK[237]SGHTRIYGPDGEPISDLVPAETEGIAYAEIDIEK[271]IIDFK

[276]YYIDPVGHYSNQSLSMNFNQSPNPVVRKIGERDSTVFTYDDLNLSVSDEEPVVRSLRK

4.4 Further analysis

After these experiments were performed, the cyanide dihydratase gene of *B. pumilus* was cloned and sequenced by Jandhyala and Benedik. (An alignment of the *P. stutzeri* and *B. pumilus* sequences is presented in Chapter 8.) With the full sequence available, it became possible to reassess the data. This was done by comparing each of the original experimental mass peaks with theoretical sizes computed from *B. pumilus* sequence, assuming partial digestion by trypsin (allowing for up to seven consecutive uncleaved trypsin sites). Twenty-two of the 59 experimental peaks could be accounted for in this way.

The nine proposed regions of sequence identity of the *P. stutzeri* and *B. pumilus* enzymes were also examined. Six of the experimental *B. pumilus* peaks did not match any of the calculated sizes. Of the remaining three, the experimental mass of 2926.3 Da (present in Figure 4.1 (b) and Table 4.5) matched to within 1.1 Da the fragment spanning amino acids 42-66 in *B. pumilus*, and this is indeed a region of sequence identity between the *P. stutzeri* and *B. pumilus* cyanide dihydratases. The experimental mass of 3346.85 Da corresponded to the region spanning amino acids 9-41 in *B. pumilus*, which has a theoretical mass of 3347.75 Da. Interestingly, the corresponding region of *P. stutzeri* is similar but not identical in sequence. However, the six amino acid differences counterbalance one another in such a way that the overall effect on the total mass is small: the fragment in *P. stutzeri* has a mass of

3343.80 Da. Lastly, the experimental mass of 3791.7 Da matched (to within 0.5 Da) the region spanning amino acids 93-126 of *B. pumilus*. The corresponding region of *P. stutzeri* differ in four positions, but again these differences counterbalance one another: the mass of the *P. stutzeri* region is 3789.37 Da.

Conclusions

The analyis by MALDI-TOF spectrometry of native *B. pumilus* cyanide dihydratase gave consistent peaks within the range 600-4000Da. Analysis of the amino acid sequence of *P. stutzeri* cyanide dihydratase pointed to nine instances in which experiment mass peaks of the *B. pumilus* enzyme matched theoretical trypsin fragments of the *P. stutzeri* enzyme. One such match, corresponding to amino acids 8-40 in the *P. stutzeri* sequence, was used in the work of Dakshina Jandhyala and Michael Benedik to design a degenerate oligonucleotide primer for the 5' end of a PCR reaction carried out on genomic DNA from *B. pumilus*. This degenerate primer, termed Pum-7, is based on the sequence AAAVQAAPVY, which in the *B. pumilus* enzyme reads AAAVQAAPIY. Pum-7 was one of the degenerate primers that was used to amplify a fragment of the cyanide dihydratase gene, which in turn led to the cloning of the entire gene.

It is important to observe that six of the nine proposed matches turned out to be false. The predictive power of this method could be improved by using a source of trypsin or other peptide cleaving agent that is able to cut at all recognition sites and nowhere else.

The MALDI-TOF spectra of three different bands extracted from SDS polyacrylamide gels of the native *B. pumilus* enzyme had many common peaks. This indicates that the polypeptides extracted from these bands are closely related in sequence, and strengthens the finding that these three bands have identical N-terminal sequences (Meyers *et al.*, 1993a).

In retrospect, degenerate primers could have been rationally designed without the use of MALDI, by picking residues proximal to the catalytic cys, glu and lys residues. The rationale is that these residues would have to have been conserved in order to

preserve the geometry at the active site. The hindsight of a sequence comparison (see chapter 8) shows that these residues are indeed highly conserved. This suggestion, of Professor DB McIntosh, is gratefully acknowledged.

Chapter 5. Chemical crosslinking of *B. pumilus* cyanide dihydratase

In this chapter a quaternary structural investigation of the *B. pumilus* cyanide dihydratase by chemical crosslinking and SDS PAGE analysis is presented. The technique of crosslinking has been used to determine the number of subunits in various oligomeric enzymes using crosslinking reagents such as dimethylsuberimidate and glutaraldehyde (Davies and Stark, 1970; Tong and Duckworth, 1975; Watanabe *et* al., 1981; Mitchell *et al.*, 1995). At sufficiently dilute concentrations of protein, crosslinking takes place more rapidly amongst subunits of an oligomer than it does between subunits of separate oligomers. The number of subunits per oligomer can be determined by counting the number of bands appearing as a ladder of crosslinked species on SDS PAGE, provided that the possibility of intermolecular crosslinks has been eliminated.

5.1 Initial crosslinking with formaldehyde and glutaraldehyde

In a preliminary experiment, the enzyme was incubated overnight at 4.8 mg/ml with crosslinking reagent (formaldehyde or glutaraldehyde). Over the 100-fold range of glutaraldehyde concentration tested (0.002% to 0.2%), the extent of crosslinking rose from zero to completion (Figure 5.1 (a)). The time-scale of the experiment and concentration of formaldehyde used was not sufficient to allow crosslinking to take place. However, the primary purpose of this experiment was to determine the approximate concentration of glutaraldehyde necessary to achieve crosslinking.

5.2 Further crosslinking with glutaraldehyde

Glutaraldehyde crosslinking was examined in greater detail. To reduce the possibility of inter-molecular crosslinking, the enzyme was diluted to 0.2 mg/ml in glutaraldehyde buffer at concentrations spanning the range 0.002% to 0.2% and incubated at room temperature for 75 minutes. A ladder of increasing molecular weight bands was observed on SDS PAGE, as shown in Figure 5.1 (b). The proportion of higher molecular weight bands increased with increasing concentrations of glutaraldehyde. In particular, three closely spaced bands of similar intensity appear

in the position assumed (for the moment) to be that of a dimer. In addition, all the bands at the monomer position disappear as the glutaraldehyde concentration is increased. A faint band in the position of a trimer is barely visible throughout, whereas a putative tetramer band is clearly visible at increasing concentrations of glutaraldehyde.

These crosslinked products are plotted according to migrational distance in Figure 5.2 (a), assuming a molecular weight of 37.5 kDa for a monomer, and assuming the successive bands correspond to the dimer, trimer, tetramer, pentamer and so on. These points do not coincide with the standard curve generated from molecular weight markers but are nevertheless collinear. This does not however necessarily justify all the assignments of subunit numbers since higher molecular weight species may migrate anomalously as the diameter of the molecules approaches the sizes of pores in the gel.

The glutaraldehyde reagent used in this experiment was diluted to 10mM in 20mM NaCl and analysed by MALDI mass spectrometry. Mass peaks were observed at increments of 100Da, which is the molecular weight of glutaraldehyde (Figure 5.2 (b)). No peak was observed at a mass larger than 1000 Da. This confirmed that the glutaraldehyde had formed polymers, but that these polymers consisted of no more than 10 glutaraldehyde molecules (bringing the total molecular weight of the largest polymer to a maximum of 1000Da).

5.3 Conclusions

The anomalously slow migration of the products of crosslinking is entirely consistent with the fact that the monomer migrates at an apparent size of 41.4 kDa although its actual size is 37.4 kDa. This may be accounted for by an intrinsic property of the polypeptide, such as incomplete denaturation, which causes anomalous migration in the polyacrylamide gel.

The disappearance of the bands in the monomer position supports the notion that all of these bands are polypeptides in the enzyme complex and not merely contaminants. The triplet of bands in the dimer position may reflect three distinct conformations that

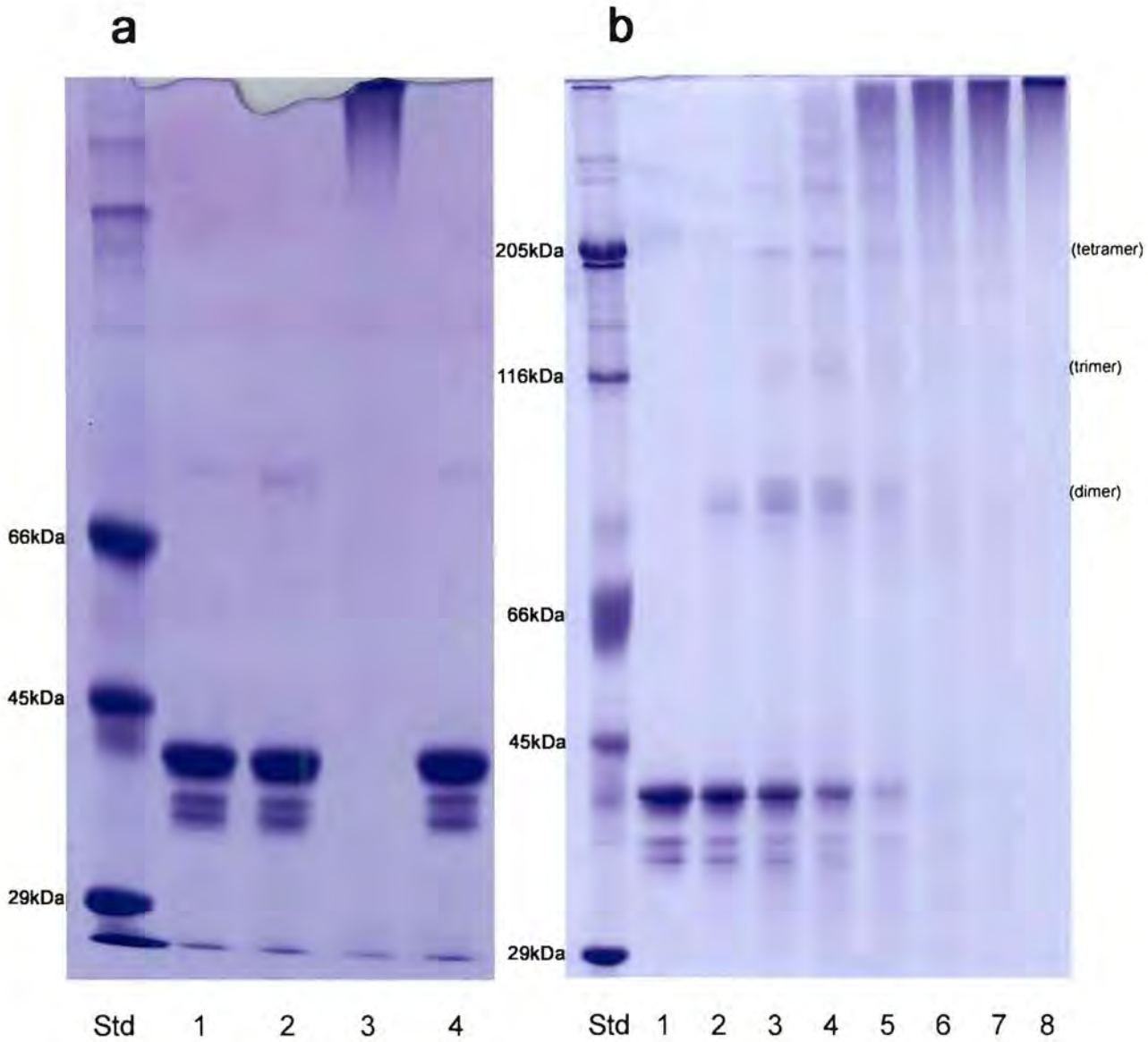

Fig 5.1. 10% SDS PAGE of crosslinked native *B. pumilus* cyanide dihydratase. In two separate experiments, crosslinking reagents were added as follows. (**a**) Lane 1, 0.0002% formaldehyde; lane 2, 0.002% glutaraldehyde; lane 3, 0.2% gluraraldehyde; lane 4, no crosslinker. (**b**) Glutaraldehyde was added to the following concentrations. Lane 1, none; lane 2, 0.002%; lane 3, 0.005%; lane 4, 0.01%; lane 5, 0.02%; lane 6, 0.05%; lane 7, 0.1%; lane 8, 0.2%. Enzyme per reaction: (a) 12μg at 4.8mg/ml; (b) 6μg at 0.2 mg/ml. Molecular weight markers: (a) Carbonic anhydrase, Ovalbumin, BSA;
(b) Carbonic anhydrase, Ovalbumin, BSA, β-Galactosidase, Myosin

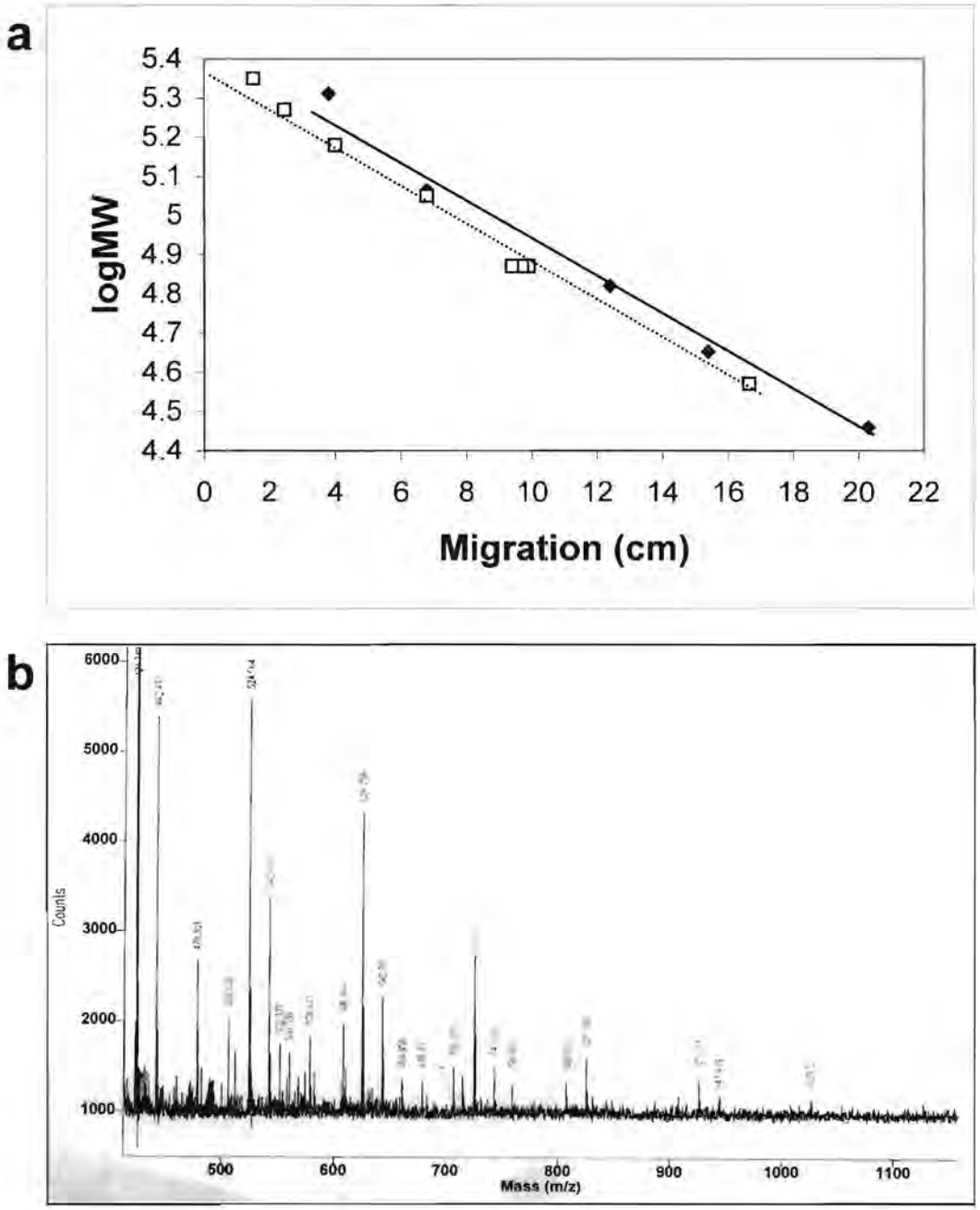

Figure 5.2 (a) Migration of molecular weight markers (solid diamonds) and crosslinked cyanide dihydratase of *B. pumilus* C1 (open squares) on 10% SDS PAGE. Molecular weights are calculated on the assumption that all possible crosslinked products are formed (dimer, trimer, tetramer, pentamer, and so on) **(b)** MALDI-TOF mass spectrum of unbuffered 10mM glutaraldehyde in 20mM NaCl. The matrix used for mass spectrometry was 2,5-dihydroxybenzoic acid (DHB).

can be adopted by a crosslinked dimer. Higher-order positions may also have complex banding patterns, as is just visible in the tetramer position, lanes 6 and 7 of Figure 5.1 (b).

Mass spectrometry of the glutaraldehyde reagent revealed polymers limited in size to 1000Da, indicating that the glutaraldehyde contained a mixture of polymers not exceeding 10-mers. Together with the low protein concentration used in the reaction (0.2mg/ml), this suggests that intramolecular- rather than intermolecular crosslinks were favoured. Further experiments with varying concentrations of enzyme would be needed to verify this.

Chapter 6. Single particle reconstructions

The single particle technique is a methodology used to determine a low resolution (~3nm) three-dimensional model of a macromolecule from electron micrographs of individual particles (Penczek *et al.*, 1992). It is particularly well-suited to homogenous preparations of a macromolecular complex. The technique, in its simplest form, relies on the collection of electron micrographs of an untilted specimen containing negatively stained or ice-embedded molecules in random or pseudo-random orientations. These images can be used together with computer programmes to reconstruct a three dimensional model of the complex. For a general overview of the technique, the reader is referred to Frank *et al*, 1996b.

In this chapter reconstructions of the purified cyanide dihydratases are described.

6.1 Preparation of specimens

Native *B. pumilus* and recombinant *P. stutzeri* and *B. pumilus* cyanide dihydratases were purified as described in Chapter 3. Negative staining was attempted with a variety of buffers of varying pH. The native *B. pumilus* enzyme was prepared in TEA buffer pH 8. Better staining was subsequently achieved with the recombinant enzyme in MES buffer pH 6. Staining of the *P. stutzeri* cyanide dihydratase was better in TEA buffer pH 8 than in MES pH 6. The optimal protein concentrations of these enzymes in the respective buffers were found to be 0.15mg/ml (*B. pumilus*) and 0.32mg/ml (*P. stutzeri*).

Negatively stained specimens were imaged by transmission electron microscopy, using the minimum dose technique. The micrographs were digitised and found to be well-stigmated, underfocussed and lacking evidence of beam damage. Focussing was facilitated by an intensified CCD camera with television display.

6.2 Reconstructions

Table 6.0 summarises the three reconstructions. Image analysis was performed using SPIDER routines (Frank *et* al., 1996). Typical micrographs are shown in Fig 6.1. In

each of these images the particles were seen in diverse, recurring shapes, and were homogeneous in size. Putative GroEL particles were seen in all the preparations. These were excluded whenever possible from the picking. Particles of *B. pumilus* were occasionally seen in an extended form of approximately twice the normal length.

Images were filtered to reduce noise. Raw and corresponding filtered images are shown in Figure 6.2 (a). After classifying the images *ab initio*, initial models of the recombinant enzymes were produced using the method of common lines (Penczek *et* al., 1996). These crude models were successively refined by repeated projection, classification and back-projection (i.e. creation of a new model from class averages and a fixed set of angles). A typical example of a class of mutually correlated images and their class average is shown in Figure 6.2 (b).

The models independently converged to spiral structures as shown in Figures 6.3 and 6.4. The model of native *B. pumilus* (Figure 6.5) was not generated *ab initio* but instead was refined from model 111 of the recombinant *B. pumilus* enzyme. Different views of the three structures are given in Figure 6.6, with successive 60° rotations of the models about a vertical axis, followed by 30° tilts about a horizontal axis.

Note that the handedness of the models could not be determined with the available data. A handedness determination was attempted by means of shadowing experiments, but the results were inconclusive (data not shown).

Terminal subunits of the *P. stutzeri* enzyme appeared to be truncated (Figure 6.3, model 31). This was believed to arise from the fact that the box used to excise images and the radius used in the backprojections were too small to accommodate the molecule. Therefore, in further cycles of refinement, the images were excised from the original micrographs, using a larger box size of 80×80 pixels, and the radius used for backprojection was increased to 38 pixels. This led to expansion of the terminal subunits in the resulting models.

Table 6.0. Summary of the three reconstructions

	Recombinant *P. stutzeri*	Recombinant *B.pumilus*	native *B. pumilus*
No. of micrographs	15	16	26
Particles picked	7008	11661	13019
Starting model	*ab initio*	*ab initio*	MB2890 model 111
Initial templates	84	84	n/a
No. of cycles of initial template refinement	5	4	n/a
No. of templates used to generate starting angles	49	40	n/a
No. of cycles of model refinement, radius 26 pixels	30	30	n/a
No. of cycles of model refinement, radius 31 pixels	24	39	n/a
No. cycles of model refinement, radius 38 pixels, 2-fold symmetry enforced	22	41	89
No. of cycles of model refinement, radius 38 pixels, no enforced symmetry	6	6	6

In all the mature models the spiral structure possessed striking two-fold symmetry across a global dyad axis. In order to exploit the symmetry, the position of this dyad

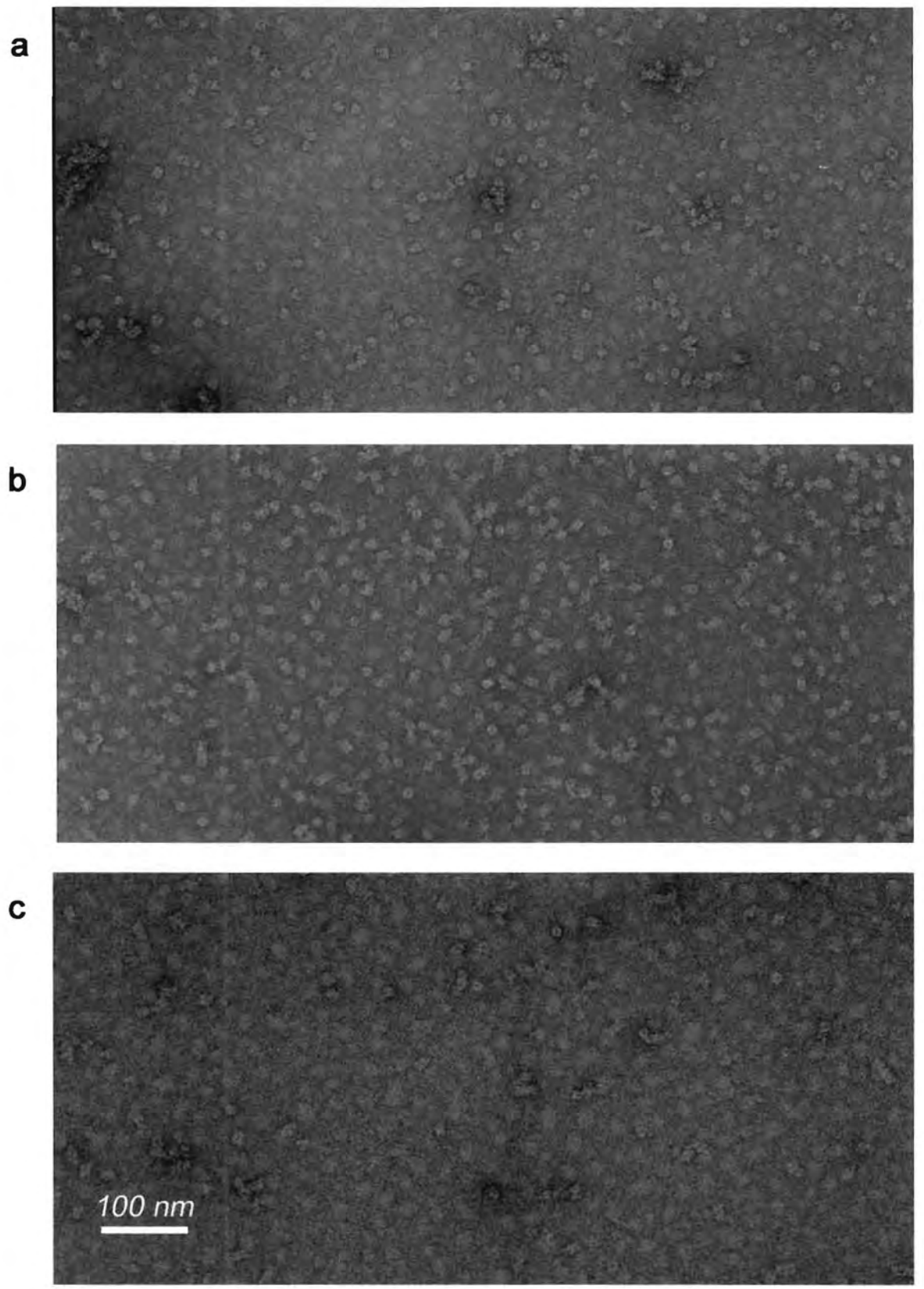

Figure 6.1. Micrographs of single particles used for reconstruction. Recombinant cyanide dihydratases of **(a)** *P. stutzeri* and **(b)** *B. pumilus*; **(c)** native cyanide dihydratase of *B. pumilus;* each at 50 000 times magnification.

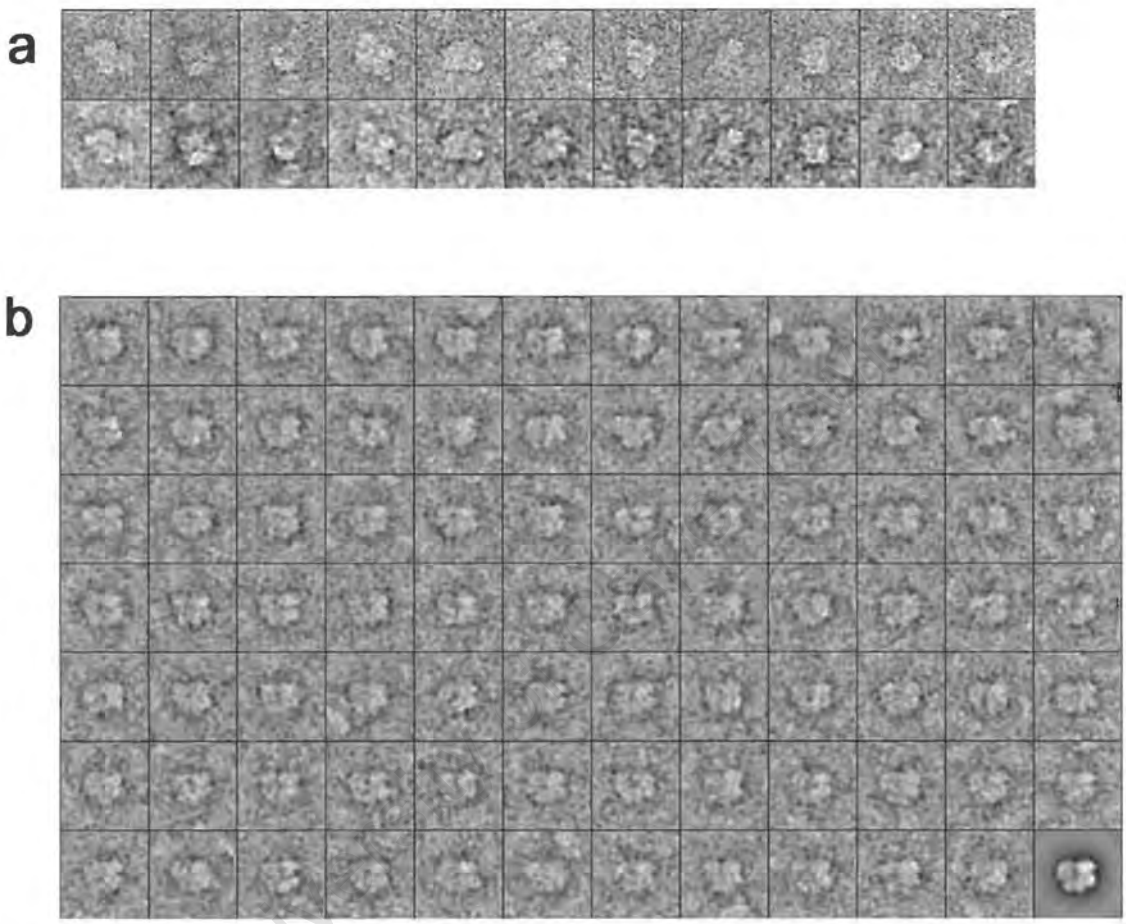

Figure 6.2 (a) Raw and corresponding filtered images, with Gaussian low-pass filter at 15Å. **(b)** Class 40 of model 83, recombinant *P. stutzeri* cyanide dihydratase, and the corresponding class average.

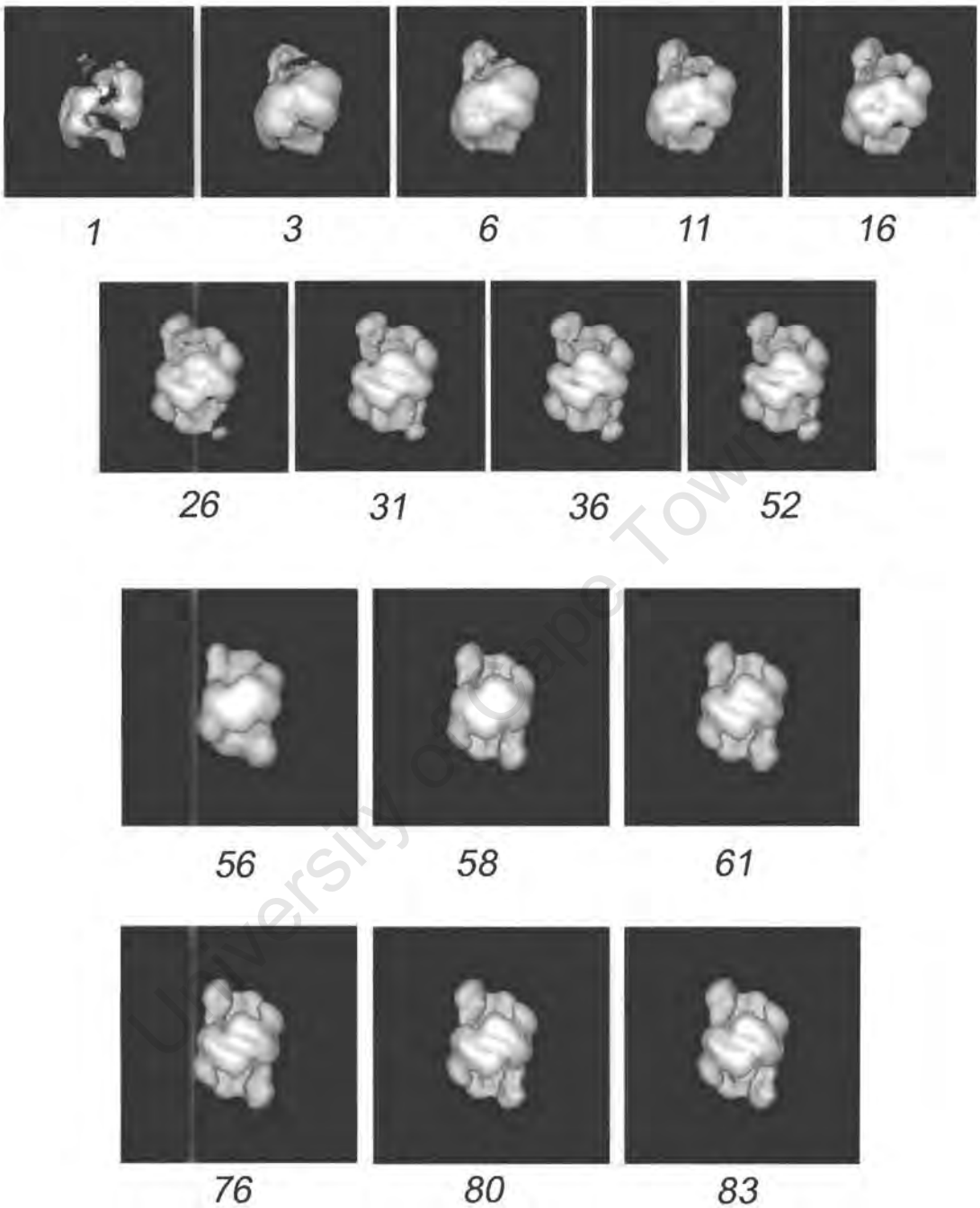

Figure 6.3. Refinement of models produced *ab initio* from single particle electron micrographs of recombinant *P. stutzeri* cyanide dihydratase. Radius for reconstruction as follows. Models 1-31, r = 26; models 32-55, r=31; models 56-83, r = 38. Box sizes of images as follows. Models 1-55, 64 by 64 pixels; models 56-83, 80 by 80 pixels. Two-fold symmetry was imposed on models 56-76.

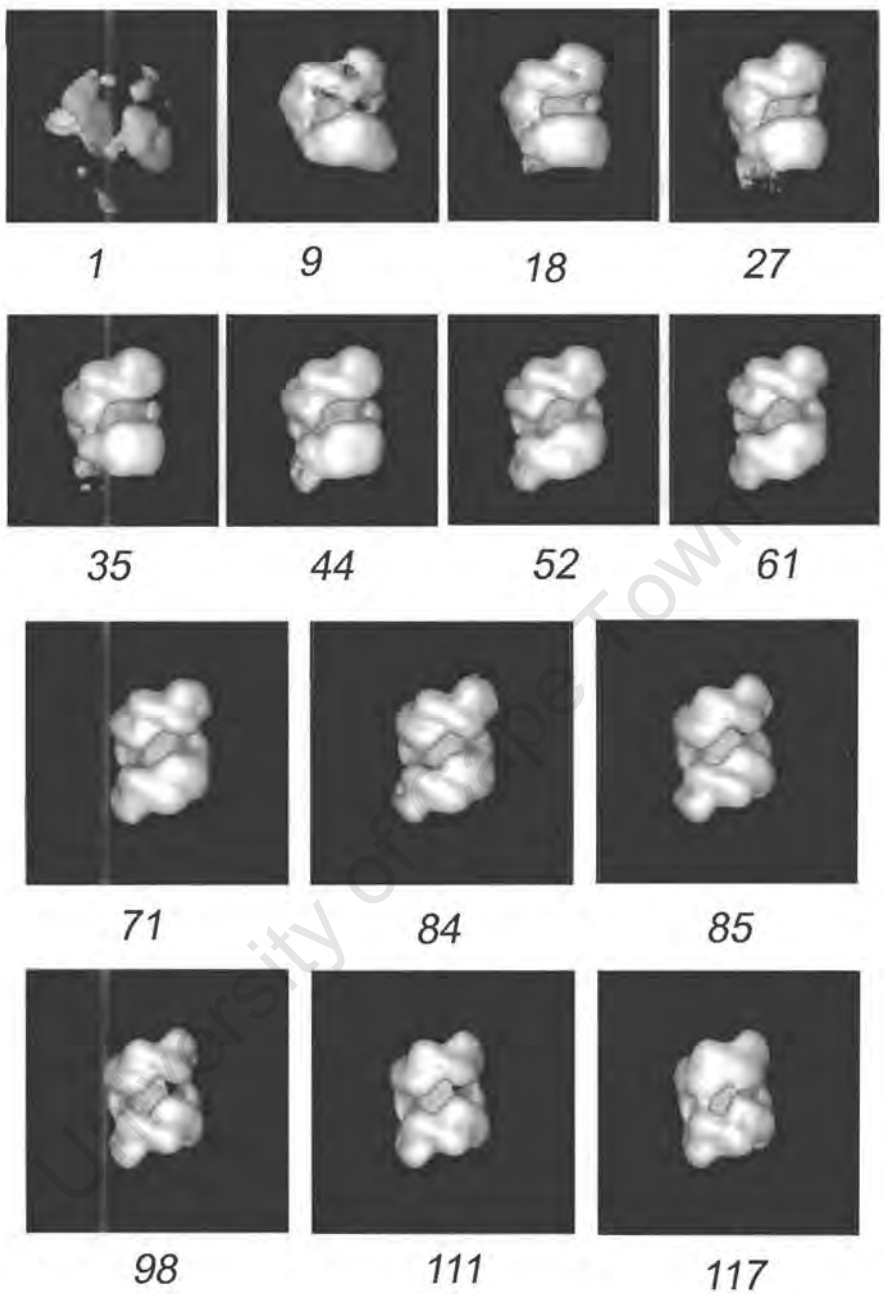

Figure 6.4. Refinement of recombinant *B.pumilus* cyanide dihydratase model, *ab initio.* Radius for reconstruction as follows. Models 1-31, r = 26; models 32-70, r = 31; models 71-117, r = 38. Box size of images as follows. Models 1-70, 64 by 64 pixels; models 71-117, 80 by 80. Two-fold symmetry was imposed on models 85-111.

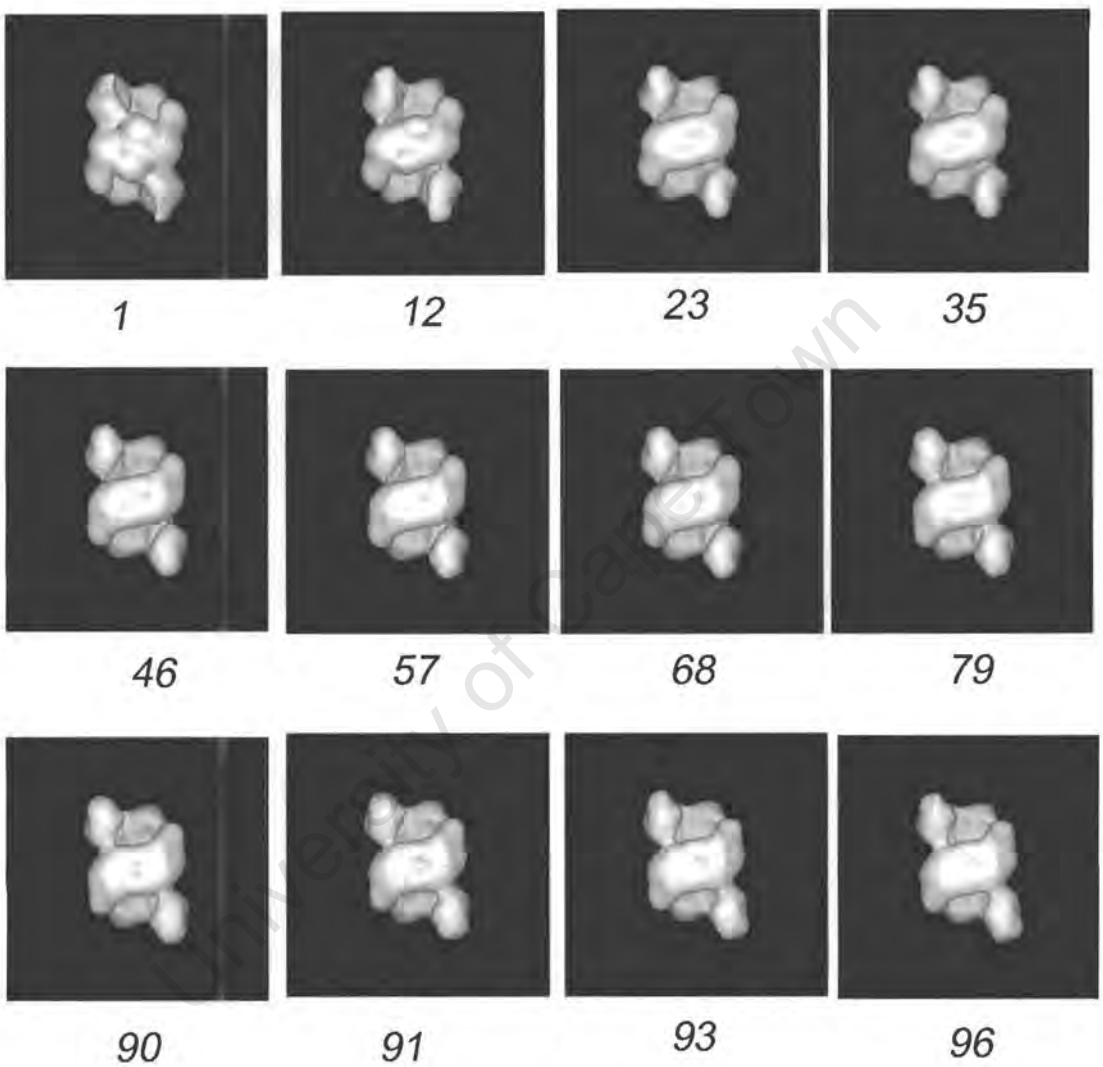

Figure 6.5. Model refinement of native *B.pumilus* cyanide dihydratase. Model 111 of recombinant *B.pumilus* cyanide dihydratase was used as the initial model. Radius for reconstruction was 38 and image box size 80 by 80 pixels for all models. Two-fold symmetry was imposed on models 1-90.

axis was estimated manually and the model was symmetrised by superposition with its two-fold related image. The chosen axis of symmetry was then fixed, and the model was further refined with symmetrisation imposed on each successive model. To test whether or not this imposition of symmetry was artificial, a final six rounds of iteration were performed without symmetrisation. The final models were carefully examined using the programme MODEL VIEWER and were seen to be effectively unchanged.

6.3 Quality and resolution of the models

The quality of each of the structures was assessed in several ways. Classes were examined and found to contain images consistently resembling the class average. A typical example is shown in Figure 6.2 (b). Projections of each of the final models were compared with class averages and found to agree very well (Figures 6.7, 6.8 and 6.9), indicating that the images were compatible with the model. Stability of the converged models after many rounds of refinement, as seen in Figures 6.3, 6.4 and 6.5, further supported the integrity of the model. The histograms in Figure 6.10 show that projections from most angles are represented in the image sets.

One of the most important means of assessing the quality of a structure is by Differential Phase Residual (DPR) and Fourier Shell Correlation (FSC) (Harauz and van Heel, 1986). The principle is to randomly divide the image set into two halves, produce two separate models from these and quantitate the difference between these models. This test was applied to each of the structures and yielded the graphs shown in Figure 6.11. An estimate of the resolution of each model can be made by reading off the resolution at which the DPR is 45 degrees or the FSC is 0.5. This gives a resolution of approximately 2.9nm for recombinant *P. stutzeri* enzyme, 3.2nm for the recombinant *B. pumilus* enzyme and 3.4nm for the native *B. pumilus* enzyme. These values apply to the models formed after relaxation of symmetry. Although enhanced resolution can be expected for the symmetrised models, such values were not calculated in the current study.

6.4 Structural features

The *P. stutzeri* cyanide dihydratase structure at pH 8 consists of a two-fold symmetric spiral of 14 subunits. The complex possesses a large central core of zero density. Two types of intersubunit contact can be inferred from the structure, indicated by arrows in Figure 6.6(a), view 5. One of these coincides with the global two-fold axis and is clearly defined. The other is not clearly defined except at high contour level. A protrusion is visible on the inside surface of the spiral, which appears on every subunit (indicated in Figure 6.6 (a), view 8). The distance between the centroids of subunits and the helical axis decreases from 4.7nm for the central subunits to 3.4nm for the terminal subunits. The overall dimensions of the structure are 17.9 nm by 12.3 nm. The number of subunits and helical radii of these subunits were determined by increasing the contour level until small, discrete units of density (the cores of the subunits) remained. These were assumed to be positioned at the centroids of subunits. The imposed two-fold symmetry ensured that the helical axis was perfectly centred, and thus allowed direct measurement of the helical radius.

The recombinant *B. pumilus* structure at pH 6 consists of a two-fold symmetric spiral of 16 subunits. It shares some of the features of the *P. stutzeri* enzyme, such as the large central core and the two types of intersubunit contact. Decreasing the contour level reveals regions of density attached to each terminal subunit (Figure 6.12 (a,b)). This indicates partial occupancy of a further pair of subunits at the two terminal locations (Figure 6.12 (a,b)). The distance between the centroids of subunits and the helical axis decreases from 5.3nm for the central subunits to 4.6nm for the terminal subunits and the overall dimensions of the structure are 17.6 nm by 12.9 nm.

The native *B. pumilus* structure at pH 8 consists of a two-fold symmetic spiral of 18 subunits. It is different to the other structures in that it has a larger hollow central core, and its subunits protrude prominently on the exterior of the spiral. Decreasing the contour level reveals a pair of unidentified regions of density, attached to exterior surface of the complex (Figure 6.12 (c,d)). These are attached to two subunits that straddle the central dimer. At the original contour level the local surface topology is modified at the positions of the central subunits, lacking the strong protrusions seen at

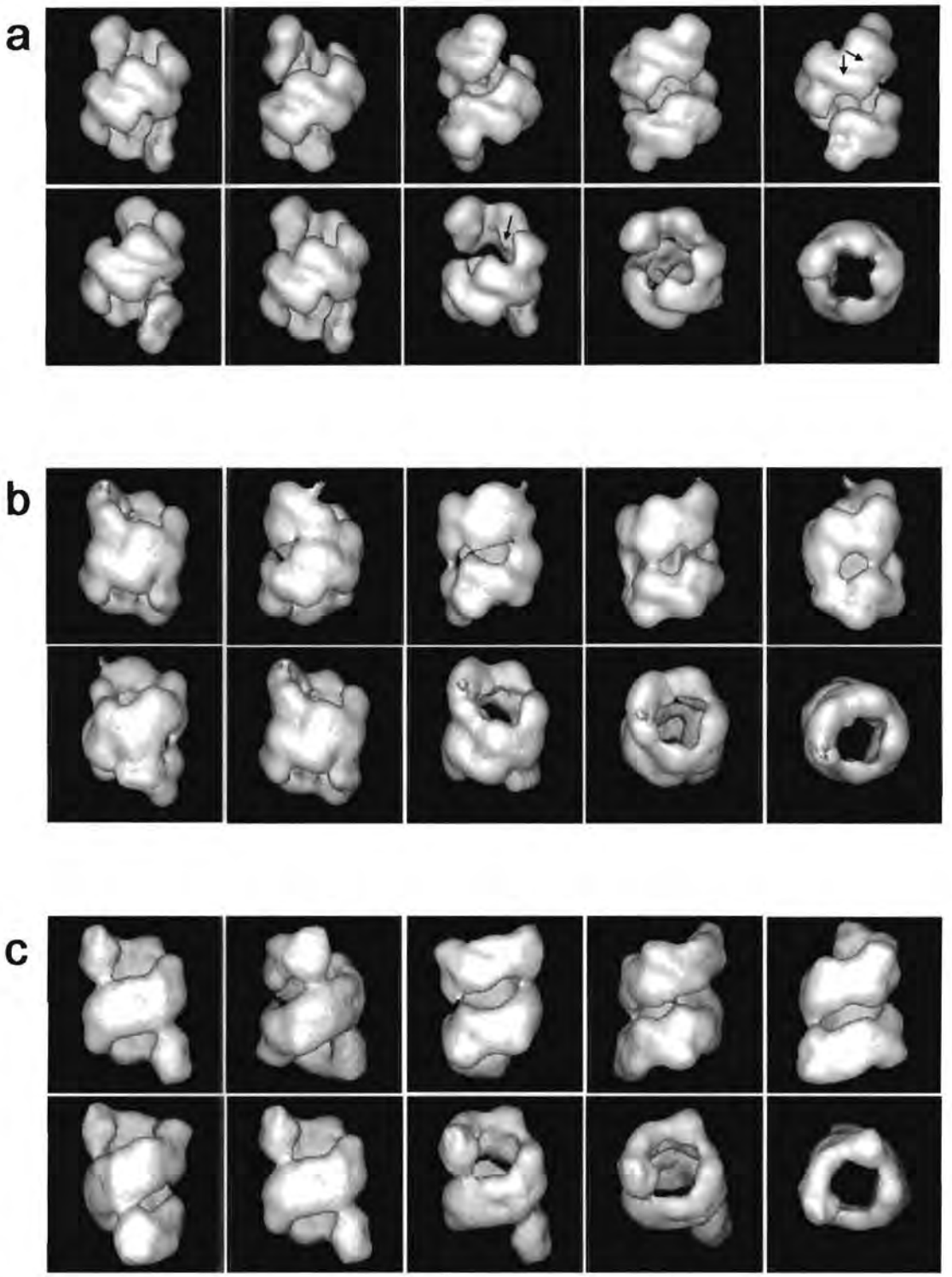

Figure 6.6. Final models rotated at 60 degree increments about the z-axis, and then at 30 degree increments about the y-axis. **(a)** Model 83 of recombinant *P.stutzeri* cyanide dihydratase. **(b)** Model 117 of recombinant *B.pumilus* C1 cyanide dihydratase. **(c)** Model 96 of native *B. pumilus* C1 cyanide dihydratase.

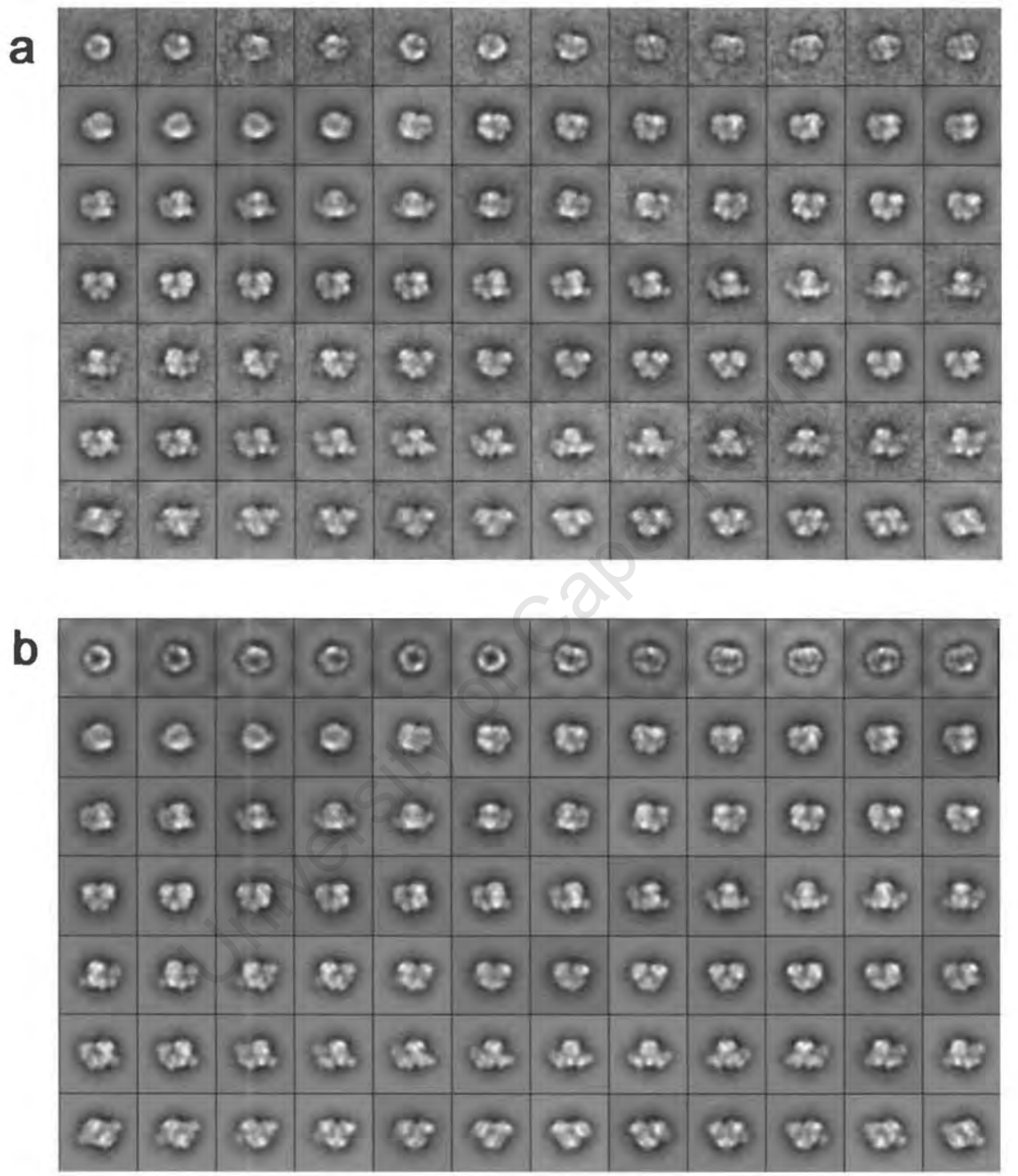

Figure 6.7 **(a)** Class averages used to generate model 83 of recombinant *P. stutzeri* cyanide dihydratase. **(b)** Corresponding projections of this model.

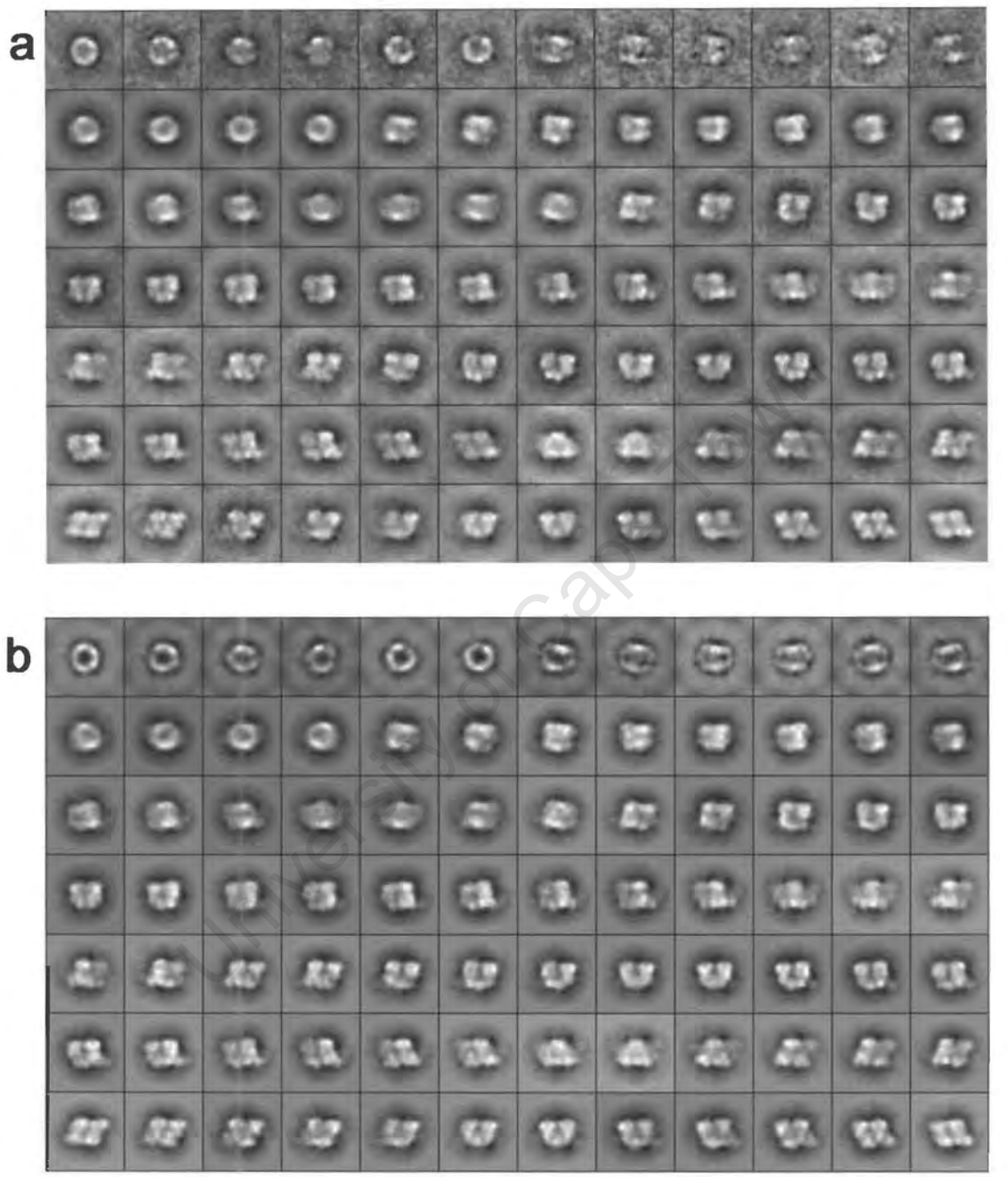

Figure 6.8. **(a)** Class averages used to generate model 117 of recombinant *B. pumilus* C1 cyanide dihydratase. **(b)** Projections of this model.

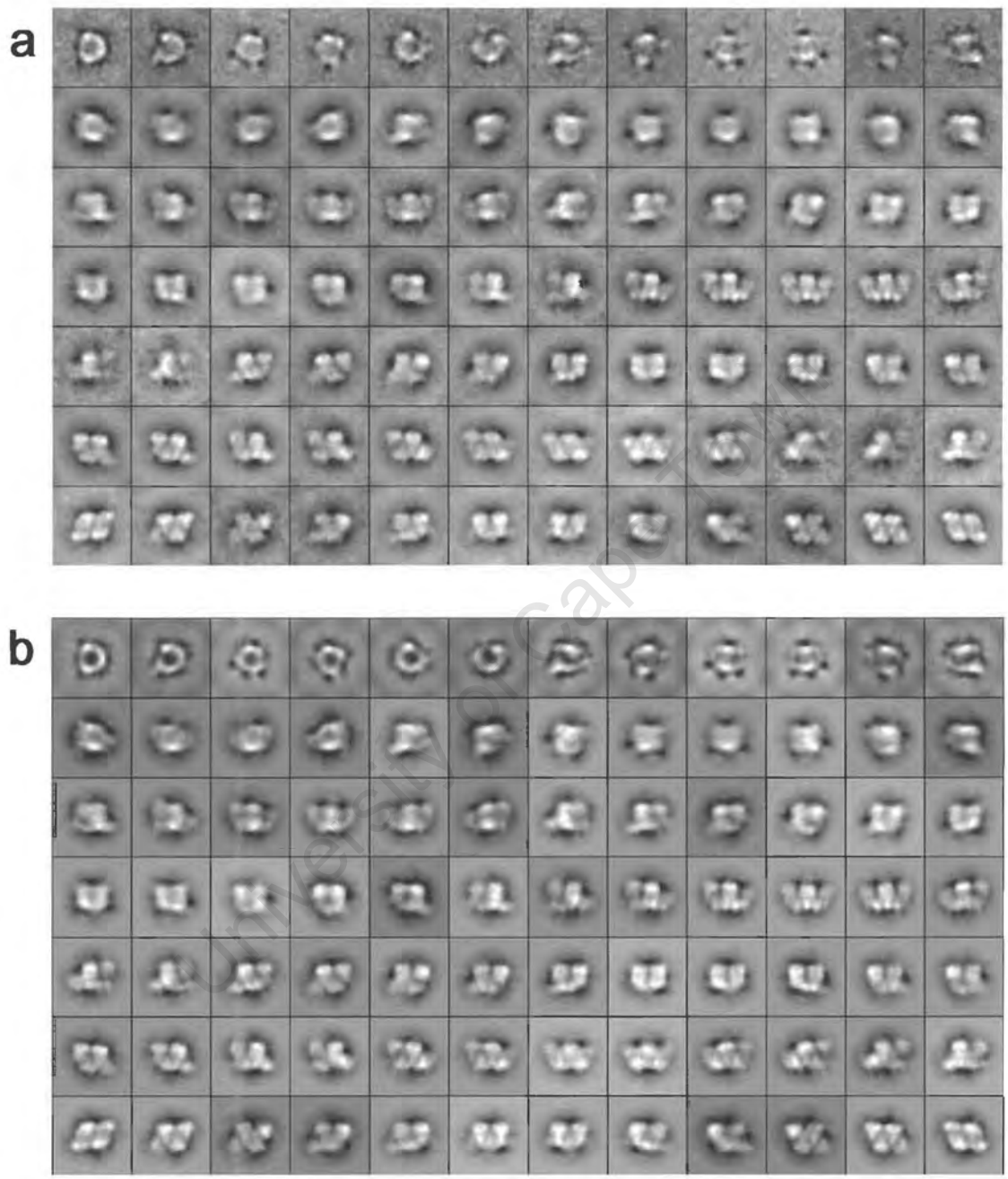

Figure 6.9. **(a)** Class averages used to generate model 96 of native *B. pumilus* cyanide dihydratase. **(b)** Projections of this model.

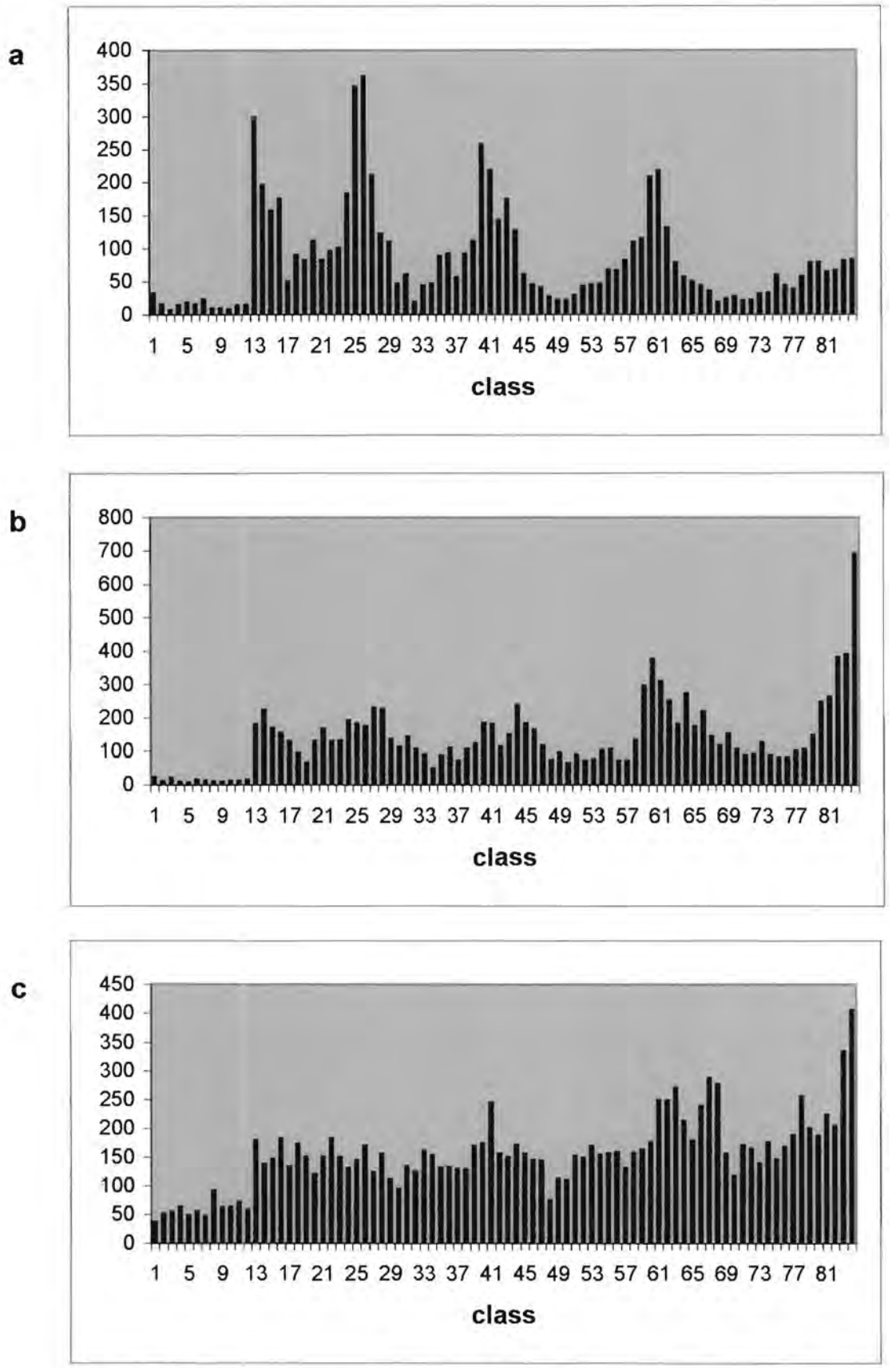

Figure 6.10. Numbers of images in each class for final reconstructions of **(a)** recombinant *P.stutzeri*, **(b)** recombinant *B. pumilus* and **(c)** native *B. pumilus* cyanide dihydratase.

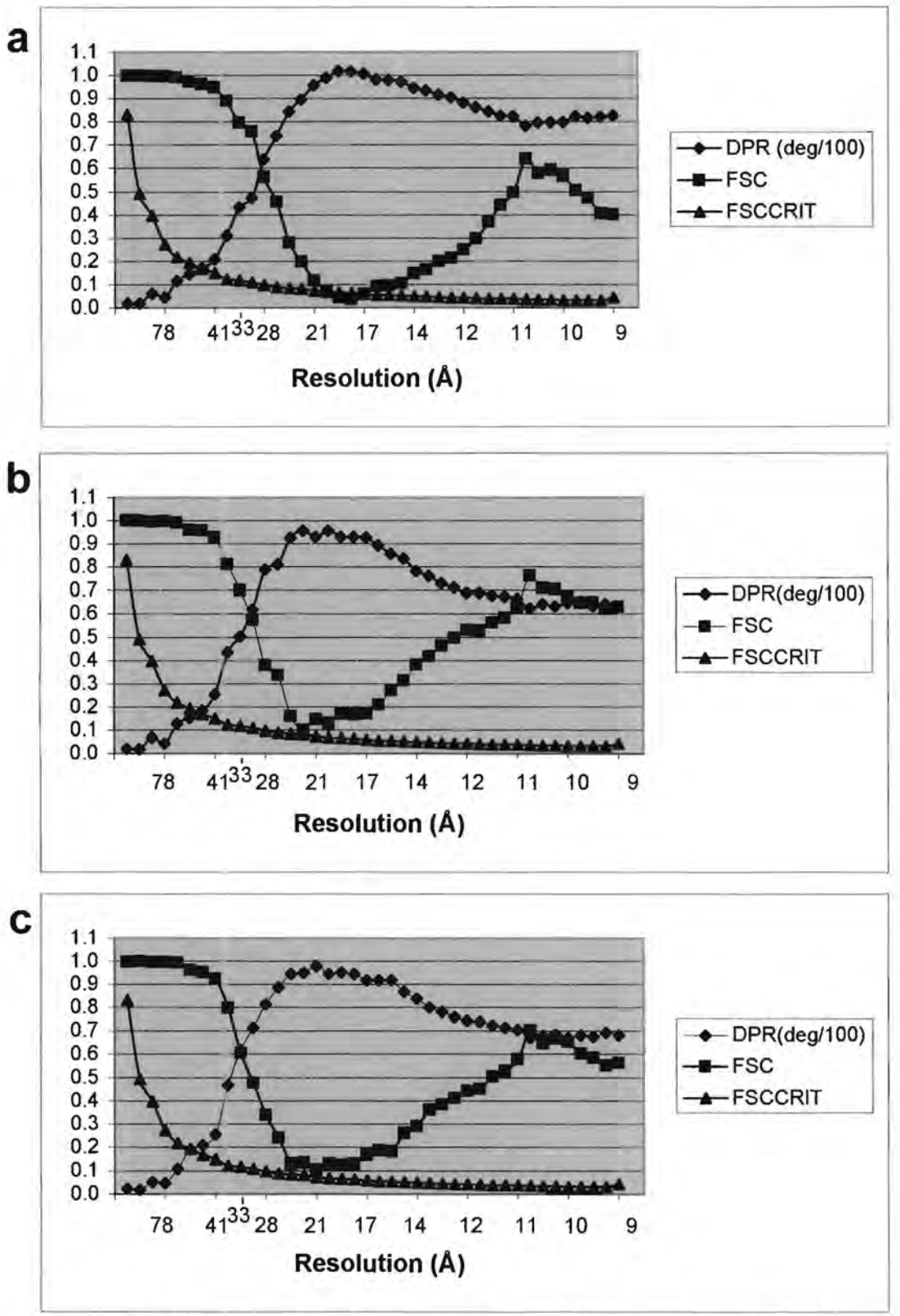

Figure 6.11. Resolution tests for models of **(a)** recombinant *P.stutzeri*, **(b)** recombinant *B. pumilus* and **(c)** native *B. pumilus* cyanide dihydratase. Differential Phase Residual (DPR) of 45 degrees or Fourier Shell Correlation (FSC) of 0.5 gives the approximate resolution of the model.

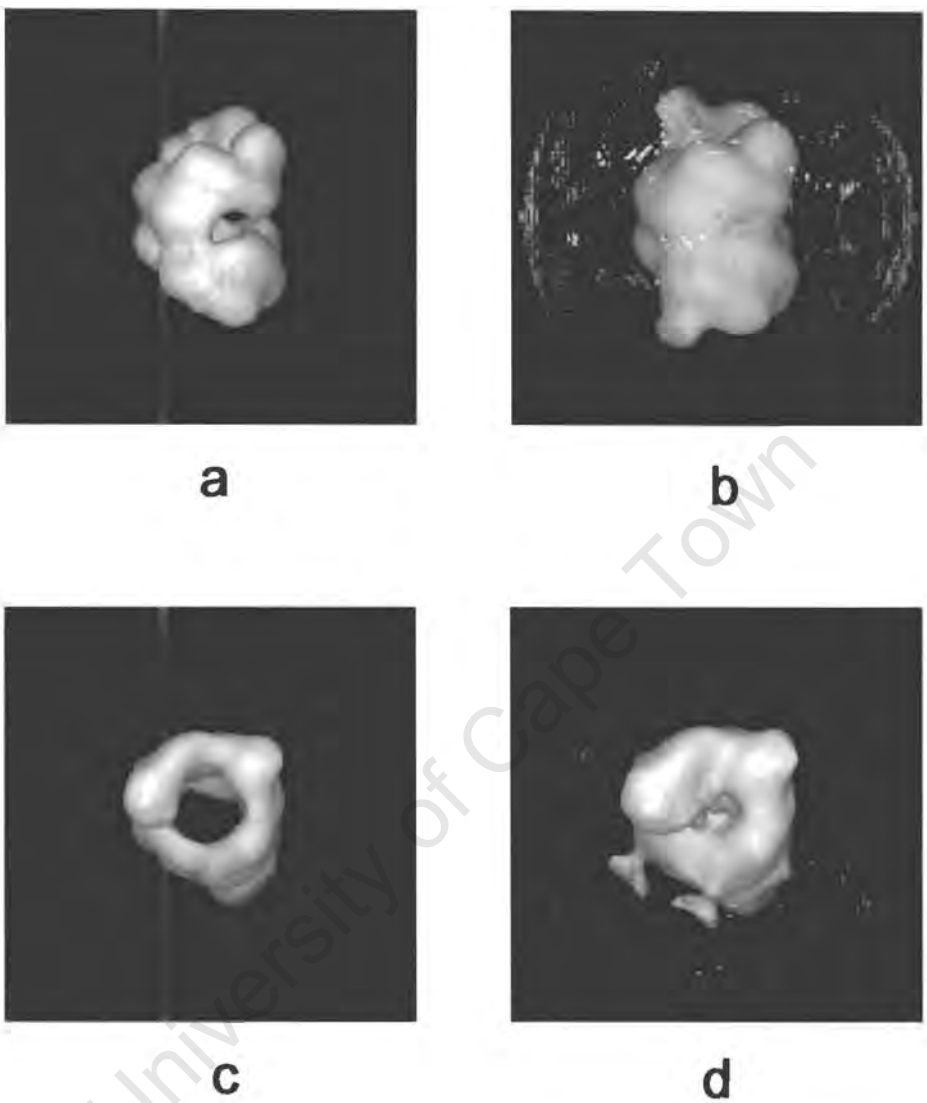

Figure 6.12. **(a,b)** Recombinant *B. pumilus* cyanide dihydratase with contour enclosing a volume of **(a)** 821nm^3 or **(b)** 1562 nm^3 **(c,d)** Native *B. pumilus* cyanide dihydratase with contour enclosing a volume of **(c)** 924nm^3 or **(d)** 1607nm^3

corresponding sites on other subunits, and displaying two prominent ridges (Figure 6.6 (c)). The overall dimensions of the structure are 19.8nm by 12.9 nm.

6.5 Conclusions

The structures of recombinant cyanide dihydratases of *P. stutzeri* AK61 and *B. pumilus* C1 and of native cyanide dihydratase of *B. pumilus* C1 have been solved to resolutions of 2.9, 3.2 and 3.4nm respectively. These structures clearly show the positions of the subunits and define two types of dimerisation interfaces. The complexes form short spirals of 14, 16 and 18 subunits respectively. It is not clear which of these differences are intrinsic and which are pH dependent, since the ambient pH for the three preparations was 8, 6 and 8 respectively.

Together with the known sizes of the polypeptides, these models give total molecular weights of 523kDa, 597kDa and 672kDa respectively for the *P. stutzeri* oligomer and the two observed forms of the *B. pumilus* enzyme oligomer. The previous estimate for the size of the the *B. pumilus* enzyme was 417kDa, as determined by gel filtration (Meyers *et al.*, 1993a).

A decrease in the helical radius is observed at the termini of the spiral, which is most pronounced in the model of the *P. stutzeri* enzyme. The significance of this observation is discussed in Chapter 8.

Two additional subunits are present at low occupancy in the structure of the recombinant *B. pumilus* enzyme, indicating weak association at the termini of the spiral.

Two unidentified regions of density are attached at low occupancy straddling the central dimer of the native *B. pumilus* enzyme. This may account for the slightly larger molecular weight of the native enzyme (observed in Chapter 3). It is conceivable that a small protein binds to the enzyme and that this protein is only present in the native organism.

Chapter 7. Structural transition in *B. pumilus* cyanide dihydratase

In this chapter, the *B. pumilus* cyanide dihydratase is shown to undergo a major structural transition from single particles to fibres upon dialysis with water. Factors inducing this transition are described.

7.1 Formation of fibres

The *B. pumilus* cyanide dihydratase was dialysed against distilled water, further diluted in distilled water and examined by electron microscopy. Quite unexpectedly, the removal of salt and buffer had a dramatic effect on the quaternary structure. The enzyme molecules assembled into long fibres several hundred nanometers in length. Formation of long fibres was observed in both the native and recombinant *B. pumilus* enzyme (Figure 7.1 (a) and (b)). The dialysed recombinant enzyme maintained this structure when diluted in 10mM citrate, 50mM NaCl pH 5.4 instead of water (Figure 7.1 (c)). Whereas visualisation by negative staining for single particles or for fibres in water was optimal at enzyme concentrations of 150 to 300μg/ml, for fibres in citrate it was much lower - around 20μg/ml.

7.2 Effects of NaCl concentration and pH

Purified native *B. pumilus* enzyme, at a concentration of 6mg/ml in 10mM TEA, 50mM NaCl pH 8, was diluted in buffers of various pH values (Figure 7.2). The enzyme was unstable in glycine at pH 2-3, formed fibres at pH 4.6-5.4 in acetate or citrate, and remained as single particles at pH 6 in MES or pH 8 in TEA. In every experiment the salt concentration was either 25 or 50mM, and the buffer concentration 10-20mM. Whereas pH was critical, ionic strength was not - for example, the enzyme formed fibres in 0.5 M NaCl at pH 5.4, thus discounting the possibility that dialysis against water promotes fibre formation simply by lowering the ionic strength.

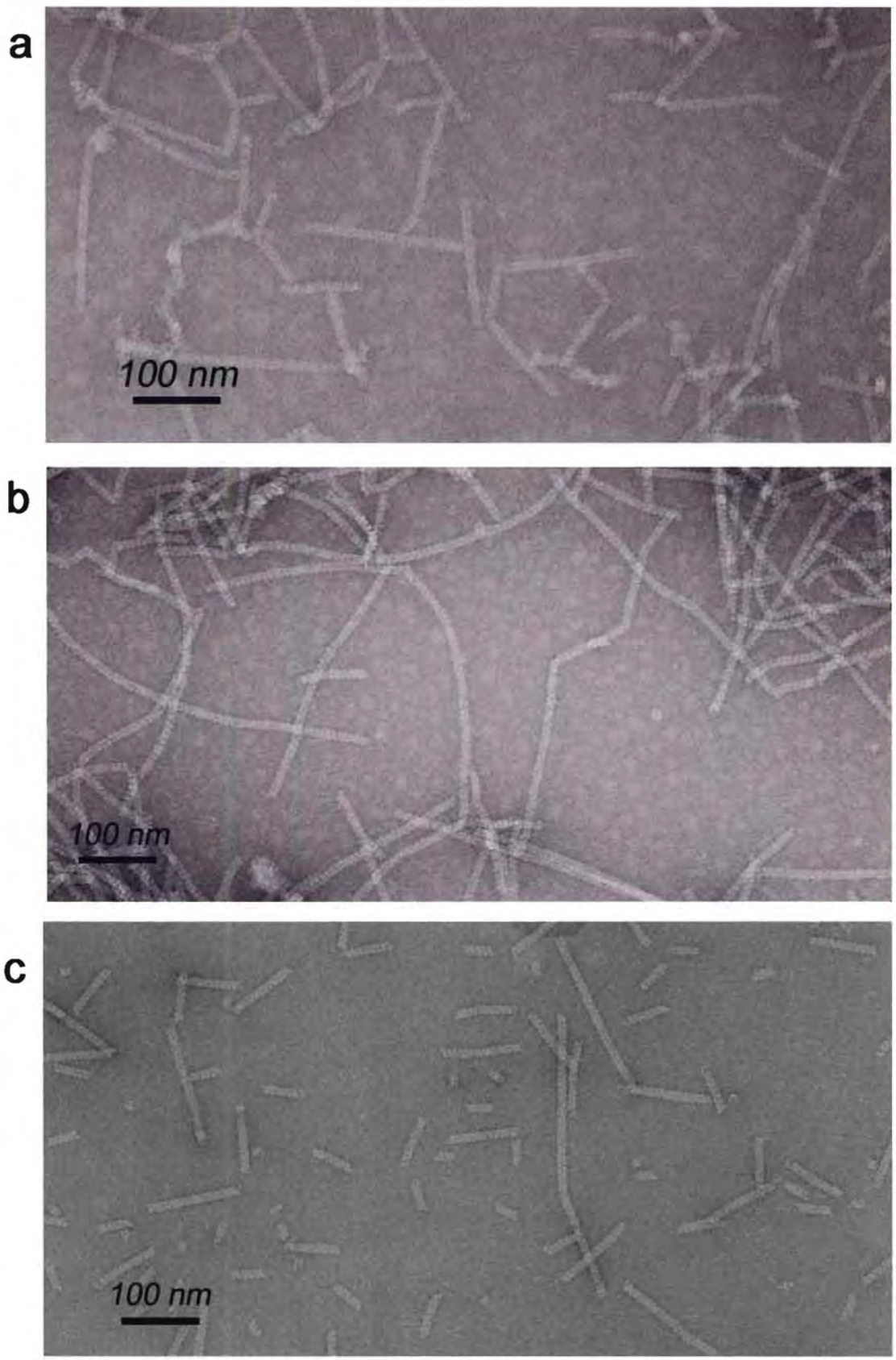

Figure 7.1. Negative stain electron micrographs of fibres obtained by dialysing purified **(a)** native and **(b,c)** recombinant *B. pumilus* cyanide dihydratase against distilled water. Prior to staining samples were diluted down in **(a,b)** distilled water; **(c)** 10mM citrate, 50mM NaCl pH 5.4.

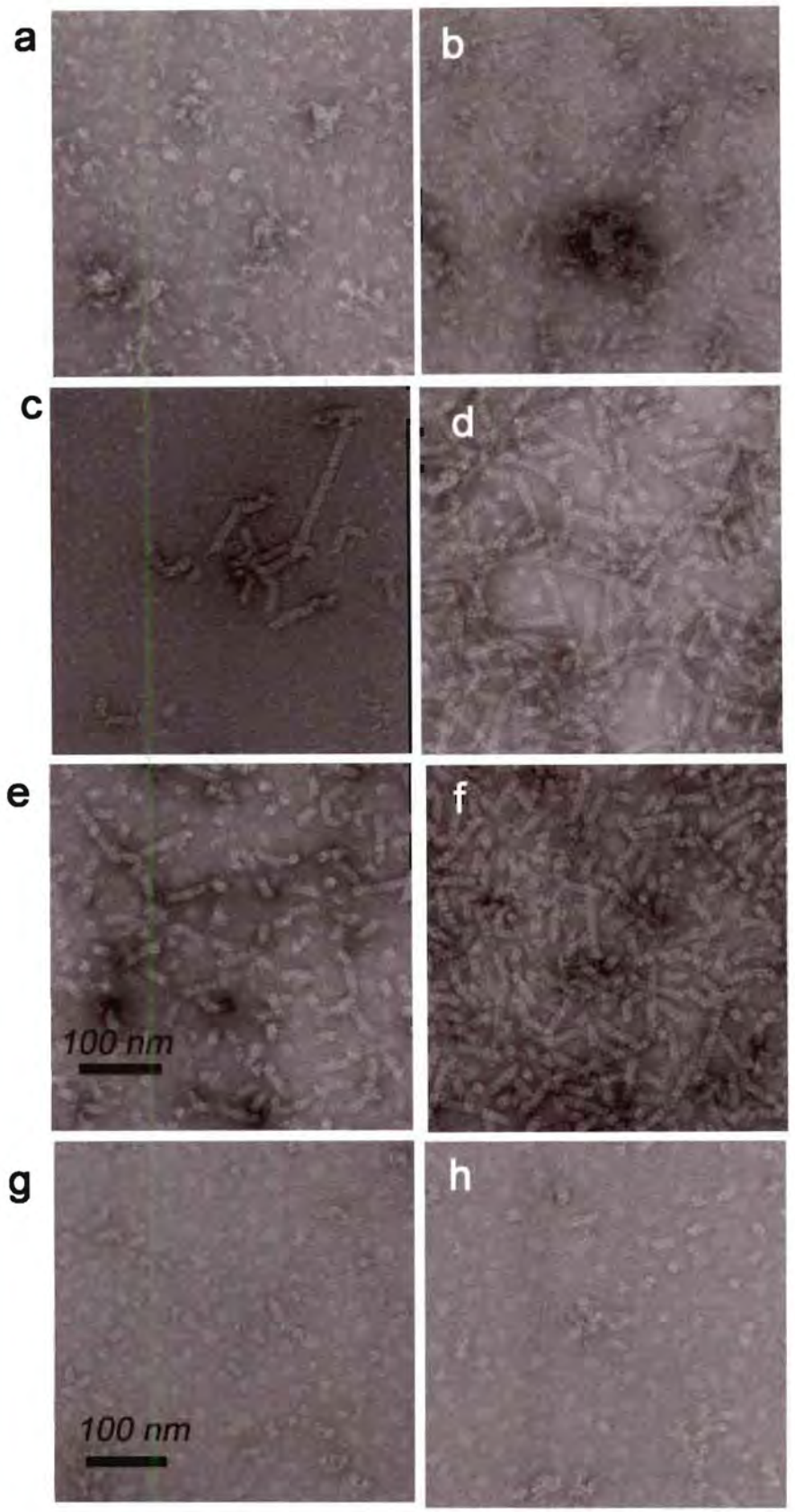

Figure 7.2. Negative stain electron micrographs of native *B. pumilus* cyanide dihydratase in 10mM TEA, 50mM NaCl, diluted 10-fold in buffers as follows. **(a)**: glycine, pH 2; **(b)**: glycine, pH 3; **(c)**: sodium acetate, pH 4.6; **(d)**: sodium acetate, pH 5; **(e)**: sodium citrate, pH 5.4; **(f)**: 10mM sodium citrate, 0.5 M NaCl, pH 5.4; **(g)**: MES, pH 6; **(h)**: 10mM TEA, 50mM NaCl, pH 8. Buffer concentrations were 20mM and [NaCl] = 25mM unless otherwise stated.

Purified recombinant *B. pumilus* enzyme was diluted in 10mM citrate, 360mM NaCl pH 5.4 and applied to the Sephacryl 300HR gel filtration column in the same buffer. The elution profile is compared in Figure 7.3 with the elution profile of blue dextran. Also shown is the elution profile for *P. stutzeri* cyanide dihydratase under the same conditions. Whereas the *Bacillus* enzyme eluted in the void volume, the *P. stutzeri* enzyme eluted well within the exclusion limit. This is compatible with the observation that the *B. pumilus* enzyme forms fibres under these conditions (Figure 7.3 (a)) whereas the *P. stutzeri* enzyme does not (Figure 7.3 (b)).

A series of micrographs was taken of the fibres which included the micrograph shown in Figure 7.1 (c). A helical reconstruction of the enzyme should be possible from these images, using a modified version of the single particle technique (Egelman, 2000). This was not attempted in the current study.

7.3 Conclusions

Under conditions of zero salt and buffer, or at pH 4-5.4 in the presence of salt, the cyanide dihydratase of *B. pumilus* C1 formed fibres of variable length. When the enzyme was first dialysed against distilled water and then diluted in either water or a buffer containing citrate pH 5.4, these fibres were several hundred nanometers in length. The formation of fibres was shown to be pH dependent. Denaturation occurred at pH 2-3, whereas single particles occurred at pH 6 or above. Fibre formation was shown to be salt independent, with fibres occurring in citrate pH 5.4 with either 25 or 500mM sodium chloride. The cyanide dihydratase of *P. stutzeri* did not form fibres under conditions that induced fibre formation in the *B. pumilus* enzyme.

Jandhyala in his PhD thesis (2002) produced an activity curve of recombinant, histidine-tagged *B. pumilus* cyanide dihydratase. Activity increases steadily with increasing pH in the range 5.0 to 7.0, with a shoulder of elevated activity at around 6.0. This suggests that fibre formation may enhance the activity of the enzyme. It would be interesting to investigate the effect of substrate or inhibitor binding on the transition from single particles to fibres.

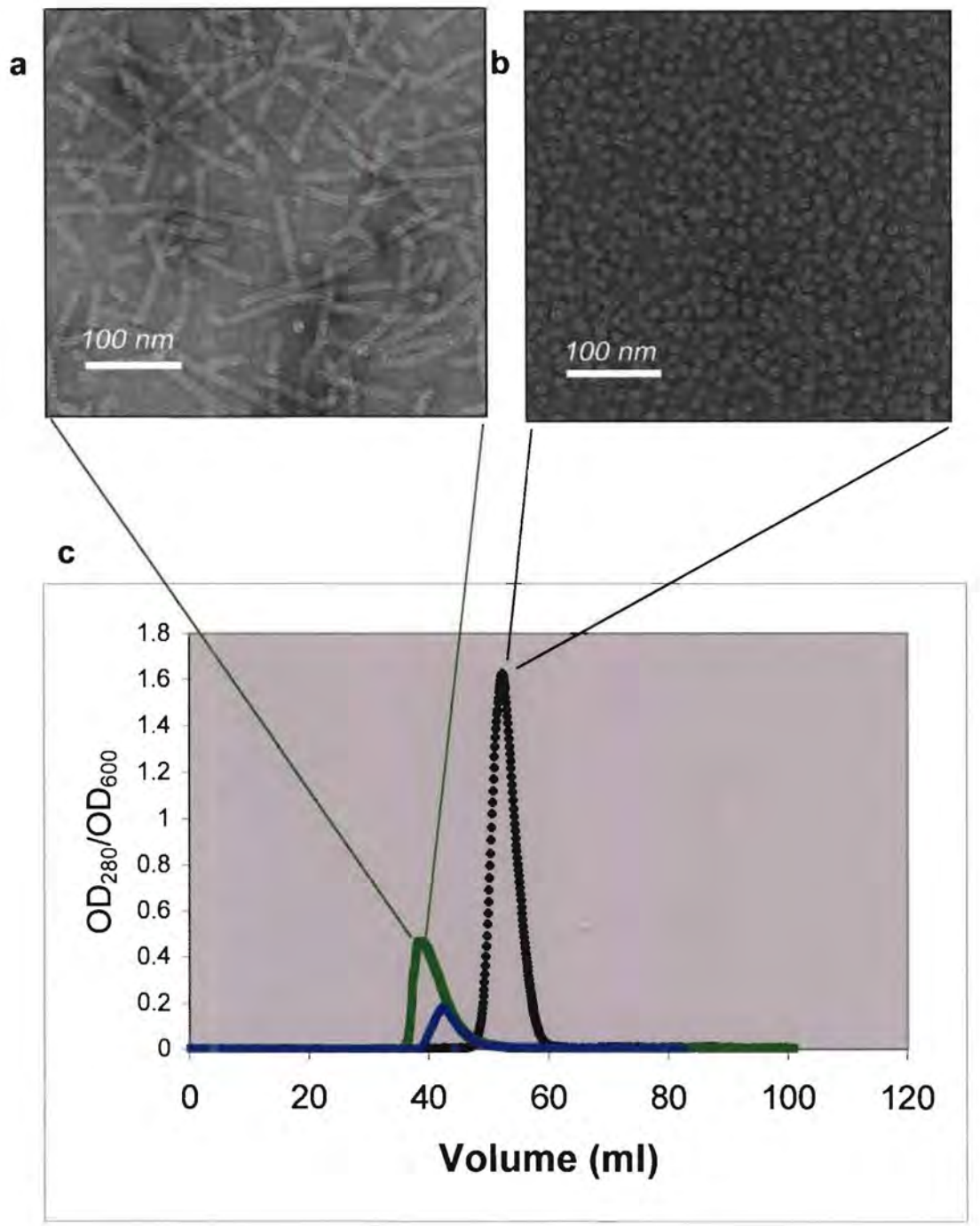

Fig 7.3. Electron micrographs of **(a)** recombinant *B. pumilus* and **(b)** recombinant *P. stutzeri* cyanide dihydratase after gel filtration in 10mM citrate, 360mM NaCl, pH 5.4. **(c)** Superimposed elution profiles. Blue dextran (blue circles); cyanide dihydratase of *B. pumilus* (green squares) and *P. stutzeri* (black diamonds).

Chapter 8. Discussion

8.1 Sequence comparison

The sequence of *B. pumilus* cyanide dihydratase (Jandhyala *et al.*, 2003), can now be compared with that of *P. stutzeri*. The full sequence is shown in Figure 8.1, aligned with sequences of *P. stutzeri* cyanide dihydratase, *G. sorghi* cyanide hydratase and the Nit domain of *C. elegans* NitFhit protein, using the programme GenThreader (Jones, 1999) to align the sequences on the basis of known and predicted secondary structure. The two cyanide dihydratase sequences are 77% identical at the amino acid level, while the cyanide hydratase and Nit sequences are respectively 32% and 15% identical to that of *B. pumilus* cyanide dihydratase. The *B. pumilus* sequence contains the presumptive cys-glu-lys catalytic residues (indicated in green). These sequences differ substantially at their C-termini. It is remarkable that despite such low sequence identity the proteins are predicted by GenThreader to share a common fold. One question that arises is whether the C-terminal extension plays a role in determining the distinct quaternary structures of these four enzymes. Another challenge will be to identify the residues that define substrate specificity.

8.2 The structures

The structures of cyanide dihydratases of *P. stutzeri* and *B. pumilus* have been solved at 2.9-3.4 nm resolution. The structure is a two-fold symmetric spiral consisting of 14 subunits in the *P. stutzeri* enzyme and 16 or 18 in the *B. pumilus* enzyme (depending on the source and preparation of the latter). Two types of interacting surfaces hold the complex together, and terminal subunits are positioned closer to the helical axis than are the two central subunits.

The crosslinking data given in Chapter 5 supports this model. In Figure 8.2 two types of interacting surfaces are indicated in red and orange. Subunits can conceivably be crosslinked across either the red or the orange contacts, or between closely positioned regions of alternate subunits such as the blue region of subunit J and the green region of subunit H in the diagram.

Figure 8.1. Alignment of amino acid sequences based on predicted and solved secondary structures, using the programme GenThreader (Jones, 1999). Sequences shown are the cyanide dihydratases of *Bacillus pumilus* C1 (Bpum) and *Pseudomonas stutzeri* AK61 (Pstu), the cyanide hydratase of the fungus *Gloeocercospora sorghi* (Gsor) and the Nit domain of the *Caenorhabditis elegans* NitFhit protein. Amino acid residues where the Bpum and Gsor sequences are identical, according to this alignment, are highlighted in yellow. The cys-glu-lys catalytic triad is highlighted in green.

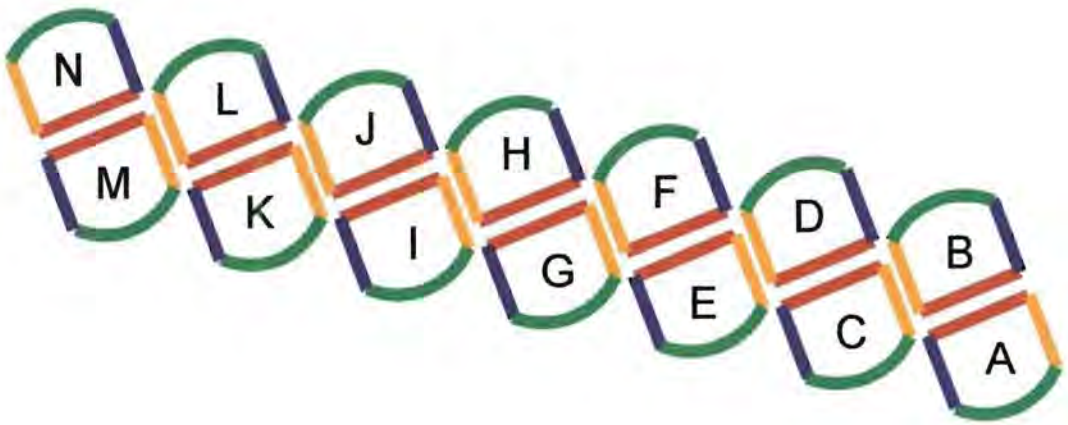

Figure 8.2. Schematic diagram of the subunit arrangement in *P. stutzeri* cyanide dihydratase.

It is thus possible to envisage at least three putative forms of crosslinked dimer, which differ in their contact points along the two polypeptide chains. This is illustrated in Figure 8.3, with polypeptide chains indicated in black and crosslinks in red (this diagram should be viewed qualitatively – the positions of crosslinks within the polypeptides are not known).

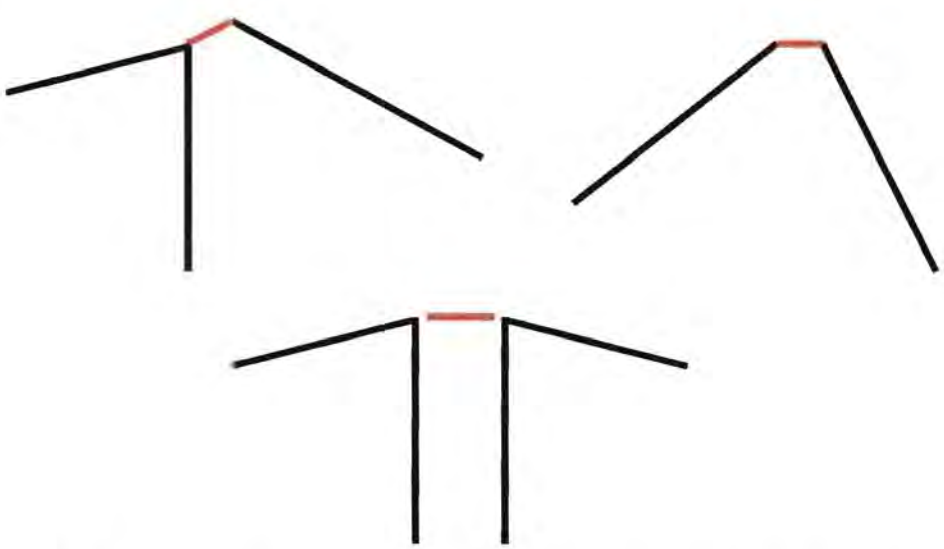

Figure 8.3. Schematic diagram suggesting three possible ways in which a pair of subunits may be crosslinked.

The gel of crosslinked *B. pumilus* cyanide dihydratase (Chapter 5) shows a triplet of bands of equal intensity in the position of a dimer. This indicates the presence of three distinct species of dimer that migrate through the pores in the polyacrylamide gel at different rates depending on where they have been crosslinked. It cannot be explained by different forms of incompletely denatured polypeptides (as was proposed for the monomers), since the predominant monomer band is much stronger than the subsidiary monomer bands.

The absence of a band in the trimer position can be understood if it is supposed that either the red or the orange interface (Figure 8.2) can be crosslinked more readily than the other. Crosslinking across only one of these interfaces would then occur throughout the spiral before crosslinking at other sites. This would lead to very little formation of crosslinked trimer, pentamer, heptamer and larger odd-numbered oligomers.

With the available data it is not possible to assign crosslinked species having five or more subunits (see Chapter 5). Nevertheless, the virtual absence of a crosslinked trimer is compelling evidence for preferential crosslinking at one type of interface, and fully supports the spiral model generated independently by single particle reconstruction.

8.3 Interpretation of the structures

The three-dimensional model immediately raises the question of why spiral assembly terminates at a defined length rather than at a range of different lengths. A possible mechanism can be inferred from the observation that the terminal subunits of the spiral are placed closer to the helical axis than are the central subunits. This breaking of helical symmetry may result from an accumulation of interactions across the groove of the spiral. The altered geometry at the termini of the growing spiral may preclude the addition of further subunits.

This could also account for the structural transition of *B. pumilus* cyanide dihydratase. The pH at which this occurs is between 5.4 and 6, which is similar to the pK_a of histidine (6.0). It is possible that a histidine residue forms an ionic interaction (either

attractive or repulsive) that will favour the restoration of helical symmetry only when this histidine is positively charged. If this is so, helical symmetry would be promoted at pH 5.4 and this could lead to indefinite extension of the spiral. The observation that this is a sharp transition is sensible for entropic reasons: the addition of many subunits would be associated with a large free energy change, and therefore would be driven forward as soon as the histidine residue becomes protonated.

The pH-dependent structural transition is observed in the *B. pumilus* enzyme but not in the *P. stutzeri* enzyme, despite the fact that the predicted sequences are 77% identical at the amino acid level. One possible explanation for this is that the *P. stutzeri* enzyme lacks either the histidine residue or its charged partner involved in the breaking of helical symmetry. Alternatively, one could observe that distortion of helical symmetry (distance from a terminal subunit to the helical axis) is more pronounced in the *P. stutzeri* enzyme than in the *B. pumilus* enzyme. Accordingly, the *P. stutzeri* enzyme only forms oligomers of 14 subunits, whereas the *B. pumilus* enzyme forms 16-mers or 18-mers. Restoration of helical symmetry would require a substantially greater structural change in the former enzyme than in the latter, and the protonation of a histidine residue may not be sufficient to overcome other charge-charge interactions that may be present in the *P. stutzeri* enzyme.

It is puzzling that there are 16 subunits in the model of recombinant *B. pumilus* cyanide dihydratase and 18 subunits in the model of the native enzyme at pH 8. Given that the structural transition takes place at pH 5.4, one would expect if anything the addition of further subunits at pH 6.

The appearance of two small regions of density proximal to the central subunits in native *B. pumilus* cyanide dihydratase is curious. These partially attached masses may be small proteins that bind to the enzyme complex in the native organism but not when the enzyme is expressed in *E. coli*. Given that the role of cyanide dihydratase in the native organism is unknown, it is impossible to speculate on the functional significance of any such protein-protein interactions.

8.4 Biological significance

The quaternary structure of cyanide dihydratase provides an explanation for the wide range of sizes of nitrilases reported in the literature. At one extreme are the cyanide hydratases, which form complexes of several megadaltons. These are predicted to form perfectly regular spirals of indefinite length, as seen already in the *B. pumilus* cyanide dihydratase at pH 5.4 and recently confirmed for the *G. sorghi* cyanide hydratase by Price *et al.*, 2002. Intermediate sizes of nitrilases range from 6 to 16 subunits. These enzymes are predicted to be spiral structures in which the extent and strength of interactions breaking helical symmetry dictate the length of the spiral. The existence of a hexamer is not readily explained by this mechanism as steric hindrance is unlikely to play a role in such a short spiral. There is only one representative of this type, the arylacetonitrilase of *Alcaligenes faecalis* JM3.

There is another report in the literature of a spiral homo-oligomeric structure of defined length, namely the giant protease TPP II of Drosophila (Rockel *et al.*, 2002). This structure consists of two intertwined spiral assemblies, and apparently has a different mechanism of termination.

If the spiral structure is indeed a common structural motif amongst nitrilases, this raises the question as to why it has been conserved across a diverse set of organisms. One possibility is that nitrilases act as a protein scaffold in the cell, upon which other proteins can dock. For instance, it is possible that enzymes in the same metabolic pathway as a nitrilase may bind to the scaffold and in so doing increase the efficiency of metabolism. Another possibility is that oligomerisation is regulated *in vivo* and that this modulates the activity of the enzyme through the conformation changes transmitted to the active site. Support for this is limited to three Rhodococcal aromatic nitrilases which oligomerise in the presence of substrate (Harper, 1977; Stevenson, 1992; Nagasawa *et al.*, 2000). This is probably not a general phenomenon, as the cyanide dihydratases only occur as large oligomers *in vitro*. However it remains to be seen whether unidentified factors that are present *in vivo* control the process of association and dissociation, and in particular whether the structural transition in *B. pumilus* (presented in Chapter 7) has any functional significance.

8.5 Future work

Atomic structures exist for two nitrilase homologues, Nit and DCase (Nakai *et al.*, 2000; Wang *et al.*, 2001; Brenner, 2002). With these it will theoretically be possible to fit the polypeptide backbone of either *B. pumilus* or *P. stutzeri* cyanide dihydratase into the molecular envelope of the low resolution model by identifying conserved structural elements. Such modelling could provide more detailed insights into the mechanism of termination of the spiral. It will be of particular interest to locate the carboxy termini of the polypeptides within the complex. As a highly variable region (see Figure 8.1), this part of the polypeptide may influence the degree of oligomerisation of nitrilases. Residues involved in intersubunit contacts may be identified through site-directed mutagenesis. These mutants will provide evidence as to whether full assembly of the complex is necessary for activity.

The outcome of this work invites similar studies to be carried out on other nitrilases that are oligomeric (see Table 1.2). Of particular interest would be the nitrilases of *R. rhodochrous* sp. NCIMB 11216, *R. rhodochrous* J1 and *Rhodococcus* ATCC 39484. The solutions of these structures by single particle reconstruction is feasible, and would provide further insights into the formation and flexibility of this novel quaternary structure.

References

Almatawah QA, Cramp R and Cowan DA (1999) Characterization of an inducible nitrilase from a thermophilic bacillus. *Extremophiles* **3,** 283-291.

Bandyopadathy AK, Nagasawa T, Asano Y, Fujishiro K, Tani Y and Yamada H (1986) Purification and characterization of benzonitrilases from *Arthrobacter* sp. strain J-1. *Applied and Environmental Microbiology* **51**, 302-306.

Banerjee A, Sharma R and Banerjee UC (2002) The nitrile-degrading enzymes: current status and future prospects. *Applied Microbiology and Biotechnology* **60,** 33-44.

Barclay M, Tett VA and Knowles CJ (1998) Metabolism and enzymology of cyanide/metallocyanide biodegradation by *Fusarium solani* under neutral and acidic conditions. *Enzyme and Microbial Technology* **23**, 321-330.

Bartling D, Seedorf M, Schmidt RC and Weiler EW (1994) Molecular characterization of two cloned nitrilases from *Arabidopsis thaliana*: key enzymes in biosynthesis of the plant hormone indole-3-acetic acid. *Proceedings of the National Academy of Sciences U S A* **91**, 6021-6025.

Bengis-Garber C and Gutman AL (1989) Selective hydrolysis of dinitriles into cyano-carboxylic acids by *Rhodococcus rhodochrous* NCIB 11216. *Applied Microbiology and Biotechnology* **32**, 11-16.

Bhalla T, Miura A, Wakamoto A, Ohba Y and Furuhashi K (1992) Asymmetric hydrolysis of α-aminonitrilase to optically active amino acids by a nitrilase of *Rhodococcus rhodochrous* PA-34. *Applied Microbiology and Biotechnology* **37**, 184-190.

Bollag DM and Edelstein SJ (1991) Protein Methods. *Wiley-Liss, Inc., New York*, 96-115.

Bradford, M. (1976) A rapid and sensitive method for the quantitation of microgram quantities of protein utilizing the principle of protein-dye binding. *Analytical Biochemistry*. **72,** 248-254.

Brenner C (2002) Catalysis in the nitrilase superfamily. *Current Opinion in Structural Biology* **12**, 775-782.

Brown DT, Turner PD and O'Reilly C (1995) Expression of the cyanide hydratase enzyme from *Fusarium lateritium* in *Escherichia coli* and identification of an essential cysteine residue. *FEMS Microbiology Letters* **134,** 143-146.

Chen CY, Chiu WC, Liu JS, Hsu WH and Wang WC (2003) Structural basis for catalysis and substrate specificity of *Agrobacterium radiobacter* N-carbamoyl-D-amino-acid amidohydrolase. *Journal of Biological Chemistry*, epub ahead of print.

Cluness MJ, Turner PD, Clements E, Brown DT and O'Reilly C (1993) Purification and properties of cyanide hydratase from *Fusarium lateritium* and analysis of the corresponding chy1 gene. *Journal of General Microbiology* **139**, 1807-1815.

Crowther, R. A., Henderson, R. and Smith, J. M. (1996) MRC image processing programs. *Journal of Structural Biology* **116**, 9-16.

Dadd MR, Claridge TD, Walton R, Pettman AJ and Knowles CJ (2001) Regioselective biotransformation of the dinitrile compounds 2-, 3- and 4-(cyanomethyl) benzonitrile by the soil bacterium *Rhodococcus rhodochrous* LL100-21. *Enzyme and Microbial Technology* **29,** 20-27.

Davies GE and Stark GR (1970) Use of dimethyl suberimidate, a cross-linking reagent, in studying the subunit structure of oligomeric proteins. *Proceedings of the National Academy of Sciences U S A.* **66**, 651-656.

Dubey SK and Holmes DS (1995) Biological cyanide destruction mediated by microorganisms. *World Journal of Microbiology and Biotechnology* **11**, 257-265.

Effenberger F and Osswald S (2001) Selective hydrolysis of aliphatic dinitriles to monocarboxylic acids by a nitrilase from *Arabidopsis thaliana. Synthesis* 1866-1872.

Egelman E (2000) A robust algorithm for the reconstruction of helical filaments using single particle methods. *Ultramicroscopy* **85,** 225-234.

Farnaud S, Tata R, Sohi MK, Wan T, Brown PR and Sutton BJ (1999) Evidence that cysteine-166 is the active-site nucleophile of Pseudomonas aeruginosa amidase: crystallization and preliminary X-ray diffraction analysis of the enzyme. *Biochemical Journal* **340,** 711-714.

Fisher FB and Brown JS (1952) Colorimetric determination of cyanide in stack gas and waste water. *Analytical Chemistry* **24**, 1440-1444.

Frank J, Radermacher M, Penczek P, Zhu J, Li Y, Ladjadj M and Leith A (1996a) SPIDER and WEB: Processing and visualization of images in 3D electron microscopy and related fields. *Journal of Structural Biology* **116,** 190-199.

Frank J (1996b) Three-dimensional electron microscopy of macromolecular assemblies. *Academic Press, San Diego*, 12-246.

Fry WE and Munch DC (1975). Hydrogen cyanide detoxification by *Gloeocercospora sorghi. Physiological Plant Pathology* 7, 23-33.

Goldlust A and Bohak Z (1989) Induction, purification, and characterization of the nitrilase of *Fusarium oxysporum* f. sp. *melonis. Biotechnology and Applied Biochemistry* **11,** 581-601.

Gradley ML and Knowles CJ (1994) Asymmetric hydrolysis of chiral nitriles by *Rhodococcus rhodochrous* NCIMB 11216 nitrilase. *Biotechnology Letters* **16**, 41-46.

Harper DB (1977a) Microbial metabolism of aromatic nitriles. Enzymology of C-N cleavage by *Nocardia* sp. (Rhodococcus group) N.C.I.B. 11216. *Biochemical Journal* **165**, 309-319.

Harper DB (1977b) Fungal degradation of aromatic nitriles. Enzymology of C-N cleavage by *Fusarium solani*. *Biochemical Journal* **167**, 685-92.

Harper DB (1985) Characterization of a nitrilase from *Nocardia* sp. (Rhodochrous group) N.C.I.B. 11215, using *p*-hydroxybenzonitrile as sole carbon source. *International Journal of Biochemistry*, **17**, 677-83.

Harauz G and van Heel M (1986) Exact filters for general geometry three dimensional reconstruction. *Optik* **73**, 146-156.

Hook RH and Robinson WG (1964) Ricinine nitrilase II. Purification and properties. *Journal of Biological Chemistry* **239**, 4263-4267 (see also Robinson and Hook, 1964).

Hoyle AJ, Bunch AW, and Knowles CJ (1998) The nitrilases of *Rhodococcus rhodochrous* NCIMB 11216. *Enzyme and Microbial Technology* **23**, 475-482.

Ingvorsen K, Højer-Pedersen B and Godtfredsen SE (1991) Novel cyanide hydrolysing enzyme from *Alcaligenes xylosoxidans* subsp. *denitrificans*. *Applied and Environmental Microbiology* 57, 1783-1789.

Jandhyala DM (2002) Cyanide degrading nitrilases for detoxification of cyanide containing waste waters. PhD thesis, University of Houston, 77-78.

Jandhyala D, Berman MN, Meyers PR, Sewell BT, Willson RC and Benedik MJ (2003) CynD, the cyanide dihydratase from *Bacillus pumilus*: Gene cloning and structural studies. *Applied and Environmental Microbiology*, **69**, 4794-4805.

Jones DT (1999) GenTHREADER: an efficient and reliable protein fold recognition method for genomic sequences. *Journal of Molecular Biology* **287**, 797-815.

Joyeux L and Penczek PA (2002) Efficiency of 2D alignment methods. *Ultramicroscopy* **92**, 33-46.

Kobayashi M, Nagasawa T and Yamada H (1988) Regiospecific hydrolysis of dinitrile compounds by nitrilase from *Rhodococcus rhodochrous* J1. *Applied Microbiology and Biotechnology* **29**, 231-233.

Kobayashi M, Nagasawa T and Yamada H (1989) Nitrilase of *Rhodococcus rhodochrous* J1. Purification and characterization. *European Journal of Biochemistry* **182**, 349-356.

Kobayashi M, Yanaka N, Nagasawa T and Yamada H (1990a) Purification and characterization of a novel nitrilase of *Rhodococcus rhodochrous* K22 that acts on aliphatic nitriles. *Journal of Bacteriology* **172**, 4807-4815.

Kobayashi M, Yanaka N, Nagasawa T and Yamada H (1990b) Monohydrolysis of an aliphatic dinitrile compound by nitrilase from *Rhodococcus rhodochrous* K22. *Tetrahedron* **46**, 5587-5590.

Kobayashi M, Komeda H, Yanaka N, Nagasawa T and Yamada H (1992a) Nitrilase from *Rhodococcus rhodochrous* J1. Sequencing and overexpression of the gene and identification of an essential cysteine residue. *Journal of Biological Chemistry*. **267**, 20746-20751.

Kobayashi M, Yanaka N, Nagasawa T and Yamada H (1992b) Primary structure of an aliphatic nitrile-degrading enzyme, aliphatic nitrilase, from *Rhodococcus rhodochrous* K22 and expression of its gene and identification of its active site residue. *Biochemistry* **31**, 9000-9007.

Kobayashi M, Izui H, Nagasawa T and Yamada H (1993) Nitrilase in biosynthesis of the plant hormone indole-3-acetic acid from indole-3-acetonitrile: cloning of the *Alcaligenes* gene and site-directed mutagenesis of cysteine residues. *Proceedings of the National Academy of Sciences U S A* **90**, 247-251.

Kobayashi M and Shimizu S (1994) Versatile nitrilases: Nitrile-hydrolysing enzymes. *FEMS Microbiology letters* **120**, 217-224.

Kobayashi M, Goda M and Shimizu S (1998) Nitrilase catalyzes amide hydrolysis as well as nitrile hydrolysis. *Biochemical and Biophysical Research Communications* **253,** 662-666.

Laemmli UK (1970) Cleavage of structural proteins during the assembly of the head of bacteriophage T4. *Nature* **227,** 680-685.

Layh N, Parratt J and Willetts A (1998) Characterization and partial purification of an enantioselective arylacetonitrilase from *Pseudomonas fluorescens* DSM 7155. *Journal of Molecular Catalysis B: Enzymatic* **5**, 467-474.

Lévy-Schil S, Soubrier F, Crutz-Le Coq AM, Faucher D, Crouzet J and Pétré D (1995) Aliphatic nitrilase from a soil-isolated *Comamonas testosteroni* sp.: gene cloning and overexpression, purification and primary structure. *Gene* **161**, 15-20.

Mahadevan S and Thimann KV (1964) Nitrilase II. Substrate specificity and possible mode of action. *Archives of Biochemistry and Biophysics* **107**, 62-68.

Meyers PR, Gokool P, Rawlings DE and Woods DR (1991) An efficient cyanide-degrading *Bacillus pumilus* strain. *Journal of General Microbiology* **137**, 1397-1400.

Meyers P, Rawlings DE, Woods DR and Lindsey GG (1993a) Isolation and characterization of a cyanide dihydratase from *Bacillus pumilus* C1. *Journal of Bacteriology* **175**, 6105-6112.

Meyers PR (1993b) Cyanide degradation by *Bacillus pumilus* C1: Cellular and Molecular Characterization. PhD thesis, University of Cape Town.

Mitchell CG, Anderson SC and el-Mansi EM (1995) Purification and characterization of citrate synthase isoenzymes from *Pseudomonas aeruginosa*. *Biochemical Journal* **309,** 507-511.

Nakai T, Hasgawa T, Yamashita E, Yamamoto M, Kamasuka T, Ueki T, Nanba H, Ikenaka Y, Takahashi S, Sato M and Tsukihara T (2000) Crystal structure of *N*-carbamyl-D-amino acid amidohydrolase with a novel catalytic framework common to amidohydrolases. *Structure* **8,** 729-737.

Nagasawa T, Mauger J and Yamada H (1990) A novel nitrilase, arylacetonitrilase, of *Alcaligenes faecalis* JM3. Purification and characterization. *European Journal of Biochemistry.* **194**, 765-772.

Nagasawa T and Yamada H (1995) Microbial production of commodity chemicals. *Pure and Applied Chemistry* **67,** 1241-1256.

Nagasawa T, Wieser M, Nakamura T, Iwahara H, Yoshida T and Gekko K (2000) Nitrilase of *Rhodococcus rhodochrous* J1 - Conversion into the active form by subunit association. *European Journal of Biochemistry* **267**, 138-144.

Nolan L, Harnedy P, Hearne A and O'Reilly C (2003) The cyanide hydratase enzyme of *Fusarium lateritium* also has nitrilase activity. *FEMS Microbiology Letters* **221**, 161-165.

Novo C, Farnaud S, Tata R, Clemente A and Brown PR (2002) Support for a three-dimensional structure predicting a Cys-Glu-Lys catalytic triad for *Pseudomonas aeruginosa* amidase comes from site-directed mutagenesis and mutations altering substrate specificity. *Journal of Biochemistry* **365**, 731-738.

Osswald S, Wajant H and Effenberger F (2002) Characterization and synthetic applications of recombinant AtNIT1 from *Arabidopsis thaliana*. *European Journal of Biochemistry* **269**, 680-687.

Pace HC, Hodawadekar SC, Draganescu A, Huang J, Bieganowski P, Pekarsky Y, Croce CM and Brenner C (2000) Crystal structure of the worm NitFhit Rosetta Stone protein reveals a Nit tetramer binding two Fhit dimers. *Current Biology* **10**, 907-917.

Pace HC and Brenner C (2001) The nitrilase superfamily: classification, structure and function. *Genome Biology* **2**, reviews0001.1-0001.9

Penczek P, Rademacher M, and Frank J (1992) Three-dimensional reconstruction of single particles embedded in ice. *Ultramicroscopy* **40**, 33-53.

Penczek P, Zhu J and Frank J (1996) A common-lines based method for determining orientations for N>3 particle projections simultaneously. *Ultramicroscopy* **63**, 205-218.

Piotrowski M, Schonfelder S and Weiler EW (2001) The *Arabidopsis thaliana* isozyme NIT4 and its orthologs in tobacco encode beta-cyano-L-alanine hydratase/nitrilase. *Journal of Biological Chemistry* **276**, 2616-2621.

Price B, Chang P, Jandhyala DM, Benedik M and Sewell BT (2002) The quaternary structure of *Gloeocercospora sorghi* nitrilase (cyanide hydratase) as revealed by negative staining. *Proceedings of the 15th International Congress on Electron Microscopy*, 565-566.

Richards FM (1974) The interpretation of protein structures: total volume, group volume distributions and packing density *Journal of Molecular Biology* **82**, 1-14.

Robinson WG and Hook RH (1964) Ricinine nitrilase I. Reaction product and substrate specificity. *Journal of Biological Chemistry* **239,** 4257-4262.

Rockel B, Peters J, Kuhlmorgen B, Glaeser RM and Baumeister W (2002) A giant protease with a twist: the TPP II complex from *Drosophila* studied by electron microscopy. *EMBO Journal* **21,** 5979-5984.

Romão MJ, Turk D, Gomis-Rüth F-X and Huber R (1992) Crystal structure analysis, refinement and enzymatic reaction mechanism of *N*-carbamoylsarcosine amidohydrolase from *Arthrobacter* sp. at 2.0 Å resolution. *Journal of Molecular Biology* **226**, 1111-1130.

Stalker DM and McBride KE (1987) Cloning and Expression in *Escherichia coli* of a *Klebsiella ozaenae* plasmid-borne gene encoding a nitrilase specific for the herbicide Bromoxynil. *Journal of Bacteriology* **169**, 955-960.

Stalker DM, Malyj LD and McBride KE (1988a) Purification and properties of a nitrilase specific for the herbicide bromoxynil and corresponding nucleotide sequence analysis of the *bxn* gene. *Journal of Biological Chemistry* **263** 6310-4.

Stalker DM, McBride KE and Malyj LD (1988b) Herbicide resistance in transgenic plants expressing a bacterial detoxification gene. *Science* **242**, 419-423.

Stevenson DE, Feng R and Storer AC (1990) Detection of covalent enzyme-substrate complexes of nitrilase by ion-spray mass spectroscopy. *FEBS Letters* **277**, 112-114.

Stevenson DE, Feng R, Dumas F, Groleau D, Mihoc A and Storer AC (1992) Mechanistic and structural studies on *Rhodococcus* ATCC 39484 nitrilase. *Biotechnology and Applied Biochemistry* **15**, 283-302.

Thimann KV and Mahadevan S (1964) Nitrilase I. Occurrence, preparation, and general properties of the enyzme. *Archives of Biochemistry and Biophysics* **105,** 133-141 (see also Mahadevan and Thimann (1964)).

Tong EK and Duckworth HW (1975) The quaternary structure of citrate synthase from *Escherichia coli* K12. *Biochemistry* **14**, 235-241.

Wang P, Matthews DE and VanEtten HD (1992a) Purification and characterization of cyanide hydratase from the phytopathogenic fungus *Gloeocercospora sorghi*. *Archives of Biochemistry and Biophysics* **298**, 569-575.

Wang P and VanEtten HD (1992b) Cloning and properties of a cyanide hydratase gene from the phytopathogenic fungus *Gloeocercospora sorghi*. *Biochemical and Biophysical Research Communications* **187**, 1048-1054.

Wang W-C, Hsu W-H, Chien F-T and Chen C-Y (2001) Crystal structure and site-directed mutagensis studies of *N*-Carbamoyl-D-amino-acid amidohydrolase from *Agrobacterium radiobacter* reveals a homotetramer and insight into a catalytic cleft. *Journal of Molecular Biology* **306**, 251-261.

Wang P, Sandock RW and vanEtten HD (1999) Disruption of the cyanide hydratase gene in *Gloeocercospora sorghi* increases its sensitivity to the phytoanticipin cyanide but does not affect its pathogenicity on the cyanogenic plant sorghum. *Fungal Genetics and Biology* **28,** 126-134.

Watanabe A, Yano K, Ikebukuro K and Karube I (1998a) Cyanide hydrolysis in a cyanide-degrading bacterium, *Pseudomonas stutzeri* AK61, by cyanidase. *Microbiology* **144**, 1677-1682.

Watanabe A, Yano K, Ikebukuro K and Karube I (1998b) Cloning and expression of a gene encoding cyanidase from *Pseudomonas stutzeri* AK61 *Applied Microbiology and Biotechnology* **50**, 93-97.

Watanabe A, Yano K, Ikebukuro K and Karube I (1998c) Investigation of the potential active site of a cyanide dihydratase using site-directed mutagenesis. *Biochimica et Biophysica Acta* **1382**, 1-4.

Watanabe Y, Iwakura M, Tokushige M and Eguchi G (1981) Studies on Aspartase. VII. Subunit arrangement of *Escherichia coli* Aspartase *Biochimica et Biophysica Acta*, **661,** 261-266.

Yamamoto K and Komatsu K (1991) Purification and characterization of nitrilase responsible for enantioselective hydrolysis from *Acinetobacter* sp. AK 226. *Agricultural and Biological Chemistry* **55,** 1459-1466.